

Preliminary Design of a Stand-Alone Mars CubeSat Mission Integrating DLR In-House Technologies

MSc Thesis

Héctor Juan Marí

Delft University of Technology



Preliminary Design of a Stand-Alone Mars CubeSat Mission Integrating DLR In-House Technologies

by

Héctor Juan Marí

to obtain the degree of Master of Science

at the Delft University of Technology,

to be defended publicly on Tuesday October 10, 2023 at 14:00.

Student number: 5620325

Project duration: February, 2023 – September, 2023

Supervisors: Ir. R. Noomen TU Delft

Dr. T.M. Ho DLR

Thesis committee: Ir. B.T.C. Zandbergen TU Delft, committee chair

Ir. R. Noomen TU Delft

Dr.ir. E. van Kampen TU Delft

Dr. T.M. Ho DLR

Voler l'impossible ens cal,

i no que mori el desig.

- Marià Villangómez, Eivissa, 1948

Preface

Two years ago, I arrived at Delft with my heart full of excitement for the things to come. As I look back, it all seems out of the most beautiful of dreams. During these two years, I have had the chance to meet some of the most incredible people in my life. Together, we danced in the smoking chaos of life, cried with both laughter and pain and, through it all, grew as tall as giants. I owe them every bit of happiness that they have gifted me with, so I can only thank them for existing and the universe for bringing us together. I cannot name them all here, but know that if we have so much as shared a smile during these years, you have been part of this amazing journey. However, I will make two exceptions. First, I am grateful to my Bagijnhof 99 family for giving me not only a house, but also a home a thousand-five hundred kilometers away from it. I will forever cherish my memories of our *gezellig* family dinners and our adventures in and out of the house. Another piece of home came to me in the form of a beautiful group of Spanish people. Thank you for making me laugh with your dumb jokes, for cheering by my side when a green car went by, for helping me fix the world with hammer blows and a beer and for letting me cook for you just so we could all be together. I like to think that I have become a better person during my time in Delft. If that is the case, it is all because of you. Thank you all for giving me the best two years of my life.

Delft has also helped me realize how much home means to me. Back home - a little piece of land in the middle of the Mediterranean - my family has made this all possible with their unconditional and unwavering love and support. This thesis is the culmination of all the hard work we have done together for me to finally become an engineer. This is all for them. To my Mum and Dad, for always believing in me and being by my side throughout it all. To my niece and nephew, the reason I wake up every day wanting to be a better man. To my grandma, my brother, my sister-in-law and my beloved friends back home. To Inés, for dancing with me through thick and thin. To Mateu, for letting me explore this amazing world with him. Also, to the ones that we have lost along the way but will always be alive as long as we are.

Finally, I must thank my supervisors at both TU Delft and DLR. To Ron Noomen, for guiding me through this long journey always with a smile on his face. I have the honour to be the last of a long list of thesis students after his retirement. From now on, TU Delft will be missing not only a passionate professor, but also a great human being. To Tra-Mi Ho and Jan Thimo Grundmann for giving me the opportunity to join DLR and learn from you. I came out of Bremen a better space engineer, with lessons learnt that I will treasure forever. Thank you all for letting me stand on your shoulders so I could see further.

I really love you all with all my heart. I hope I can keep making you proud.

Héctor Juan Marí
Delft, September 2023

Abstract

Recent progress in CubeSat technology has allowed miniaturized satellites to venture away from Earth's orbit. In 2018, NASA's MarCO mission performed a Mars fly-by to provide relay communications between the InSight lander and Earth. In 2022, LICIACube carried out an observational analysis of the Didymos asteroid binary system after DART's impact on Dimorphos. More recently, ten 6U CubeSats built by universities and research centres were launched as secondary payloads of the Artemis 1 mission. These missions will independently explore cislunar and interplanetary space with the lowest cost up to date. Thus, the next significant advancement should encompass a dedicated CubeSat mission to explore a planet in Earth's proximity.

To contribute to this goal, the Institute of Space Systems of the German Aerospace Center (DLR) has developed radiation-hardened small satellite technologies, including communications, power and onboard computer subsystems. This study presents a stand-alone Mars exploration mission using the CubeSat standard that will demonstrate DLR's in-house technologies in deep space. The concept of operations is planned for a 2-year mission. After deployment, the spacecraft will carry out a stand-alone Earth-Mars transfer propelled by a low-thrust propulsion system. Upon arrival at Mars, the spacecraft will execute a ballistic orbital insertion into a highly elliptical orbit. Once in orbit around the Red Planet, the spacecraft will perform aerobraking to position itself in a Primary Science Orbit (PSO) in the altitude of 250 km, where the science operations will take place. This PSO will be a frozen and Sun-synchronous orbit to take advantage of Mars' gravitational parameters to enable a near-circular orbit [36]. During this phase, the spacecraft will tackle two of the most relevant scientific objectives of space missions around Mars [54]: gathering data on its lower atmosphere and gravity field. Finally, the spacecraft will be placed into a graveyard orbit for disposal.

A system concept is created to accomplish this mission by integrating the in-house technologies, investigating the necessary Commercial-Off-The-Shelf (COTS) components, and performing a feasibility assessment. The resulting 12U CubeSat has a wet mass of 20 kg, 5.1 km/s manoeuvring capability, and can generate up to 90 W of power at Mars. Its main payloads are a 2U infrared spectrometer, a 1U gravimeter and a 12 Mpx CMOS camera. The DLR ICA stack will be used, which combines multiple avionics systems (i.e., onboard computer, communications, and power) into a single unit. The DLR ScOSA onboard computer will be used, which integrates two computing nodes to ensure robustness. The reliable computing node comprises the OBC used on the MASCOT lander developed by DLR [31]. The high-performance computing node consists of a COTS-based processing module for application acceleration. The spacecraft uses the radiofrequency X-band in order to communicate with its ground segment. The in-house developed GSDR is used as a transceiver. The system also features a main reflectarray antenna as used by MarCO [32] and secondary patch antennas. Electrical power is generated using two linear solar arrays with 32% efficiency triple junction solar cells developed by Azur Space. The power control and distribution unit, as well as the batteries, will be adapted from those used by the DLR PLUTO mission [4]. For other subsystems, COTS components have been chosen that satisfy the needs of the mission. The propulsion system is a Busek BIT-3 gridded-ion engine as used in the Lunar IceCube and LunaH-Map missions [69]. This system features an expanded tank to accommodate the needed 4.3 kg of propellant. The XACT-50 developed by Blue Canyon Technologies is used as the integrated attitude control and determination system [74]. Thermal coating and heaters are used for thermal management; a preliminary

thermal analysis is presented that demonstrates their feasibility. All of these systems are housed in an EnduroSat 12U XL main structure [24]. A ground segment architecture is presented using a combination of DLR's antennas, ESA's European Space Tracking (ESTRACK) infrastructure and NASA's Deep Space Network (DSN). These are also used for navigation using ranging, Doppler and Delta-Differential One-Way Ranging (Delta-DOR) measurements. Different launch opportunities are studied, favouring a piggyback on another Mars-bound launch.

A preliminary mission analysis is performed using the TU Delft Astrodynamics Toolkit (Tudat) to assess the feasibility of the mission. Assuming the piggyback launch method as mentioned above, a set of porkchop plots is generated to constrain the two possible launch windows using Lambert's problem. Thus, the two departure date search spaces are: for the 2028/2029 launch window, from 2028-10-15 to 2029-05-01; and for the 2030/2031 launch window, from 2030-11-01 to 2031-06-15. The hodographic-shaping method [29] is then used to efficiently calculate the available low-thrust Earth-Mars trajectories and their Delta-V. An optimization process is implemented using a grid search over the potential departure dates and times of flight for these trajectories. For each point in the grid search, a differential evolution algorithm is used to find the free parameters in the hodographic-shaping velocity functions that result in an optimal Delta-V trajectory. An optima region has been found for the studied departure dates with TOFs in the range of 1000 to 1400 days. A 25% increase over the first estimate of Delta V for the Earth-Mars transfer enables feasible trajectories for 80% of the departure dates studied, with room for improvement. These trajectories exhibit maximum thrust values in the same order of magnitude as the system requirements, which is encouraging for a first estimation. An updated space segment is proposed with a wet mass of 20.8 kg, a Delta-V budget of 6.3 km/s and an increased mission lifetime of ~ 4 years. An orbit insertion strategy is proposed involving a ballistic capture. Finally, a study of a Mars science orbit that enables the scientific objectives of the mission is presented.

Contents

Preface	ii
Abstract	iv
Nomenclature	viii
1 Introduction	1
1.1 Motivation and objectives	1
1.2 Research questions and hypotheses	2
1.3 Document structure	3
2 Background	4
2.1 CubeSat ecosystem	4
2.2 Interplanetary CubeSat missions	6
2.3 DLR in-house small spacecraft technologies	8
2.3.1 Integrated Core Avionics	8
2.3.2 Communications	9
2.3.3 On-board computer	11
2.3.4 Software	12
3 Mission engineering	13
3.1 Goals, stakeholders and mission requirements	13
3.1.1 Needs, goals and objectives	13
3.1.2 Stakeholder identification	15
3.1.3 Mission requirements	15
3.2 Concept of operations	17
3.2.1 System context	17
3.2.2 Mission timeline	18
3.3 System requirements	19
3.4 System architecture	21
3.4.1 Functional decomposition	21
3.4.2 Physical decomposition	23
4 System design	27
4.1 Space segment	27
4.1.1 Payloads	27
4.1.2 Propulsion	31
4.1.3 Attitude determination and control	34
4.1.4 Guidance, navigation and control	38
4.1.5 Avionics stack	40
4.1.6 On-board computer	41
4.1.7 Telemetry, tracking and command	42
4.1.8 Electrical power	48
4.1.9 Thermal control	50
4.1.10 Structure	53

4.1.11	Configuration and budgets	55
4.1.12	Space segment overview	59
4.2	Ground segment	60
4.2.1	Ground station	60
4.2.2	Operations	61
4.3	Launch segment	62
4.3.1	Launcher	62
4.3.2	Deployer	63
4.4	Development, integration and testing	64
4.4.1	Development	64
4.4.2	Integration	65
4.4.3	Testing	66
4.5	Risk management	67
4.6	Requirement compliance	71
5	Mission analysis	72
5.1	Earth-Mars transfer	72
5.1.1	Hodographic-shaping method	72
5.1.2	Simulation	74
5.1.3	Departure date analysis	78
5.1.4	Optimization	78
5.1.5	Verification	91
5.2	Mars orbit insertion	91
5.3	Mars science orbit	92
6	Conclusions and future work	95
6.1	Summary	95
6.2	Conclusions	97
6.3	Future work	98
	References	99
A	Mission requirements	104
B	System requirements	106
C	Subsystem requirements	109

Nomenclature

Abbreviations

Abbreviation	Definition
ADCS	Attitude Determination and Control System
APR	Array Power Regulator
BBE	Baseband Equipment
BOL	Beginning Of Life
CDS	CubeSat Design Specification
CNES	Centre National d'Études Spatiales
ConOps	Concept of Operations
DE	Differential Evolution
Delta-DOR	Delta-Differential One-Way Ranging
DSN	Deep Space Network
EDL	Entry, Descent and Landing
EOL	End Of Life
EPS	Electrical Power System
EQM	Engineering Qualification Model
ESTRACK	European Space Tracking
FFBD	Functional Flow Block Diagram
FPGA	Field Programmable Gate Array
GNC	Guidance, Navigation and Control
GS	Ground Segment
GSDR	Generic Software Defined Radio
GSOC	German Space Operations Center
HGA	High Gain Antenna
HPN	High Performance Node
JAXA	Japan Aerospace Exploration Agency

Abbreviation	Definition
LEOP	Launch and Early Orbit Phase
LGA	Low Gain Antenna
LS	Launch Segment
MCS	Mission Control System
MMX	Mars Moons eXploration
MOI	Mars Orbit Insertion
MRO	Mars Reconnaissance Orbiter
NAIF	Navigation and Ancillary Information Facility
OBC	On-Board Computer
OUTPOST	Open modular software Platform for Spacecraft
PCDU	Power Conditioning and Distribution Unit
PSO	Primary Science Orbit
PUS	Packet Utilization Standard
RCN	Reliable Computing Node
RF	Radiofrequency
SC	Spacecraft
ScOSA	Scalable On-board Computing for Space Avionics
SOI	Sphere of Influence
SSO	Sun-Synchronous Orbit
TC	Telecommand
TCS	Thermal Control System
TID	Total Ionizing Dose
TOF	Time of Flight
TT&C	Telemetry, Tracking and Telecommand
Tudat	TU Delft's Astrodynamics Toolbox

Symbols

Symbol	Definition
A_d	Drag reference area, m^2
A_r	Radiator area, m^2
A_s	Sunlit surface area, m^2
a	Semi-major axis, m
B	Magnetic field, T
C_d	Drag coefficient
c	Speed of light, 2.99×10^8 m/s
c	Free shaping function parameter
cm	Center of mass, m
cp_a	Center of aerodynamic pressure, m
cp_s	Center of solar radiation pressure, m
D	Spacecraft residual dipole moment, Am^2
e	Eccentricity
f	Thrust acceleration, m/s^2
G_{rms}	Root mean square acceleration, m/s^2
H_p	Periapsis altitude, m
H_a	Apoapsis altitude, m
I_y	Moment of inertia about the Y-axis, kg/m^2
I_z	Moment of inertia about the Z-axis, kg/m^2
i	Inclination
M	Magnetic moment of Earth multiplied by the magnetic constant, Tm^3
m	Mass, kg
$Q_{backload}$	External heat load on the spacecraft surfaces, W
Q_{int}	Internal heat load generated by the spacecraft, W
q	Unitless reflectance factor
q_{albedo}	Albedo heat load per unit area, W/m^2
$q_{EarthIR}$	Black body radiation heat load from Earth per unit area, W/m^2
q_{solar}	Solar heat load per unit area, W/m^2
R	Distance between the spacecraft and the center of a celestial body, m
r	Radial distance, m

Symbol	Definition
s	Distance from the central body, m
T_a	Atmospheric drag torque, Nm
T_g	Gravity-gradient torque, Nm
T_m	Magnetic torque, Nm
T_{max}	Maximum radiator temperature, K
T_s	Solar radiation pressure torque, Nm
t	Time, s
V	Spacecraft orbital velocity, m/s
v_{eq}	Effective exhaust velocity, m/s
z	Axial distance, m
α	Absorptivity
ϵ	Radiator emissivity
σ	Stefan-Boltzmann constant, $5.67 \times 10^{-8} \text{ W}/(\text{m}^2\text{K}^4)$
ΔV	Velocity change, m/s
θ	Polar angle, rad
λ	Function of the magnetic latitude
μ	Gravitational parameter, m^3/s^2
ρ	Atmospheric density, kg/m^3
Φ	Solar constant adjusted for actual distance from the Sun, W/m^2
ϕ	Angle of incidence of the Sun, rad
ψ	Angle between the local vertical and the Z principal axis, rad
Ω	Right ascension of the ascending node, rad
ω	Argument of periapse, rad
\square_0	Initial value
\square_f	Final value
\square_r	Radial component
\square_z	Axial component
\square_θ	Transverse component
$\dot{\square}$	Derivative w.r.t time
$\ddot{\square}$	Second derivative w.r.t time

1

Introduction

In this chapter, an introduction to the research project is presented. First, the motivation for the research and the main objectives are established. Then, the main research questions are posed, along with their corresponding hypotheses. Finally, the structure of the complete document is discussed.

1.1. Motivation and objectives

The first wave of interplanetary CubeSats is already underway. In 2018, NASA's MarCO mission launched two 6U CubeSats into interplanetary space alongside the InSight Mars lander. These CubeSats enabled the success of the InSight mission by providing a crucial real-time communication link between the spacecraft and Earth during its entry, descent, and landing (EDL). In 2022, LICIACube carried out an observational analysis of the Didymos asteroid binary system after DART's impact on Dimorphos. More recently, ten 6U CubeSats built by universities and research centres were launched as secondary payloads of the Artemis 1 mission. These missions will independently explore cislunar and interplanetary space with the lowest cost up to date.

The primary motivation for this research is to propose the next significant advancement in the interplanetary CubeSat mission ecosystem. This next step shall encompass a stand-alone CubeSat mission to explore a planet in Earth's proximity. Since Mars was previously visited using CubeSats to support a larger mission, the most logical progression would involve a mission to the Red Planet with the purpose of conducting independent scientific research. To contribute to this goal, the Institute of Space Systems of the German Aerospace Center (DLR) has developed radiation-hardened small-satellite technologies, including communications, power, and onboard computer subsystems. Therefore, the mission will also serve as a technology demonstration for these technologies.

The key word for this mission is "stand-alone". This term signifies that the mission, once it has been launched, will fulfil all its objectives without the support of a larger mission. Therefore, the system shall perform the Earth-Mars transfer, orbit insertion and science measurements on its own. This is to result in a system that can accommodate a wide range of launch opportunities and is therefore more probable to advance into the following stages of development. The mission will tackle two of the most relevant scientific objectives around Mars [54]: collecting data on its lower atmosphere and on its gravity field.

As a result, the objectives of this research are:

- Establish an overall system design that enables a stand-alone CubeSat mission to Mars.
- Provide a system solution that integrates the available small-satellite DLR in-house technologies.
- Study the trajectory design of the mission to demonstrate its feasibility.
- Advance the understanding of interplanetary CubeSats and foster their ecosystem.

1.2. Research questions and hypotheses

The primary research questions and the corresponding hypotheses are as follows:

1. What are the design and performance characteristics that enable a stand-alone interplanetary CubeSat system to Mars?
 - Hypothesis: After the first wave of interplanetary CubeSats, the previous concerns in terms of telecommunications, propulsion and radiation tolerance have now been mitigated. In 2018, NASA's MarCO mission performed a Mars fly-by using CubeSats to provide relay communications between the InSight lander and Earth. More recently, ten 6U CubeSats built by universities and research centres were launched as secondary payloads of the Artemis 1 mission. These missions will independently explore cislunar and interplanetary space with the lowest cost up to date. Thus, the next significant advancement should encompass a dedicated CubeSat mission to explore a planet in Earth's proximity. The feasibility of such a mission shall be analyzed.
 - Sub-questions:
 - 1.1. What is the most feasible timeline for a stand-alone Mars CubeSat mission?
 - 1.2. How can DLR's in-house technologies be evaluated and combined with COTS components to provide a solution for the space segment?
2. What are the trajectory characteristics of a stand-alone CubeSat mission to Mars?
 - Hypothesis: Chemical propulsion systems have been proven to be unfeasible for stand-alone CubeSat missions to other Solar System planets given their size and mass constraints. However, electric propulsion systems are being developed that could facilitate low-thrust trajectories to these celestial bodies. Missions such as Lunar IceCube and LunaH-Map are set to perform stand-alone low-thrust transfers to the Moon. Therefore, the CubeSat ecosystem might be prepared to enable low-thrust transfers to Mars. A study is required to assess the feasibility of these trajectories.
 - Sub-questions:
 - 2.1. What is the feasibility of a low-thrust CubeSat transfer to Mars and what are the associated requirements?

1.3. Document structure

In this chapter, the motivation, objectives, and questions to be answered during this research project have been established. Including this chapter, the document is divided primarily into six chapters.

Chapter 2 deals with the necessary background information to delve into the study. The general CubeSat ecosystem is discussed showing the advancements that have recently enabled interplanetary missions using the standard. The main interplanetary CubeSat missions are then analyzed, focusing on MarCO and the Artemis 1 CubeSats. Finally, the DLR in-house small spacecraft technologies to be integrated into the system are reviewed.

Chapter 3 outlines the first steps in the system design process. First, the stakeholder expectations are analyzed, resulting in the first set of mission requirements. From there, the concept of operations is defined through a system context diagram and a mission timeline. This is then used to formulate the system requirements. Finally, the system architecture is presented by studying the functions that the system needs to perform and assigning them to physical subsystems and components.

Chapter 4 presents an analysis of the main subsystems of the space, ground, and launch segments. An individual solution is found for every subsystem within the different segments. Then, the configuration of the space segment and its mass budget are analyzed. A development plan for the following stages of the mission is introduced, as well as a risk analysis.

Chapter 5 describes the mission analysis. It mainly focuses on the calculation of low-thrust Earth-Mars trajectories using the hodographic shaping method. An optimization procedure is performed on these trajectories in order to study their feasibility using the proposed system solution. An orbit insertion strategy around Mars is then presented. The chapter ends with the study of a Mars science orbit that enables the scientific objectives of the mission.

Finally, the conclusions of this research project are drawn in Chapter 6. The initial research questions are answered and some recommendations for future work are given.

2

Background

In this chapter, a brief background study is presented. Initially, an overarching perspective of the CubeSat ecosystem is given. Subsequently, this viewpoint is focused specifically on the initial wave of interplanetary CubeSats. To conclude, a review is performed on the DLR in-house technologies to be assessed and potentially applied in the mission.

2.1. CubeSat ecosystem

The CubeSat has allowed sectors with little to no experience and resources to access space. By using standardized systems and riding as secondary payloads on launchers, small companies and universities can now also push the boundaries of space exploration.

The first CubeSat was the result of a collaboration between Stanford University and California State Polytechnic University back in 1999. The OPAL (Orbiting Picosat Automated Launcher) aimed to demonstrate the viability of the concept of picosatellites (i.e., satellites with a mass from 0.1 kg to 1.0 kg) as well as introduce an innovative orbital deployment system. The success of the mission meant the start of a new era in space exploration. [11]

To make these CubeSats compatible with a standardized orbital deployer, a physical standard was established: a CubeSat of 1 unit (1U) would have the dimensions of a 10 x 10 x 10 cm cube and a mass of no more than 1.33 kg [15]. These units can be joined together resulting in 2U, 3U or even bigger configurations, with 16U CubeSats being the largest to be sent to orbit. This scalability provides great flexibility in the design of the spacecraft and the payload selection.

The philosophy of the CubeSat is to provide an architecture for the design of a spacecraft that can be developed by a student team in a relatively short time frame (i.e., around 1-2 years) and at a low cost (i.e., less than \$100.000). To do so, the design of the CubeSat [72] needs to:

1. Reduce development costs by reducing the size of the satellite.
2. Reduce launch costs.
3. Reduce design choices.
4. Protect the primary payload.

5. Develop a market for COTS components.
6. Attract new companies to the sector.

While the CubeSat form factor was designed to educate and train university students, it has been adopted by the commercial space industry as a quick and inexpensive way of bringing certain payloads to Earth's orbit. The production and launch of CubeSats have skyrocketed during the last decade, as can be seen in Figure 2.1. In this figure and from here onwards, the term 'nanosatellite' refers to all spacecraft in the range of 1.1 - 10 kg. Smaller CubeSats are considered nanosatellites, while larger configurations (i.e., 6U or more) are considered 'microsatellites'. As of May 2023, 2105 CubeSats have been launched, with 15 of them going to interplanetary space [43]. Among these, the Delfi-C3 launched in 2008 was the first Dutch university satellite to be flown. As can be seen in Figure 2.1, CubeSats were not launched beyond LEO until 2018. Mostly thanks to the ten 6U CubeSats launched on the Artemis I mission, this number has been on an upward trend since then. The most common applications for these nanosatellites are remote sensing, technology development and communications.

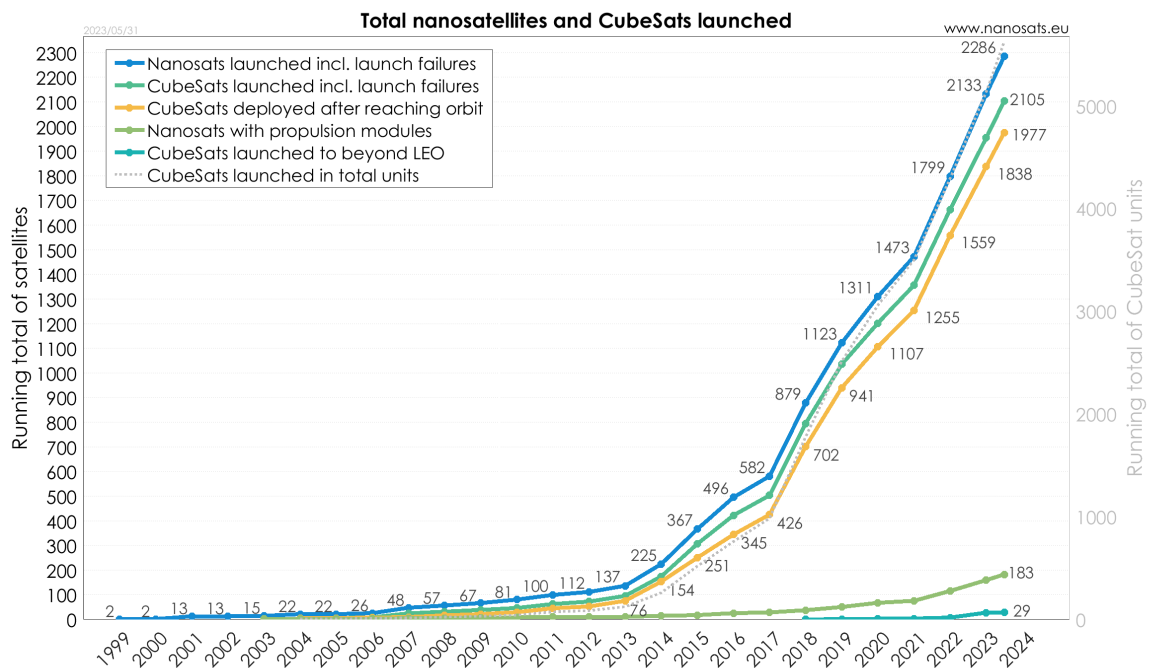


Figure 2.1: Cumulative number of nanosatellites and CubeSats launched [43].

Given the surge in satellite constellations and the increasing number of new-space companies coming into play, the era of nanosatellites is still to come, with over 2080 nanosats being set to launch in the next 6 years. Moreover, the technological advancements and the improvements in the design of nanosatellites during the last decades have improved the success rate of these missions up to 75% [70]. Since these missions have a relatively low cost, the limited budgets might not allow for the required testing for the success rates to go higher.

While the capabilities of small spacecraft have matured over the past years, technologies are still being developed to make deep space smallsat missions more common. Some aspects such as increased radiation tolerance, improved communication systems and efficient propulsion systems are critical in interplanetary CubeSat missions. MarCO's two 6U CubeSats were the first to venture into deep space in a communications relay mission that accompanied the InSight lander to Mars. This mission

proved the capabilities of such a class of spacecraft and the Guidance, Navigation and Control (GNC) fine-pointing necessary for communications in deep space. This mission sparked interest in designing microsats for environments beyond low-Earth orbit. Such interest culminated with the launch of Artemis 1 in November 2022, which sent 10 6U CubeSats into lunar orbit and interplanetary space. [33]

2.2. Interplanetary CubeSat missions

The use of CubeSats for deep space missions could revolutionise robotic Solar System exploration. The recent advancements in the CubeSat paradigm could open the doors of deep space exploration to students with limited experience and resources. While interplanetary CubeSats share similarities with low-Earth orbit missions, they require changes in most subsystems. These interplanetary CubeSats require propulsion systems to escape Earth's gravity field, manoeuvre in interplanetary space and/or enter an orbit around another planet. When in deep space, the CubeSat faces harsher environments and longer path distances, which require more efficient communication systems and pointing control [5]. Since they are outside of the protection of Earth's magnetosphere, they also require dedicated strategies for radiation tolerance. Moreover, less frequent contact with Earth also imposes the need for more autonomous operations. This all in turn drives the power requirements up, and therefore the need for higher energy storage capabilities. Higher power requirements also usually need more advanced thermal control solutions.

Regarding radiation tolerance, there are several considerations to take into account. First of all, single-event upset rates have proven to be less frequent than predicted in interplanetary CubeSats, which could be due to careful part selection. Also, while total ionizing dose tolerance levels are lower for commercial electronics, simple shielding techniques are sufficient since interplanetary radiation environments are generally more benign than those in GTO. On top of that, several techniques can be used for increased robustness, including redundancy, rebooting systems using watchdog timers and radiation shielding, among many others [11].

Another important challenge to overcome for interplanetary CubeSats is telecommunication. Here, significant development has been ongoing, and the success of the MarCO mission showed promising results. In order to overcome the challenges created by long path distances, higher frequencies (S-band, X-band and Ka-band) need to be used, as well as higher power and bigger antennas. MarCO, with an X-band communications system, achieved a data rate of 16 kbps at the distance of Mars, but this could be boosted by a factor of eight by switching to Ka-band and by a further factor six by using a bigger 1 m² antenna. Several missions have proven that this type of high-gain antenna can be adapted for the CubeSat platform [14]. For example, NASA's RainCube successfully flew a deployable 0.5-m-diameter Ka-band parabolic antenna. The RainCube 6U CubeSat (shown in Figure 2.2) fits the 0.5m antenna into 1.5U, the radar electronics into 3U, and the spacecraft bus into 1.5U.

In general, other aspects of spacecraft design have accomplished enough maturity over the last decades or simply do not scale. On the one hand, CubeSat subsystems like the AOCS have acquired high technology readiness levels and can be scaled up for the requirements of an interplanetary mission as was done for the MarCO CubeSats [35]. On the other hand, CubeSat navigation and flight dynamics are elements that do not scale, as they generally require the same resources as other interplanetary missions. For example, navigation information is usually gathered by measuring Doppler shifts on the spacecraft's Radio Frequency (RF) signal. This is usually done using NASA's DSN or other (smaller) networks. Therefore, the infrastructure for interplanetary navigation already exists [11].

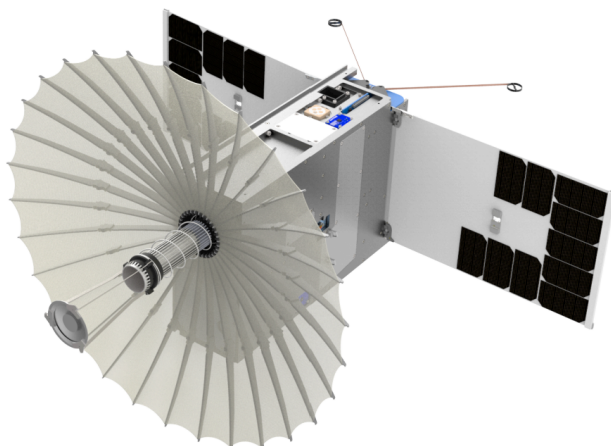


Figure 2.2: The RainCube 6U CubeSat in deployed-antenna configuration [60].

For the moment, the main destination for these interplanetary CubeSats is the inner Solar System, both in free-flying and mother-daughter configurations. On the one hand, free-flying CubeSats perform the transfer to their destination on their own. On the other hand, mother-daughter CubeSats are integrated into larger spacecraft and only detach from them when the mothership has reached a certain destination. The widespread use of gravity assists on planets in the inner Solar System could provide a viable option to bring nanosatellites to their destinations. Nonetheless, free-flying nanosats with a few kilometres per second of ΔV could also be placed in the relevant transfer orbits [11]. Moreover, the Moon, near-Earth asteroids, comets or objects that traverse the Solar System (e.g., Oumuamua) could be attractive destinations for these CubeSats. On the other hand, the outer Solar System is still only reachable using a mother-daughter configuration, since the distances to Earth and the Sun would require considerably better communication and power systems.

It was not until the decade of 2010 that interplanetary CubeSats became viable. Some key technology developments were needed for this breakthrough [38]. First of all, CubeSat sizes were on a path to the 6U and larger form factors, after the sector had favoured the 3U configuration for low-Earth orbits. On top of that, small-scale propulsion techniques such as solar sails and electric propulsion emerged which got rid of the need for pressurized propellants. Finally, the communications team at the Jet Propulsion Laboratory (JPL) did extensive work on reducing the size of the needed electronics for both optical and RF telecommunications [41]. This led to an increasing number of interplanetary CubeSat mission proposals at NASA, which culminated with the Mars CubeSat One (MarCO) mission.

The MarCO concept (Figure 2.3) was developed in 2014 and aimed to send two CubeSats to Mars autonomously after being launched along the InSight mission. This was a technology demonstration mission, which intended to advance the technology and demonstrate the feasibility of a CubeSat mission into deep space. In the end, MarCO-A and MarCO-B did a Mars flyby, during which they provided a real-time communication link between InSight and Earth during its entry, descent, and landing (EDL). These were 6U CubeSats and were fully implemented using COTS components, which were proven to be effective during deep space operations. The mission was successful, receiving the ultrahigh-frequency telemetry from InSight during its EDL phase and relaying this telemetry in the X-band to NASA's DSN [35]. Many of the lessons learned from the MarCO mission are being published, including the compensation of a drifting onboard clock and a leak in its cold-thrust propulsion system [40]. All in all, this mission enabled a new class of planetary exploration, with a cost 40 times lower than most NASA Discovery missions and a schedule that only spanned 15 months.

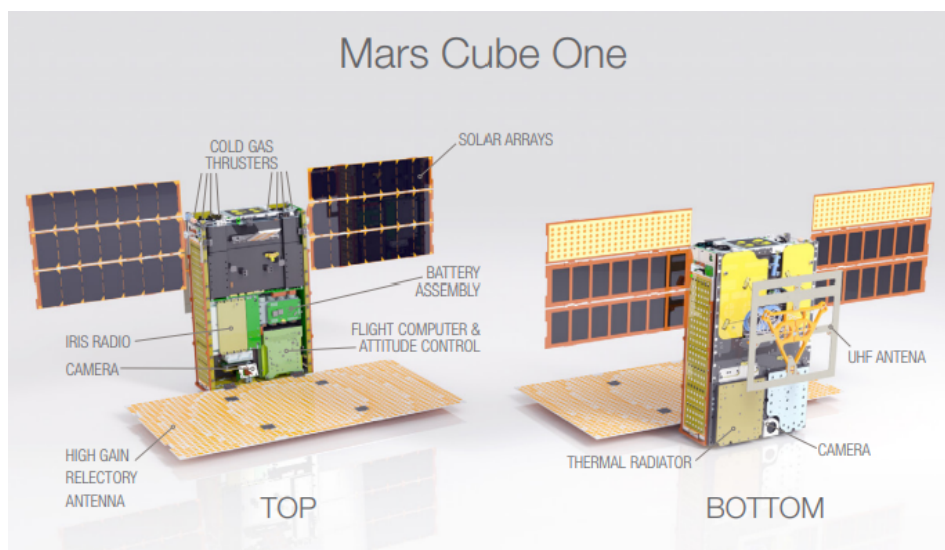


Figure 2.3: Illustration of the twin MarCO spacecraft with some key components labelled. The top cover is left out to show some internal components [35].

However, MarCO is no longer the only CubeSat mission to venture into interplanetary space. During the Artemis 1 launch, 10 CubeSats were carried as secondary payloads and are destined for cislunar and deep space [53]. Missions such as EQUULEUS, LunaH-Map and Lunar IceCube will orbit the Moon and perform measurements from cislunar space. The OMOTENASHI mission will attempt to land on the Moon using solid rocket motors. Other missions such as the Near-Earth Asteroid Scout, Team Miles, the CubeSat for Solar Particles and BioSentinel will travel beyond the limits of the Earth-Sun system. The Near-Earth Asteroid Scout will travel to a near-Earth asteroid using solar sail propulsion. Team Miles, on the other hand, will demonstrate low-thrust plasma propulsion in interplanetary space. Moreover, the BioSentinel mission will carry yeast cards into deep space in order to analyze the effects of deep space radiation. Following this trend, more opportunities for interplanetary microsattellites will arise, setting the pace for this new kind of Solar System exploration.

2.3. DLR in-house small spacecraft technologies

The German Aerospace Center has been developing various miniaturized satellite systems throughout the years, which could be used for a potential CubeSat mission to Mars. The following systems will be reviewed in order to have a first grasp of their feasibility for such a mission: communications system, power system, onboard computer, and software. These are all combined in a space avionics stack, the Integrated Core Avionics (ICA).

2.3.1. Integrated Core Avionics

ICA is a space avionics stack that can be used for different mission scenarios in an innovative and developer-friendly manner [64]. It provides an interface that integrates the full set of avionic domains of power, onboard data handling, communication, and software into a single unit. The goal was to simplify interfaces, reduce size and mass and reduce recurrent engineering efforts for subsystem integration [4]. As the design is based on previous subsystem developments, a shared form factor had to be found to allow interoperability of the components.

ICA provides solutions that can be used in a wide variety of scenarios and allows integration of the same modules in CubeSat structures or stand-alone enclosures for larger systems, as can be seen in Figure 2.4. A variety of modules can provide the required functionality, from power and data handling to communications. These modules are supported by DLR's Open modular software Platform for Spacecraft (OUTPOST). This allows the application of ICA to CubeSats, small satellites, launchers and other space equipment, with reduced redesign effort and reduced risk.

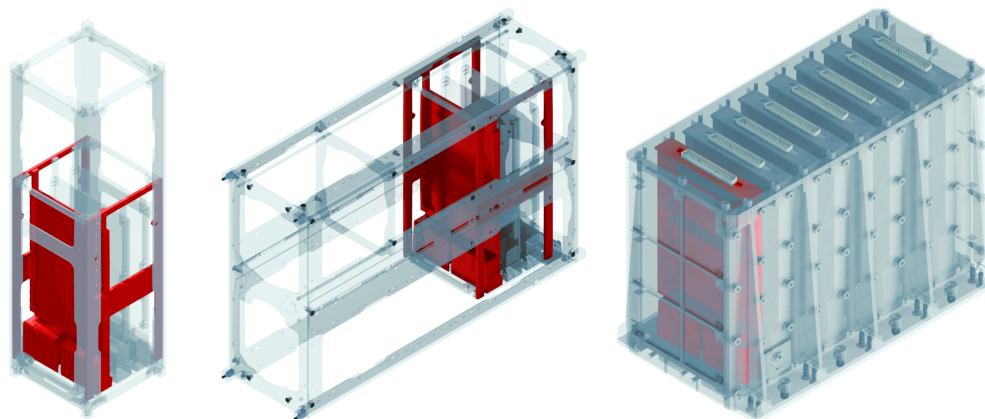


Figure 2.4: Application spectrum for ICA modules (in red) showing compatibility with 3U/6U CubeSat structures and integration with a stand-alone box for larger systems [64].

This framework also implements a wireless intra-spacecraft communication system. This allows a simplification of the harness design and routing, with the consequent reduction of harness cables and thus mass in a certain space system. The system makes use of an impulse radio ultra-wideband (IR-UWB) physical layer, which is based on short-duration and low-energy pulses that are transmitted through a wideband antenna. An optimized low-latency and deterministic network protocol was also developed to meet latency requirements on spacecraft networks [23]. This allowed the system to accomplish communication with a latency of 10 ms and less for key drivers like the Attitude and Orbit Control System (AOCS). In essence, the system allows for reliable wireless communication between the internal network nodes (e.g., sensors) for low- to medium-data rate applications.

2.3.2. Communications

The in-house communications system at DLR is based on a highly integrated and reliable Generic Software Defined-Radio (GSDR) platform. The GSDR allows the operation of multi-band RF applications in the harsh environment of space, being designed with a notable focus on its radiation hardening [9]. The system went through characterization at the system level in order to verify the radiation tolerance of the whole system and assess the mechanisms for protection from radiation effects.

This system is built around the concept of Software Defined Radio (SDR). This concept arose from the need for smaller, more flexible, and cost-efficient radio systems. Traditionally, radio communication systems use analog hardware such as mixers, filters, and amplifiers, among others. The basic principle of SDR systems is to perform most parts of the signal processing through software, which has led to systems with much simpler and less costly hardware. This also means that its functionalities are easily updated and upgraded through simple re-programming while using the same hardware.

The basic architecture for an SDR communications system can be seen in Figure 2.5. It consists

of an antenna system, a simple RF front end, a digital front end and a digital back end [7]. First of all, the antenna system gathers or sends certain RF waves from/into the environment. The RF front end is used to amplify the received and transmitted waveform. Another function of the RF front end is to down-convert the signals to an Intermediate Frequency (IF) so that they can be used by the Analog-to-Digital Converter (ADC) and Digital-to-Analog Converter (DAC). These hardware components are the interface between the analog and digital domains. The digital front end is usually implemented into Field Programmable Gate Arrays (FPGA), where basic signal processing steps are performed. Finally, the main part of the signal processing is performed in the digital baseband, which usually takes the form of a General Purpose Processor (GPP) or a personal computer. This is where the signal processing software is implemented, leading to versatile architectures that can easily be upgraded, updated and de-bugged.

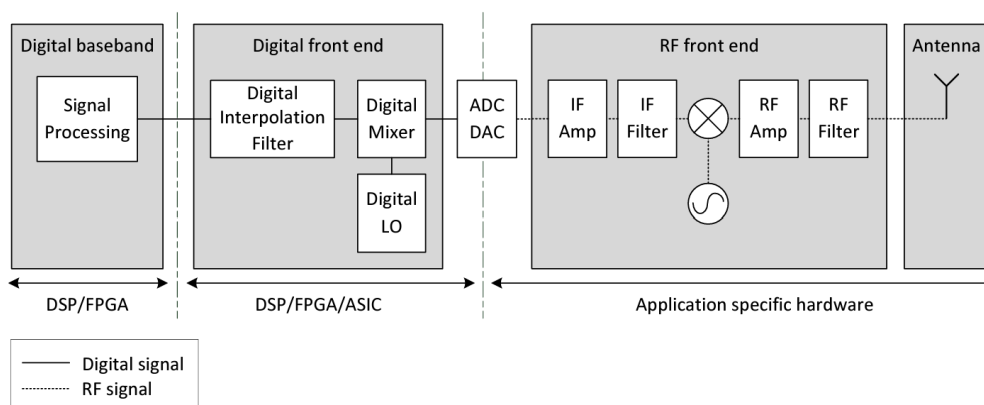


Figure 2.5: High-level system architecture of common SDR systems [7].

Being a space-borne system, the GSDR was designed with special consideration for its radiation tolerance. On the one hand, space-qualified and highly reliable technologies had low flexibility and performance, and extremely high costs. On the other hand, technologies developed for CubeSat missions using COTS devices were potentially more powerful and efficient but could fail in the harsh environment of space. A methodology was therefore designed that allowed an analytical judgement for the use of COTS components in space applications [7]. The result is a system design that is based on radiation-hardened components and evaluated COTS electrical devices. Rigorous system-level radiation testing was performed, through which no destructive event was observed.

Overall, the capabilities of the GSDR are highlighted in the following list:

- Fully software-controlled radio platform
- Radiation-tolerant and modular design
- Adjustable in RF range up to 6 GHz by software
- 4x Rx and 4x Tx design for MIMO applications
- Up to 56 MHz bandwidth per channel
- Customizable FPGA design for user-defined communication systems
- In-flight reconfiguration, redundant boot mechanism and automatic failure recovery

2.3.3. On-board computer

The Scalable on-board Computing for Space Avionics (ScOSA) is a distributed, heterogeneous, scalable and reliable On-Board Computer (OBC) with high computing performance that can be reconfigured whenever needed. One of the main reasons for its development was the demand for high computing performance needed for onboard data processing in Earth Observation (EO) or robotics missions. The increase in sensor resolution and the need for autonomous navigation require more powerful onboard computers while still ensuring the required reliability.

In order to create the system, DLR internal hardware, as well as software in the field of OBCs, were combined. It consists of several computing nodes that are interconnected via a switched SpaceWire network. These computing nodes are either reliable space-qualified or high-performance COTS components. The system can also be scaled depending on the mission requirements. In contrast to the one-to-one mapping of redundant computing units to reach better reliability, the ScOSA introduces a different concept, which is more flexible and efficient: in case of failure, the system migrates the tasks of the affected parts to other spare units, essentially re-configuring itself. [22]

Figure 2.6 shows ScOSA's system architecture. First of all, one can see that the reliable computing nodes (RCN) are the interface between the system and the telecommand and telemetry units. These RCNs are space-qualified and radiation-hardened, which makes them suitable for interplanetary space missions. The RCNs are also connected by SpaceWire routers to N high-performance nodes, which are COTS components. These RCNs are also connected to the interface nodes which connect the sensors and actuators. This modular concept allows for increased scalability to tailor the computational resources to the mission's demands. [47]

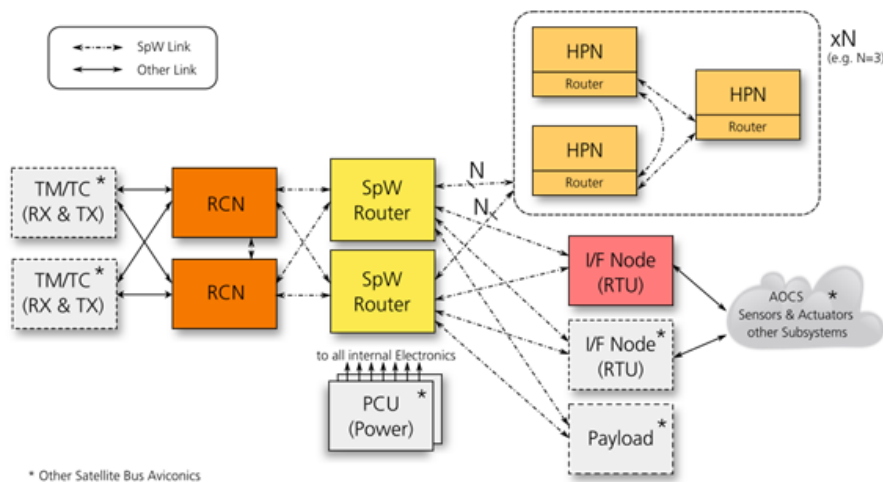


Figure 2.6: Example of ScOSA's system architecture [47].

Each of the aforementioned nodes is assigned a role to ensure early detection of faults due to hardware malfunction, radiation effects or software errors. The system has a Master Node which receives regular heartbeat messages from all other nodes. Each of the Slave Nodes continuously informs the Master Node in case it detects a malfunction in itself or in another node. In that case, a reconfiguration event is activated by the Master Node: first, the failed node is isolated from the network; then, its tasks are redistributed among the remaining nodes; and finally, the tasks are resumed from the last available checkpoint. As a result, the mission can be continued with the possibility of (limited) performance

degradation. [68]

Overall, the capabilities of the ScOSA are highlighted in the following list:

- Fault and radiation tolerant LEON3FT-based processing modules with up to:
 - 160 DMIPS / 160 MFLOPS
 - 128 MiB RAM with ECC and 4 GiB NAND flash memory
- COTS-based processing modules for application acceleration with up to:
 - 8660 DMIPS / 410 MFLOPS (double precision)
 - 1 GiB RAM with ECC and 4 GiB NAND flash memory
- Mission-specific interface modules with a selection of standard interfaces like RS422/RS485 serial, CAN, SpaceWire, and discrete I/O

2.3.4. Software

The DLR in-house developed flight software is the Open modular software Platform for Spacecraft (OUTPOST) [21]. It was developed to design and implement reusable embedded software in the early stages of a mission design and hence to be independent of the operating system and the hardware it runs on. This software uses abstraction layers, towards hardware and operating system, leading to modular and portable implementations of flight software. The key elements of OUTPOST have been released under an open-source license so that it is available for use and development by third parties.

OUTPOST implements several capabilities, including a module with Packet Utilization Standard (PUS) services. This module can be used for telemetry and telecommand verification and parsing, parameter storage with statistics and monitoring, flexible function management with time and location scheduling, data compression and housekeeping recording, among other operations. Other modules implement functionalities like internal and external communication protocols, sparse logging, ground parsing and even mission control software.

3

Mission engineering

This chapter introduces the initial phases of the system design. First, the stakeholders will be identified and their expectations will be analyzed. This will result in the formulation of the mission requirements. These mission requirements will be used to design the mission Concept of Operations (ConOps). Subsequently, the mission requirements will be specified into the system requirements. Finally, a functional and physical architecture of the system is presented.

3.1. Goals, stakeholders and mission requirements

The point from which the system design process should start is the stakeholder's expectations. They lay out the mission and drive the design, development, integration, and deployment. The primary stakeholders for this mission (i.e., the customers) are DLR and TU Delft.

3.1.1. Needs, goals and objectives

The customers have been directly consulted to identify the underlying need that will serve as the foundation for this mission. From there, the main goals and objectives of the mission can be inferred.

Need statement

By analyzing the expectations of the main customers, the following mission need statement can be retrieved:

“In the past, space exploration of celestial bodies other than Earth or the Moon has been largely restricted to missions with substantial governmental funding and resources. However, the recent proliferation of CubeSats has resulted in considerable advancements in interplanetary small spacecraft technologies. This change in paradigm culminated with the first wave of interplanetary CubeSats to Mars, Near-Earth Asteroids (NEA) and the Moon. Following this trend, DLR has been developing a number of spacecraft subsystems that could potentially be used for a deep space mission.

Having now operated CubeSats around Earth's natural satellite, there is a need to demonstrate the capabilities of interplanetary CubeSat technology applied to independently explore a planet in Earth's proximity.”

Mission statement

A mission statement can be formulated in response to the aforementioned need:

“A stand-alone CubeSat mission to Mars will be designed, leveraging DLR’s in-house technologies and conducting an orbit analysis to demonstrate the feasibility of interplanetary small spacecraft.”

Mission goals and objectives

From the mission statement, a specific set of goals and objectives for the mission has been proposed. As shown in Table 3.1 this is primarily a DLR in-house technology demonstration mission. The main technologies to be demonstrated are the communications, power and onboard computer subsystems. On top of that, the spacecraft will also conduct scientific research in a Mars orbit. To do so, the spacecraft first needs to travel to Mars independently. This substantially increases the launch and transfer possibilities when comparing it to a mothership piggyback alternative.

In order to fully demonstrate the feasibility of interplanetary CubeSats, the mission shall also tackle relevant scientific objectives in Mars orbit. These knowledge gaps have been identified by the Mars Exploration Program Analysis Group at NASA. In their last report, published in 2020 [54], one of the higher-priority goals is to characterize the dynamics, thermal structure and distribution of dust, water, and carbon dioxide in Mars’ lower atmosphere. On top of that, as a secondary scientific objective, the gravity field of Mars will be studied. As required by DLR, the mission shall also be able to carry out observational analysis of Mars.

Goals	Objectives
1. Demonstrate DLR’s in-house technology for interplanetary small spacecraft.	1.1. Demonstrate DLR’s Integrated Core Avionics stack in deep space.
	1.2. Demonstrate DLR’s ScOSA On-Board Computer (OBC) in deep space.
	1.3. Demonstrate DLR’s Power Conditioning and Distribution Unit (PCDU) in deep space.
	1.4. Demonstrate DLR’s GSDR communication system in deep space.
	1.5. Demonstrate DLR’s Solar Array system in deep space.
	1.6. Demonstrate DLR’s OUTPOST in-flight software in deep space.
2. Execute Earth-Mars transfer trajectory.	2.1. Perform an Earth-Mars transfer orbit.
	2.2. Achieve orbital insertion around Mars.
	2.3. Reach an operational orbit at Mars
3. Perform science in an orbit around Mars.	3.1. Gather data on the lower atmosphere of Mars.
	3.2. Perform measurements of the gravity field of Mars.
	3.3. Carry out observational analysis of Mars.

Table 3.1: Goals and objectives for the mission.

3.1.2. Stakeholder identification

Apart from the main customers, there are many stakeholders that will influence the development of the system. The main stakeholders have been identified and are shown in Table 3.2. A stakeholder ID has been assigned to each of them. Moreover, they have been classified as active or passive. On the one hand, an active stakeholder interacts directly with the operational system. On the other hand, passive stakeholders are involved in other activities (e.g., design, integration) but do not interact directly with the deployed system. DLR will take responsibility for the design, assembly, testing, and operations of the mission. The launch provider will provide the spacecraft testing requirements in the later stages of the mission design. On top of that, space agencies and other institutions will provide standards to be followed in the design of the mission. More specifically, Cal Poly is the entity responsible for the CubeSat standard, which is to be followed rigorously.

Type	Stakeholder	ID	Active/Passive
Customer	German Aerospace Center (DLR)	SH01	Passive
	Delft University of Technology (TU Delft)	SH02	Passive
Designer			Passive
Developer	DLR Institute of Space Systems	SH03	Passive
Integrator			Passive
Tester			Passive
Operator	DLR German Space Operations Center (GSOC)	SH04	Active
Launch provider	Arianespace, NASA	SH05	Active
Governmental space agency	European Space Agency (ESA)	SH06	Passive
	National Aeronautics and Space Administration (NASA)	SH07	Passive
Other	Committee on Space Research (COSPAR)	SH08	Passive
	International Telecommunication Union (ITU)	SH09	Passive
	Universities and research institutes (UNI)	SH10	Passive
	Space and defence industry (IND)	SH11	Passive
	Cal Poly (CAL)	SH12	Passive

Table 3.2: Principal system stakeholders for the mission.

3.1.3. Mission requirements

The expectations of the relevant stakeholders have been analyzed by direct communication or consultation of relevant documents. From these expectations, the mission requirements have been formulated and can be seen in Table 3.3. The traceability of these requirements to their corresponding stakeholder is also shown. Note that MR-08 comprises the requirements established in the CubeSat Design Specification (CDS) [18], defined by Cal Poly. These requirements are standard guidelines for preliminary design purposes and are written conservatively to allow the best chances of compatibility with any launch vehicle.

ID	Stakeholder	Statement
MR-01	SH01	The mission shall consist of a space segment or spacecraft (SC), a ground segment (GS) and a launch segment (LS).
MR-02	SH01	The mission shall cost less than 10M€.
MR-03	SH01	The mission shall be ready to launch in less than 4 years.
MR-04	SH01	The launch of the SC shall nominally occur by 2028.
MR-05	SH01	The system shall be developed, integrated and tested by DLR Institute of Space Systems.
MR-06	SH01	The system shall be operated from the GSOC.
MR-07	SH03	The mission lifetime shall be no more than 2 years including the Earth-Mars transfer.
MR-08	SH03	The SC shall implement the CubeSat form factor as established in the CDS.
MR-09	SH03	The SC shall be implemented following a 12U CubeSat configuration.
MR-10	SH12	The SC shall weigh less than 24 kg.
MR-11	SH02	The mission analysis shall be performed using the TU Delft Astrodynamics Toolkit.
MR-12	SH03	The SC shall be sized for the most demanding mechanical, thermal and electromagnetic mission scenario.
MR-13	SH03	The SC shall be launched into an Earth escape trajectory.
MR-14	SH03	The SC shall travel independently from Earth to a Mars orbit.
MR-15	SH03	The SC shall gather data on Mars' atmosphere.
MR-16	SH03	The SC shall collect information about Mars' gravitational field.
MR-17	SH03	The SC shall be able to perform observational analysis of Mars.
MR-18	SH03	The SC shall be able to establish communication with Earth during all mission phases.
MR-19	SH03	The SC shall be able to control its state so as to enable all mission phases.
MR-20	SH03	The SC shall be designed using the available DLR in-house technology.
MR-21	SH03	The SC shall use COTS components for the needed subsystems.
MR-22	SH03	Only technologies at a minimum of TRL 5 shall be implemented in the mission design.
MR-23	SH04	The GS shall be able to provide reliable communication, command, and control of the SC.
MR-24	SH04	The GS shall be able to handle the data generated by the SC.
MR-25	SH04	The GS shall be able to provide orbit and attitude determination and prediction services for the SC.
MR-26	SH05	The system shall undergo testing as defined by the launch provider.
MR-27	SH06	The mission shall implement Telemetry and Telecommand procedures as established by the applicable ECSS standards.
MR-28	SH07	The mission shall follow NASA's General Environment Verification Standard.
MR-29	SH08	The SC shall comply with the COSPAR Planetary Protection policies.

Table 3.3 continued from previous page

ID	Stakeholder	Statement
MR-30	SH09	The mission shall obtain and provide documentation of proper licenses for use of radio frequencies.
MR-31	SH10	The scientific data gathered by the system shall be made publicly available to promote research.

Table 3.3: Complete list of mission requirements with their respective ID and stakeholder.

3.2. Concept of operations

An effective approach for validating the mission requirements mentioned earlier is to create a Concept of Operations. This ConOps describes the overall top-level concept of how the system will satisfy stakeholder expectations. This will be done using a system context diagram and mission timeline.

3.2.1. System context

The first step in the generation of a ConOps is the analysis of the system environment. To do that, a system context diagram has been created which can be seen in Figure 3.1. The diagram illustrates the primary system components, its external actors, and the interactions between them.

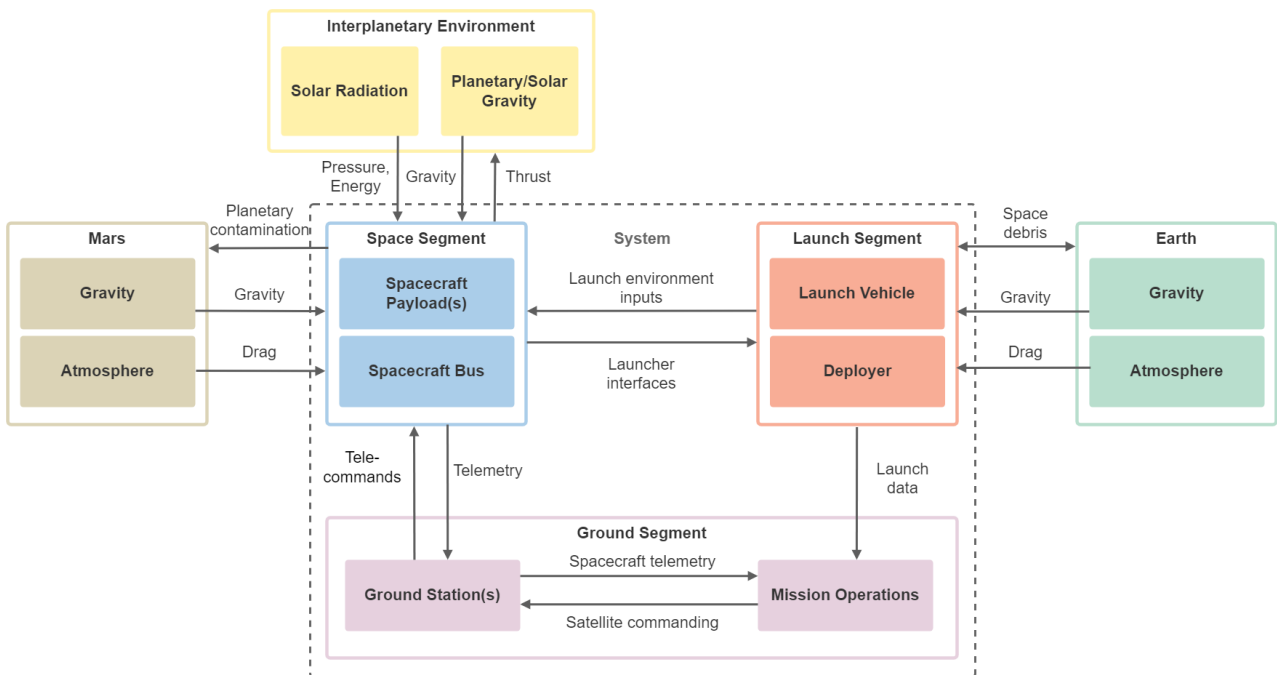


Figure 3.1: System context diagram for the mission.

The system is divided into three segments that are directly linked with each other: the space segment, the ground segment, and the launch segment. The space segment, or spacecraft, will be the cornerstone of the system that will travel to Mars and gather data once in orbit around the planet.

To do so, it will use its payload, which will be enabled by the spacecraft bus. The bus will take care of the power generation, communications, and other general tasks. The SC will communicate with Earth through the Ground Stations. These will in turn be closely connected with the Mission Operations, which will receive all the information from the SC and send commands to operate it. To send the SC to space, a launch segment will be used. This launch segment will transport the SC into orbit and deploy it, with the associated physical strains.

Similarly, the overall system also interacts with external actors, such as the Earth, Mars, or the general Solar System environment. First of all, the launch segment will interact directly with the environment around Earth. This means that it will be affected by its atmosphere and its gravity pull. In principle, this will also expose the SC to space debris. In turn, the launch vehicle could pose a potential threat as space debris. It is assumed that the SC is launched outside of the influence of Earth's gravity and atmosphere. Therefore, the SC will mainly interact with the interplanetary space environment, and more specifically, with Mars. Its trajectory will be affected to a certain extent by the gravity of all the bodies in the Solar System, as well as by solar radiation pressure. This solar radiation will also be used for power generation. Once the SC is in orbit around Mars, it will be affected mainly by the gravity of the Red Planet and its atmosphere to a smaller degree. Consequently, the SC could present a risk of planetary contamination on Mars, so the relevant guidelines should be followed.

3.2.2. Mission timeline

In order to fulfil all the goals and objectives presented in Section 3.1, a mission timeline has been proposed which can be seen in Figure 3.2. This diagram represents the sequence of events that will enable the mission's success.

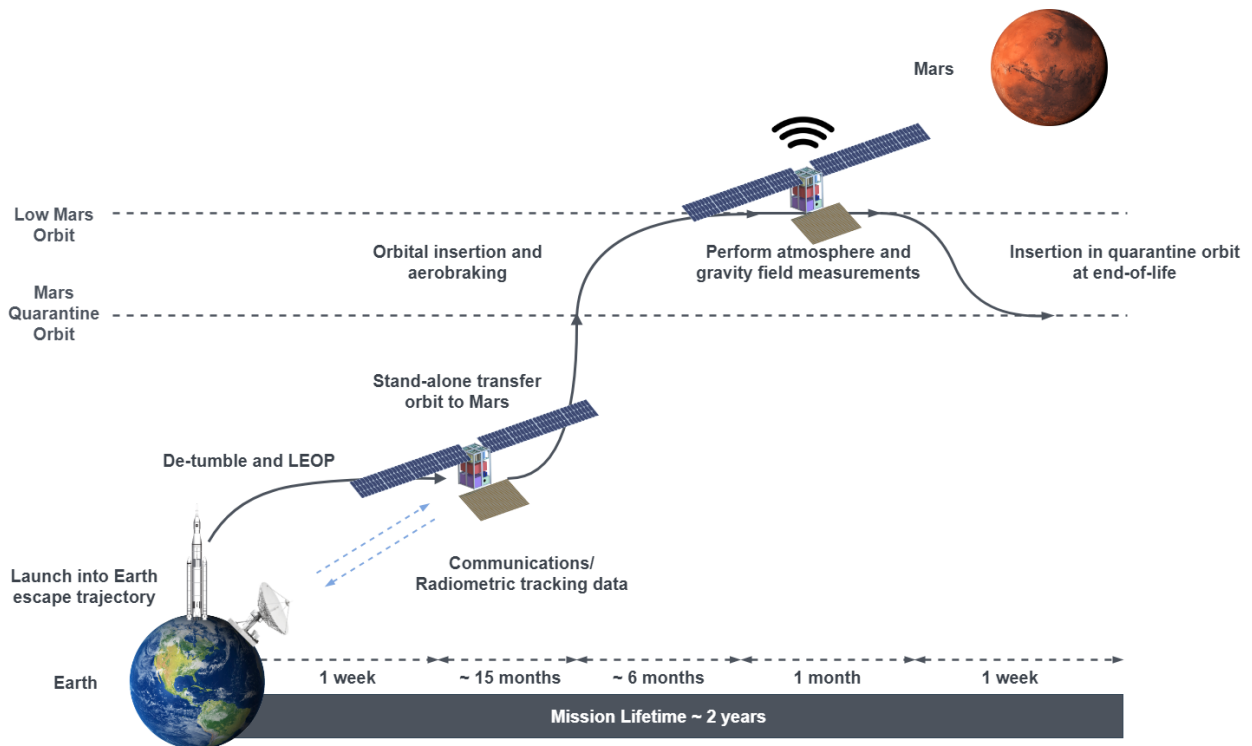


Figure 3.2: Mission timeline. Time periods are not to scale.

Once the system has been integrated and tested, the first step is to launch the SC into space. It is assumed that the launch vehicle will inject the SC into an Earth escape trajectory. This could be achieved for example through piggyback on another Mars-bound mission. Once the SC is placed on a transfer orbit to Mars, it will start the Launch and Early Orbit Phase (LEOP). During this phase, the SC will deploy its solar arrays, de-tumble and perform a first contact with the ground segment. After this, the SC will start a stand-alone interplanetary cruise to Mars, which will take approximately 15 months. During this and all subsequent phases of the mission, a communication link shall be established between the SC and the ground segment to command the system and gather radiometric data for navigation purposes. These contacts will be more frequent during the mission's most critical phases, such as the orbital insertion around Mars.

Upon arrival at Mars, the SC will perform a low-thrust orbital insertion into a highly elliptical 2-sol orbit [67]. Once in orbit around the Red Planet, the SC will perform a 6-month aerobraking phase [48] to position itself around a Primary Science Orbit (PSO) at an altitude of ~ 250 km, where the science operations will take place. An overview of the reference PSO is presented in Section 5.3. This PSO will be frozen and Sun-synchronous in order to take advantage of Mars' gravitational parameters to enable a near-circular orbit [10]. During this phase, the SC will perform measurements on the lower atmosphere and gravity field of Mars and carry out observational analysis for a nominal duration of 1 month. After this phase, another orbital change phase will be performed to raise the SC into a quarantine orbit [3]. This will allow the possibility of an extended science operations phase. Table 3.4 shows an overview of the aforementioned event sequence.

Sequence #	Event	Remarks	Time
1	Launch into Earth escape trajectory	Potentially, a piggyback on another Mars mission.	1 week
2	Early operations	Booting, deploying solar arrays and antennas, de-tumble and Sun-search	1 week
3	Stand-alone transfer orbit to Mars	Executing a low-thrust profile to arrive to Mars independently.	15 months
4	Mars orbital insertion into PSO	Performing a ballistic capture and aerobraking to the Primary Science Orbit (i.e., Low Mars Orbit).	6 months
5	Science operations	Performing measurements on the lower atmosphere and gravity field of Mars and sending the data back to Earth.	1 month
6	Orbit change for end of life	To comply with planetary protection policies, the orbit will be changed into a quarantine orbit.	1 week
7	End of life	Shutting down the spacecraft.	1 week

Table 3.4: Event sequence for the mission.

3.3. System requirements

Once the ConOps for the mission has been generated, the needed capabilities and characteristics can be translated into system requirements. These system requirements provide a technical specification to the mission requirements given in Section 3.1. At this stage of the mission design, there are many uncertainties that make it difficult to propose quantifiable system requirements. There-

fore, there is some overlap between the mission and the system requirements. Table 3.5 shows the system requirements for the mission and their specific ID. These system requirements together with their traceability and compliance with the system solution presented in Chapter 4 can be found in Appendix B.

ID	Statement
SR-SYS-01	The system shall consist of a space segment or spacecraft, a ground segment and a launch segment.
SR-SYS-02	The mission cost shall not exceed 10M€.
SR-SYS-03	The system shall be ready for launch in less than 4 years.
SR-SYS-04	The system shall be operational for a maximum of 2 years.
SR-SYS-05	The SC shall be implemented using the CubeSat standard as established in the CDS.
SR-SYS-06	The SC volume shall not exceed the configuration of a 12U CubeSat as established in the CDS.
SR-SYS-07	The total dry mass of the SC shall not be greater than 20 kg.
SR-SYS-08	The total wet mass of the SC shall not be greater than 24 kg.
SR-SYS-09	The SC shall be launched into a parabolic Earth escape trajectory.
SR-SYS-10	The SC shall perform a stand-alone Earth-Mars transfer in less than 15 months.
SR-SYS-11	The SC shall achieve autonomous orbital insertion into a Mars 2-sol orbit.
SR-SYS-12	The SC shall reach its PSO through a 6-month aerobraking phase.
SR-SYS-13	The SC shall nominally operate at a Mars frozen PSO with an altitude of 250 km.
SR-SYS-14	The SC shall maintain itself in its PSO for at least 1 month.
SR-SYS-15	The SC shall measure water, CO ₂ and dust distribution in Mars' lower atmosphere.
SR-SYS-16	The SC shall perform measurements of Mars' gravity field.
SR-SYS-17	The SC shall be able to take images in the visible part of the spectrum.
SR-SYS-18	The SC shall accommodate the science payloads and enable fulfilling all primary science measurements.
SR-SYS-19	The SC shall be able to process all the data gathered by the science payloads and bus.
SR-SYS-20	The SC shall be able to provide the required power to enable all operational phases.
SR-SYS-21	The SC shall be able to provide enough Delta-V to enable all phases of the mission.
SR-SYS-22	The SC shall be able to communicate with the GS without deployable components during LEOP.
SR-SYS-23	The system shall be able to establish long-range communication with Earth up to a distance of 1.5 AU.
SR-SYS-24	The system shall implement Telemetry and Telecommand procedures as established by the applicable ECSS standards.
SR-SYS-25	The system shall obtain and provide documentation of proper licenses for use of radio frequencies.
SR-SYS-26	The GS shall provide uninterrupted view of the spacecraft.
SR-SYS-27	The SC shall be able to maintain all subsystems within operational temperatures during all mission phases.
SR-SYS-28	The SC shall be able to provide attitude estimation and control that enable all operational phases.

Table 3.5 continued from previous page

ID	Statement
SR-SYS-29	The SC shall be able to provide state estimation and control that enable all operational phases.
SR-SYS-30	The SC shall implement the different operational modes established in the ConOps.
SR-SYS-31	The SC shall support autonomous operations according to a mission timeline uploaded from ground.
SR-SYS-32	Random vibration testing shall be performed to the levels and duration as defined by the launch provider.
SR-SYS-33	Thermal vacuum bakeout shall be performed to ensure proper outgassing of components.
SR-SYS-34	The thermal test specification will be defined by the launch provider.
SR-SYS-35	Visual inspection of the SC and measurement of critical areas will be performed as defined by the launch provider.

Table 3.5: Complete list of system requirements with their respective requirement ID.

3.4. System architecture

The aforementioned system requirements have been used to analyze the functions that the system has to perform. Subsequently, these functions are associated with specific subsystems and components.

3.4.1. Functional decomposition

First, the necessary functions of the system have been analyzed following the mission timeline presented in Section 3.2. To do so, a set of Functional Flow Block Diagrams (FFBD) has been created. Figure 3.3 shows the top-level functions of the mission, reflecting the event sequence presented in Table 3.4.

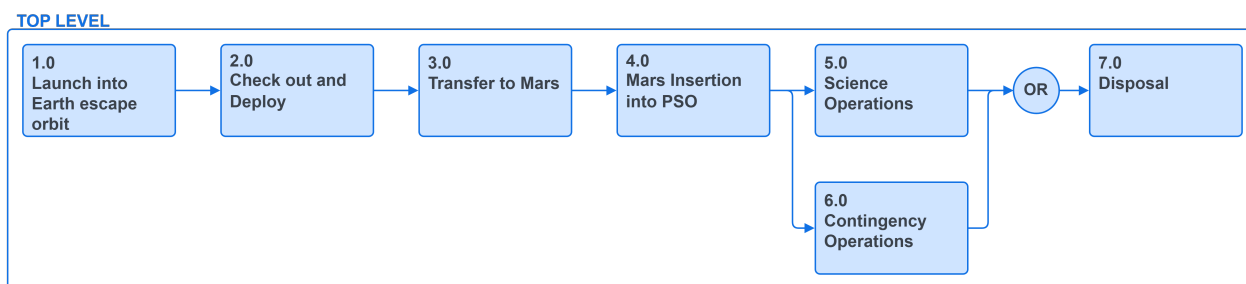


Figure 3.3: Top-level FFBD.

This diagram can be extended by analyzing the different steps on a lower level. For example, Figure 3.4 shows the various functions performed during LEO. These include booting the system, deploying the solar arrays and first contact with the ground segment, among other tasks. This functional flow has been adapted from the one designed for MarCO's LEO [39].

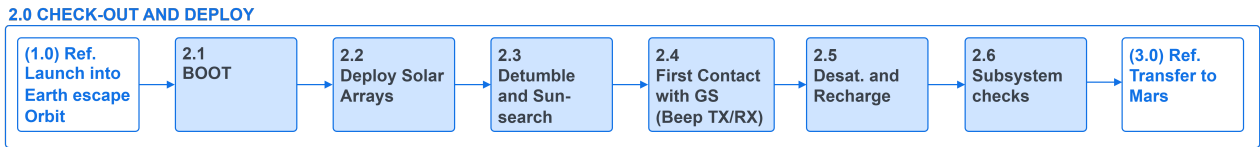


Figure 3.4: LEOP FFBD.

The subsequent steps of the mission follow a similar functional pattern. To demonstrate it, Figure 3.5 shows the functional diagram for the Earth-Mars transfer phase. As can be seen, the same activities are iterated (represented by the symbol ‘IT’) until arrival at Mars’ Sphere Of Influence (SOI). In these iterations, two activities are performed in parallel: the bus activities and either communications with Earth or trajectory control. The trajectory control activity comprises the use of propulsion to change the state of the spacecraft to follow a certain orbital trajectory. Since both communications with Earth and controlling the trajectory are quite power-demanding tasks, they have to be performed at separate times. The bus activities shown in Figure 3.6 include tasks like providing electrical power, performing attitude stabilization, providing thermal control or acquiring subsystem status data.

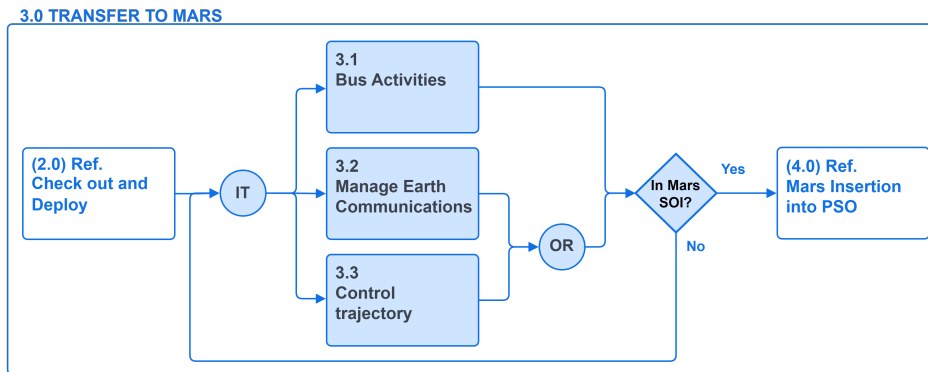


Figure 3.5: Mars transfer FFBD.

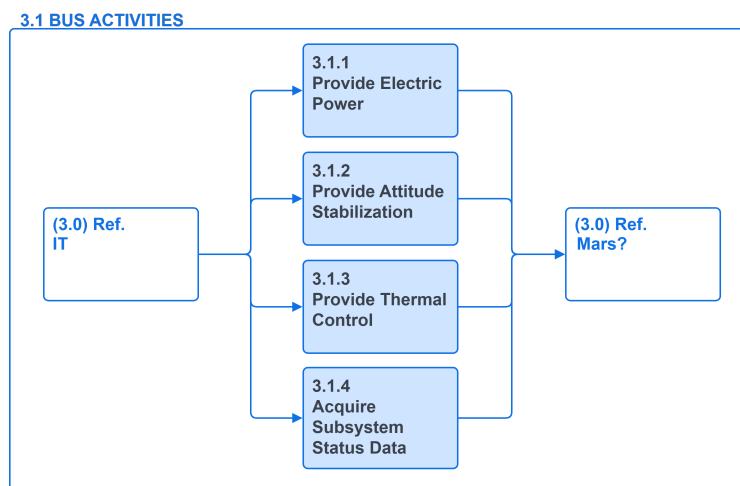


Figure 3.6: Bus activities FFBD.

In the case of the insertion into PSO, the functions are analogous to those in the Mars transfer. This also applies to the disposal phase, since the spacecraft will first thrust itself into a quarantine orbit and then shut down, as proposed in Table 3.4. The science operations phase has similar functions as can be seen in Figure 3.7. However, in parallel to the bus activities, the spacecraft will manage the communications with Earth, gather payload data and perform orbital maintenance until end-of-life. Once more, these activities are conducted separately due to their significant power requirements.

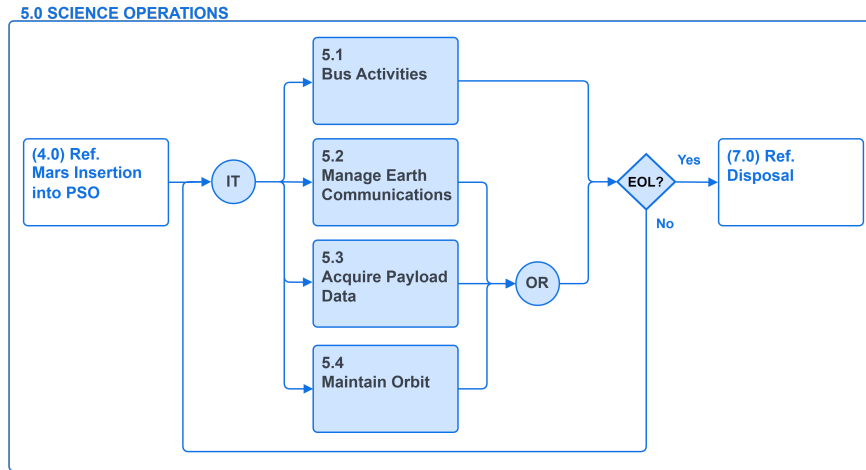


Figure 3.7: Science Operations FFBD.

3.4.2. Physical decomposition

Using the previous FFDBs, the main functions and sub-functions for the system have been identified. These sub-functions can be associated with a certain physical component, which can be grouped into sub-systems. Tables 3.6 and 3.7 show these associations for the ground segment and the space segment, respectively. The DLR in-house technologies are shown in the ‘Components’ column.

Function	Sub-function	Component	Subsystem
Tracking	Perform range measurements	Antennae	Ground Station (GS)
	Perform Doppler measurements	Antennae	
	Perform Delta-DOR measurements	Antennae	
Communicate with SC	Receive TM	Antennae	Ground Station (GS)
	Demodulate and decode TM	Ground transceiver	
	Encode and modulate TC	Ground transceiver	
	Send TC	Antennae	
Manage operations	Plan schedules	Operators	Operations (OPS)
	Solve S/C issues	Operators	
	Perform state estimation	Operators	
	Distribute science data	Operators	

Table 3.6: Functional decomposition and associated subsystems for the ground segment.

Function	Sub-function	Component	Subsystem
Perform science	Measure Mars' gravity field	Gravity payload	Payload (PL)
	Gather data on Mars' atmosphere	Atmosphere payload	
	Capture images of Mars	Imaging payload	
Provide power	Gather energy	Solar panels	Electrical Power System (EPS)
	Store energy	Batteries	
	Monitor energy levels	PCDU	
	Distribute energy	PCDU	
Communicate with GS	Receive TC	Antennae	Telemetry, Tracking and Command (TT&C)
	Demodulate and decode TC	GSDR	
	Encode and modulate TM	GSDR	
	Send TM	Antennae	
Control SC dynamics	Measure attitude	Star tracker, Sun sensor	Attitude Determination and Control (ADCS)
	Control attitude	GNC software	
	Change attitude	Reaction wheels, thruster	
	Measure state	Visual sensor, accelerometer	Guidance, Navigation and Control (GNC)
	Estimate state	GNC software	
	Control state	GNC software	
	Actuate mechanisms	ScOSA	Mechanisms (MECH)
Manage thrust	Store propellant	Propellant tank	Propulsion (PROP)
	Generate thrust	Thrusters	
	Control thrust	GNC software	
Control temperature	Generate heat	Heaters	Thermal Control System (TCS)
	Dissipate heat	Radiators	
	Transport heat	Thermal harness	
	Monitor temperatures	Thermal sensors	
Handle data	Gather data	ScOSA	On-Board Computer (OBC)
	Distribute data	ScOSA	
	Perform data analysis	ScOSA	
	Store data	ScOSA	
	Generate status reports	ScOSA	
Physically support SC	Provide structural support	Structure	Structure (STR)
	Protect against environment	Shielding	
Provide physical interface	Interface avionics	ICA	Avionics Stack (AVI)

Table 3.7: Functional decomposition and associated subsystems for the space segment. The light green indicates the components provided by DLR.

This physical decomposition enables the creation of a physical diagram for the system, shown in Figure 3.8. In this diagram, the space, ground and launch segments are represented. The interactions among them and with the external environment are represented in yellow arrows (e.g., the loads on the space segment produced by the launch segment). The different connections between subsystems are also represented: mainly the power, data, Radio Frequency (RF) and propellant links. As can be seen, the data links connect all the subsystems in the space segment to the OBC, as this subsystem commands and manages the data from each of them. Similarly, all the subsystems are connected to the EPS, as it provides power to the entire space segment. For the sake of clarity in presentation, the ICA stack is omitted. Nonetheless, the components shown in light blue are integrated into the ICA stack. A comprehensive description of each of the subsystems is given in Chapter 4.

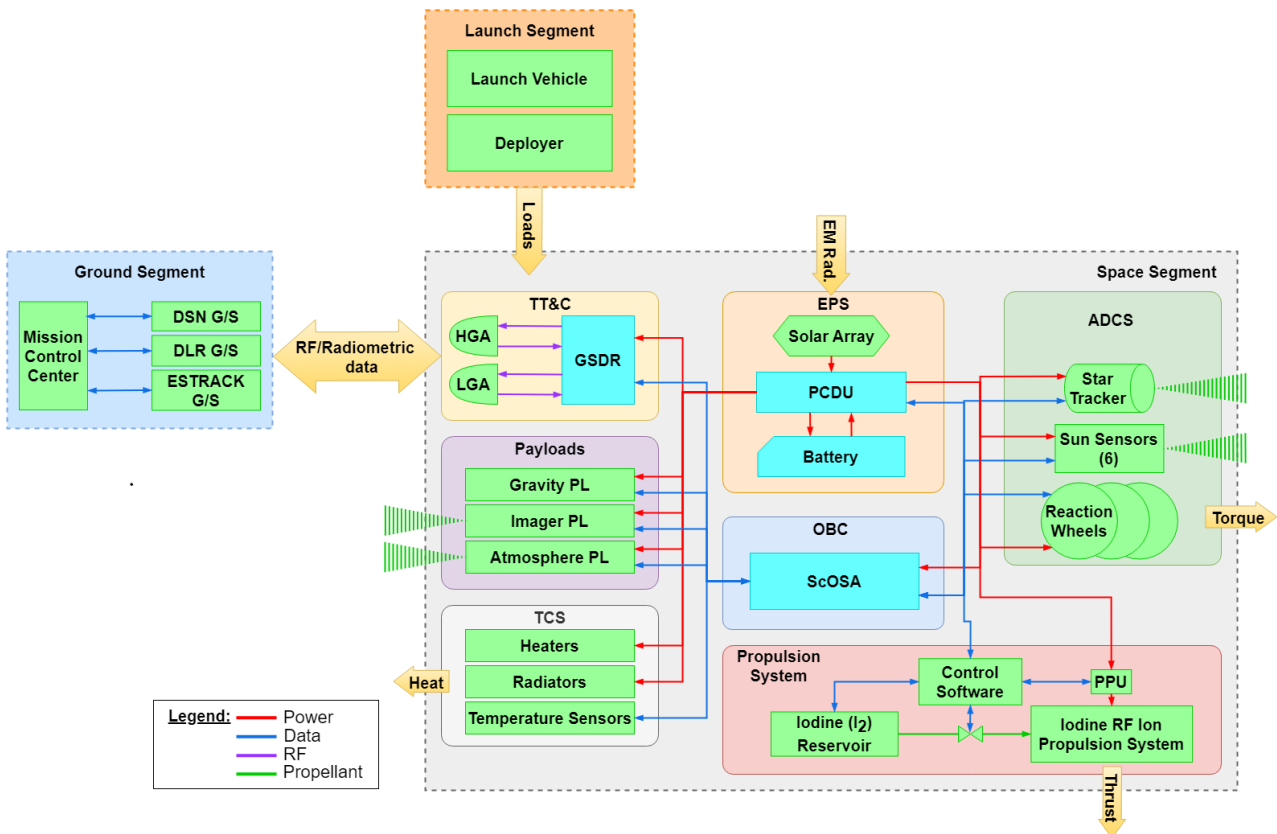


Figure 3.8: Mars CubeSat physical diagram. The light blue indicates components included in the ICA stack.

Finally, the interactions between the different subsystems are analyzed. To do so, an N-squared matrix has been created and can be seen in Figure 3.9. This matrix shows the different subsystems on its diagonal. For each of the subsystems, its associated outputs are displayed on the same row and its inputs are in the same column. The inputs and outputs to the exterior of the system are displayed in the borders of the matrix. As can be seen, all the spacecraft subsystems output loads to the Structure as it interfaces mechanically with each of them. Here one can also see that the EPS provides power to all the subsystems but the Structure, and these need an interface to receive that power. Likewise, the OBC receives data and sends commands to all the subsystems but the Structure, and these in turn provide it with their data. Here again, the Avionics Stack is omitted to enhance clarity in the representation, as it will only serve as an interface to certain components. The diagram also shows the RF link between the communications subsystem and the ground station, with its associated radiometric data (i.e., Doppler shift).

		Sunlight, EM radiation	Star distribution imagery	RF radiation, Solar system bodies imagery		Mars gravity, Mars atmosphere	RF Uplink		Solar IR, EM radiation			
	STR	Structural loads, Mechanical interface	Structural loads, Mechanical interface	Structural loads, Mechanical interface	Structural loads, Mechanical interface	Structural loads, Mechanical interface	Structural loads, Mechanical interface	Structural loads, Mechanical interface	Heat Conduction	Structural loads, Mechanical interface	Coupled launch loads, LV adapter	
	Loads, Heat, Elec ground Cond. Mech I/F	EPS	Electrical power, Power harness	Electrical power, Power harness	Electrical power, Power harness	Electrical power, Power harness	Electrical power, Power harness	Electrical power, EPS TM, Harnesses	Electrical power, Power harness	Electrical power, Power harness		
Torque	Loads, Heat, Mechanical I/F, Cond.	Electrical ground, Power harness	ADCS			Current pointing data, Data harness		ADCS data & TM, Data harness				
	Loads, Heat, Mechanical I/F, Cond.	Electrical ground, Power harness	Current Nav. Data, time	GNC		Current Nav. Data, Data harness		GNC TM (Navigation data), Data harness				
Thrust exhaust	Loads, Heat, Mechanical I/F, Cond.	Electrical ground, Power harness			PROP			Propulsion TM, Data harness				
	Loads, Heat, Mechanical I/F, Cond.	Electrical ground, Power harness		Payload data, Data harness		PL		Payload data, Data harness				
RF downlink, Doppler shift	Loads, Heat, Mechanical I/F, Cond.	Electrical ground, Power harness					TT&C	Commands, Data harness				RF TM, Doppler shift
	Loads, Heat, Elec ground Cond. Mech. I/F	EPS command Elec. ground,	ADCS commands, Data harness	GNC commands (Orbit), Data harness	Propulsion commands, Data harness	Payload commands, Data harness	Payload data, TM, Data Harness	OBC	Thermal control com., Data harness	Mechanism commands, Data harness		
Heat, EM radiation								Temp. measurements, Data harness	TCS			
	Loads, Heat, Mechanical I/F, Cond.							Mechanism TM, Data harness		MECH		
	Loads, Heat, Mechanical I/F, Cond.										Launch Vehicle	
							RF TC					G/S

Figure 3.9: Mars CubeSat N-squared matrix. The thicker border surrounds the spacecraft subsystems.

4

System design

The preceding chapter concluded with a physical breakdown of the system. This chapter delves into an examination of the space, ground, and launch segments. Within each segment, solutions that comply with the established architecture, ConOps, and system requirements are presented for their respective subsystems. The chapter wraps up with an assessment of the subsequent mission development stages and a comprehensive risk evaluation.

4.1. Space segment

The following sections provide a comprehensive analysis of each of the space segment subsystems. For each subsystem, the main requirements are stated here. These subsystem requirements flow down from the system requirements presented in Section 3.3 or are the result of a preliminary analysis of the pertinent subsystem. A complete list of these requirements and their ID, traceability and compliance with the proposed solution can be consulted in Appendix C. After that, a section is reserved for the configuration and system budgets.

4.1.1. Payloads

As explained in Section 3.1, the main scientific goals of the mission include studying Mars' lower atmosphere, mapping its gravity field, and performing observational analysis of the Red Planet. Each objective is tackled using a different payload: a 2U infrared spectrometer, a 1U gravimeter and a miniaturized imaging camera.

Payload requirements

Each of the scientific objectives of the mission flows down into different payload requirements. First, SR-SYS-15 states that the SC shall be able to measure water, CO₂ and dust distributions in the atmosphere of Mars. To do so, the payload that addresses this requirement shall operate in the absorption bands of these chemical components. A payload that operated in the wavelength range of 1-3 μm would be able to tackle most of the water-related bands as well as other chemical components such as NH₃, CO₂ [16]. On top of that, bands linked to pyroxene, olivine, iron oxides and other minerals that are present as volatiles in Mars' atmosphere could also be studied. With respect to SR-

SYS-16, the system shall perform measurements of Mars' gravity field. While gravimetry is usually performed using spacecraft tracking data, gravimetry payloads such as accelerometers can provide improved resolution in the measurements. Although miniaturized gravimeters have been used in CubeSat missions [76], it is not clear how much they can improve the resolution of the gravity field measurements. Therefore, the performance characteristics of such a gravimetry payload are To Be Determined (TBD) in a later stage of the mission design. Finally, SR-SYS-17 states that the SC shall be able to perform an observational analysis of Mars. DLR has required the capabilities of this payload to be at least comparable to the observational payload used on the MASCOT lander. Therefore, the resolution of the imager payload shall be better than 10 Mpx.

Therefore, the full list of payload requirements is:

- SR-PL-01: The atmospheric payload (PL-ATM) shall operate in the wavelength range of 1-3 μm .
- SR-PL-02: The PL-ATM shall have a spectral resolution of at least 50 nm.
- SR-PL-03: The gravity payload (PL-GRA) shall enhance the measurements of Mars' gravity field performed using tracking data.
- SR-PL-04: The imager payload (PL-IMG) shall operate in the visible spectrum.
- SR-PL-05: The PL-IMG shall take pictures with a resolution of at least 10 Mpx.

Atmospheric payload

The objective of this payload is to characterize the dynamics, thermal structure, and distributions of dust, water, and carbon dioxide in the lower atmosphere [54]. To do so, it needs to gather data on the lower atmosphere's temperature, pressure, and chemical composition. Several types of instruments can be used to perform these measurements [65], including:

- Spectrometers. These instruments measure the light absorbed or emitted by a planet's atmosphere at various wavelengths.
- Radiometers. These instruments measure the amount of radiation emitted by a planet's atmosphere at various wavelengths.
- Mass spectrometers. They analyze the chemical composition of the atmosphere of a planet by ionizing the gas molecules and measuring their mass-to-charge ratio.
- Lidars. They use laser beams to probe a planet's atmosphere, measuring the altitude and density of different layers of the atmosphere.

All of these technologies excluding Lidars have been applied to CubeSat missions. Table 4.1 shows a selection of relevant payloads that have been used in CubeSat missions to perform atmospheric research. The QB50 INMS would be an interesting option for a very low Mars orbit since it could perform in-situ measurements of its atmosphere. However, at this point in the mission design, it is not clear whether the spacecraft would be able to attain such low altitudes, so it will be discarded from the selection. The infrared (IR) spectrometers will be favoured as they operate in more interesting spectral bands for atmospheric measurements. For example, the Thoth Argus 1000 could be used to characterize certain water bands with reduced dimensions, mass and consumed power. However, it operates on a relatively narrow spectral band, which would make it unfeasible to study the concentrations of NH_3 , CO_2 , H_2S and other important volatiles.

Name	Type	Objective	Spectral band	Size [U]	Mass [kg]	Power [W]
VISION	Hyperspectral imager	Observation of the Earth's atmospheric limb during orbital solar occultation, measuring the light absorption in a certain band.	430-800 nm	1.5	0.526	3
NASA CIRAS	IR spectrometer	Measure temperature and water vapour in the lower troposphere.	4-5 μm	4	2.5	30
NASA PRE-FIRE	IR spectrometer	Provide measurements of spectral fluxes, column-water vapour, surface emissivity and broadband radiances over thermal wavelengths.	5-54 μm	3	3	4.5
NASA BIRCHES	IR spectrometer	Characterize and distinguish important volatiles (water, H_2S , NH_3 , CO_2 , CH_4 , OH, organics) and mineral bands.	1-4 μm	2	2.5	10
Thoth 1000	Argus IR spectrometer	Characterize volatiles and minerals. Measure temp and water vapour in the atmosphere. Night-imaging, temperature mapping.	1000-1700 nm	1	0.300	1
QB50 Ion/Neutral Mass Spectrometer	Mass spectrometer	Sampling of low mass ionized and neutral particles in the lower thermosphere, such as O, O_2 , NO and N_2 .	-	1	0.220	0.85

Table 4.1: Selection of relevant payloads used in CubeSat missions for remote sensing of atmospheres. [65]

From this selection, the option that provides the best spectral band performance is the BIRCHES infrared spectrometer (Figure 4.1) developed by NASA Goddard Space Flight Center [16]. This is a miniaturized version of the OVIRS infrared spectrometer used in OSIRIS-Rex. BIRCHES is a 2U, 2.5 kg, 12-25 W point spectrometer that operates in the 1 to 4-micron wavelengths. This allows the instrument to characterise and distinguish important volatiles (water, H_2S , NH_3 , CO_2 , CH_4 , OH, organics) and mineral bands. BIRCHES is the primary payload of the Lunar IceCube launched in the Artemis 1 mission. Its main scientific goal is to study the composition and distribution of volatiles in the lunar environment. As this payload was designed for a mission outside Earth's orbit, it features its own cryocooler and radiation-tolerant hardware. Once it is operationally validated, its TRL will increase, making it an appealing option for an interplanetary CubeSat to Mars. All in all, the BIRCHES IR spectrometer complies with the specified requirements: it operates in the spectral band from 1-4 μm (the required spectral band is 1-3 μm) and it provides a spectral resolution of 10 nm (the required spectral resolution is 50 nm). Therefore, it will be taken as the reference atmospheric payload for the mission.

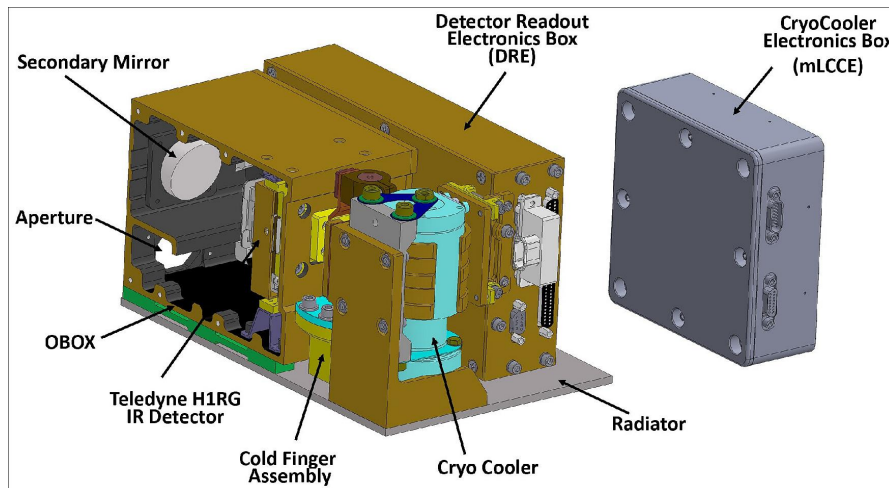


Figure 4.1: BIRCHES instrument and its main components, including a cryocooler. [16]

Gravity payload

This payload is to fulfil the objective of mapping Mars' gravity field. This has been done in the past by using tracking data from Mars orbiters or landers, such as the Mars Reconnaissance Orbiter [42]. This technique uses range and Doppler measurements to measure the changes in the spacecraft's state along its orbit caused by the variations in the planet's gravity field. Another approach could involve the use of a gravimeter. Miniaturized gravimeters have been demonstrated on CubeSat missions, such as the 1U gravimeter onboard the Star of Aoxiang, developed by Northwestern Polytechnical University [76].

These miniaturized gravimeters measure the gravitational acceleration of a planet by detecting changes in the position of a test mass relative to the spacecraft. An interesting concept is that of the Drag-Free CubeSat [77]. This mission proposal studied the feasibility of a Gravitational Reference Sensor (GRS) that could fit in a 1U space, as can be seen in Figure 4.2. The CubeSat was designed to shield a test mass from external non-gravitational forces and to minimize the effect of internally generated disturbances. The position of this test mass is measured by the GRS using an LED-based sensor system. Subsequently, this data can be used to infer the gravitational acceleration along the trajectory of the spacecraft, which can be mapped around the planet on which it orbits.

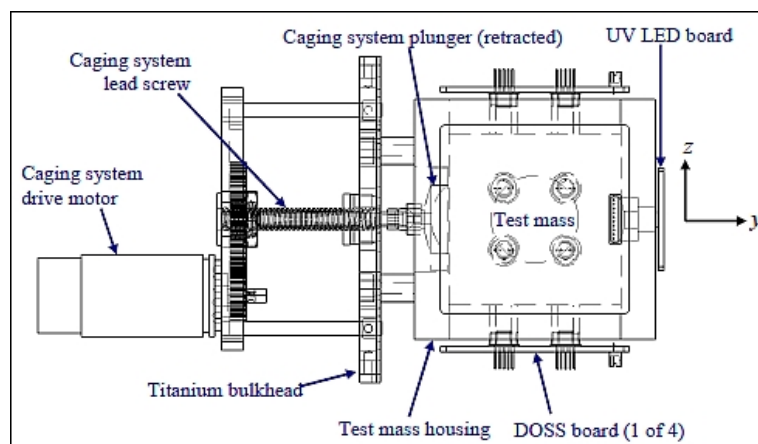


Figure 4.2: Schematic view of the 1U GRS (right) with its caging mechanism (left). [77]

Thus, a potential miniaturized 1U gravimeter developed by DLR will be used as the reference gravity payload for the mission. The readings of the test mass state will be used in combination with the spacecraft's radiometric data to study Mars' gravity field. The simplicity of its mechanisms and electronics offers reduced risk in a key aspect of the mission's science operations.

Imaging payload

A camera will be used to take images of Mars. These images can have a variety of scientific applications, such as surface feature recognition, dust storm identification, etc. On top of that, images of celestial bodies can be used as input into the navigation algorithms. While many COTS alternatives exist for space cameras, most options provide better performance than needed [33]. This usually comes at the cost of higher mass and volume, which would not be feasible given the constraints of the CubeSat form factor. Therefore, a simpler alternative is preferred.

The DLR Institute of Space Systems has recommended using the 3D Plus 12 Megapixel CMOS Space Camera. This camera is to be used in the Mars Moons eXploration (MMX) rover, designed and integrated by DLR in collaboration with the Centre National d'Études Spatiales (CNES). This will greatly simplify the integration process and reduce uncertainties in the design process. This camera, shown in Figure 4.3, provides sufficient performance in a reduced volume of $40 \times 40 \times 39 \text{ mm}^3$, a mass of 120 g and a power consumption of 5 W. It is also highly radiation tolerant, with a TID of up to 40 krad. The camera complies with the specified requirements in terms of resolution and spectral range, so it will be taken as the reference imaging payload for the mission.

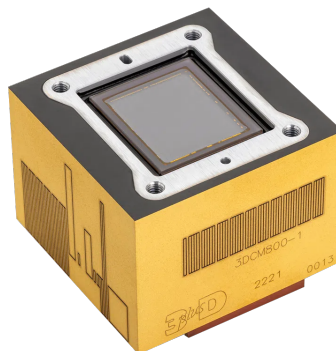


Figure 4.3: 3D Plus 12 Megapixel CMOS Camera as used in the MMX rover. [1]

4.1.2. Propulsion

Estimation of propulsion capabilities

For this to be a completely stand-alone mission, the spacecraft needs to perform an independent Earth-Mars transfer, achieve orbital insertion, and position itself into the PSO. The amount of Delta-V needed for such a mission using the CubeSat form factor has been proven unfeasible using chemical propulsion alone [11]. Combined chemical-electric propulsion systems have been studied for such a mission with promising results [51]. However, this results in a complex system that would require excessive development effort and would have consequences in terms of mass, volume, and cost. Therefore, a purely electric propulsion system is preferred.

In order to find a first approximation for the required amount of Delta-V and the time of flight for the mission, the study conducted by Ryan C. Woolley and Nathan J. Barba is used [73]. In this analysis, a variety of reference mission scenarios are presented given different starting and stopping points between Earth and Mars. For each of the combinations, the Delta-V and time of flight for a solar electric propulsion transfer can be retrieved using lookup tables. As explained in the ConOps (Section 3.2), the Earth-Mars transfer starts at Earth on a Mars-bound launch vehicle with a $C_3 = 15 \text{ km}^2/\text{s}^2$. Mars orbital insertion is then performed into a highly elliptical 2-sol orbit, with a peri- and apoapsis of 300 and 57826 km, respectively. Given the fact that the mission is in a preliminary stage, the ‘high’ values will be taken. Therefore, the total Delta-V for the transfer can be approximated to be 4.8 km/s. Furthermore, the most likely time of flight for the transfer is 15 months.

Once in a 2-sol orbit around Mars, the spacecraft will lower itself by aerobraking to a low Mars orbit (i.e., with an altitude of 300 km), so the use of propellant is considered negligible. This will increase the time of flight by at least 6 months, using the Mars Reconnaissance Orbiter mission as a reference [48]. At end-of-life, the spacecraft will be positioned into a quarantine orbit. As the look-up table suggests, the Delta-V needed to raise the spacecraft from a low Mars orbit to a Phobos orbit (i.e., 5000 km of altitude) is 3.3 km/s. However, a quarantine orbit could be achieved by raising the altitude to 600 km [3]. Therefore, 10% of that Delta-V value is considered more than sufficient to position the spacecraft into an appropriate graveyard orbit.

Therefore, the initial estimate for the needed propulsion parameters is as follows:

- Total Delta-V: 5.1 km/s
- Total time of flight (from Earth to PSO): 21 months

Propulsion requirements

As explained in the previous section, the propulsion system shall provide a total Delta-V of at least 5.1 km/s. On top of that, low-thrust trajectories to Mars for CubeSats are not feasible using chemical propulsion only [11]. Therefore, the specific impulse of the system shall be in the order of 1000 s, which can only be achieved by electric or combined propulsion systems. The propulsion system will also have to operate in a close loop with the ADCS. Therefore, it shall be compatible with the attitude modes presented in Subsection 4.1.3. Moreover, ADCS imposes the need for reaction wheel desaturation, which can be performed using the propulsion system.

Therefore, the full list of propulsion requirements is:

- SR-PROP-01: The propulsion system shall provide at least 5.1 km/s of Delta-V.
- SR-PROP-02: The propulsion system shall have a specific impulse performance of at least 1000 s.
- SR-PROP-03: The propulsion system shall be compatible with any operational SC attitude.
- SR-PROP-04: The propulsion system shall perform reaction wheel desaturation.

COTS selection

Using NASA’s 2022 State-of-the-Art of Small Spacecraft Technology Report [33], the most promising commercial electric propulsion systems have been identified. They are shown in the following Table 4.2.

Name	Type	Propellant	Max. thrust (mN)	Specific impulse (s)	Mass (kg)	Envelope (U)	Power (W)
Busek BIT-3	Gridded-Ion	Iodine	1.25	2100	2.9	1.6	75
Empulsion Micro R3	IFM Electro spray	Indium	1	3500	3.9	2.2	45
Thrustme NPT30-I2-1.5U	Gridded-Ion	Iodine	1.1	2400	1.7	1.5	65
Miles Space M1.4	Ambipolar	Water	2.8	1340	0.8	1	11.5

Table 4.2: Overview of COTS electric propulsion systems. [33]

As can be seen, these electric propulsion systems offer different advantages. The Miles Space M1.4 offers the best performance in terms of maximum thrust but also relatively low specific impulse. This would most likely result in unfeasible quantities of propellant being needed for an Earth-Mars transfer. The remaining propulsion systems provide comparable capabilities. However, from a heritage point of view, the Busek BIT-3 is the most interesting alternative. This is due to the utilization of the BIT-3 in the Lunar IceCube and LunaH-Map CubeSats, both of which were launched as part of the Artemis 1 mission [69]. In principle, this propulsion system will allow CubeSats to carry out a low-thrust trajectory to lunar orbit. The BIT-3 (Figure 4.4a) is an RF ion thruster that features a two-axis thruster gimbal capable of $\pm 10^\circ$ slew. This characteristic allows for reaction wheel desaturation. The system can be throttled depending on the input power as can be seen in Figure 4.4b. At 80 W of input power, the system can operate at 1.25 mN of thrust and 2150 s of specific impulse. Since the BIT-3 complies with the specified requirements and provides the best overall characteristics compared to other electric propulsion systems, it will be used as the reference propulsion system for the mission.

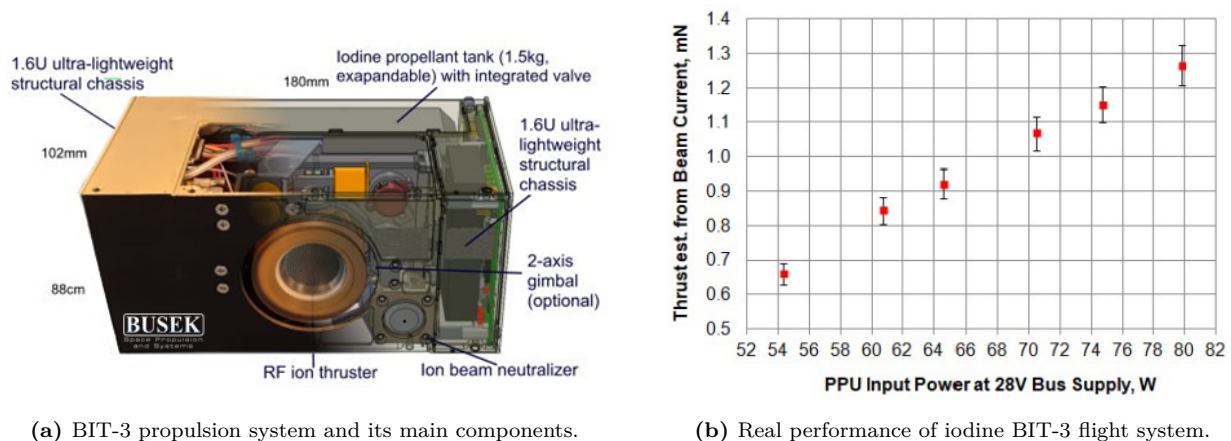


Figure 4.4: BIT-3 RF Ion Thruster. [6]

Iodine is used as a propellant as it has many advantages over other legacy electric propulsion propellants such as xenon. These include easier handling, higher launch safety, and lower cost. Most importantly, it has twice as much storage density as xenon. In that regard, the baseline system fea-

tures a 1.5 kg propellant tank, which allows for up to 2.4 km/s of Delta-V in a 14 kg CubeSat [6]. As discussed in the previous section, this will not be sufficient to achieve the proposed goals. However, Busek affirms the possibility of an expanded propellant tank. Therefore, the required amount of propellant will be calculated. Using the standard rocket equation for a 14-kg CubeSat, one can find the effective exhaust velocity for the system:

$$\Delta V = v_{eq} \cdot \ln\left(\frac{m_0}{m_f}\right) \rightarrow v_{eq} = \frac{\Delta V}{\ln\left(\frac{m_0}{m_f}\right)} = \frac{2.4}{\ln\left(\frac{14}{12.5}\right)} = 21.2 \text{ km/s} \quad (4.1)$$

And now, using the same equivalent exit velocity for a 20 kg CubeSat and the required 5.1 km/s of Delta-V, the required propellant mass can be calculated:

$$m_p = m_0 - m_f = m_0 - \frac{m_0}{e^{\Delta V/v_{eq}}} = 20 - \frac{20}{e^{5.1/21.2}} = 4.3 \text{ kg} \quad (4.2)$$

The volume of the propellant tank on the baseline system is assumed to be a third of the total volume of the system. Therefore, the total propulsion system volume with the expanded propellant tank is 2.6U. As can be seen in Figure 4.4a, the propellant tank is located at the back of the system. Therefore, the most straightforward way to expand the system is to increase its longitude towards the back of the system while keeping the front-face dimensions constant. This corresponds to the following dimensions for the expanded tank propulsion system: 88 x 180 x 165 mm.

4.1.3. Attitude determination and control

ADCS modes

The ADCS is responsible for determining the spacecraft's attitude using sensors and controlling it through sensors. First of all, the different attitude modes needed to fulfil the ConOps have been defined. They can be seen in Table 4.3.

Control Mode	Code	Description
Standby Mode	SBM	Determination of attitude and stabilization during commissioning or after a system failure.
Safe Mode	SM	Used in emergencies if nominal mode fails or is disabled. It will use less power and/or fewer components, but it shall enable Sun acquisition and precise antenna pointing.
Normal Mode	NM	Nominal mode for communications with the Ground Station and science operations.
Orbit Control Mode	OCM	Precise attitude determination and control in the loop with propulsion system during the transfer to Mars, insertion around Mars, orbit lowering to PSO, orbit maintenance, and momentum unloading.

Table 4.3: Overview of the ADCS modes for the system.

A state diagram for the different modes is presented in Figure 4.5, and can be applied to any stage of the mission. As shown, after powering up or a system failure, the spacecraft goes into SBM.

This allows for the initial determination of attitude and stabilization. Then, SM should be entered automatically. In this mode, Sun acquisition will be performed in order to provide power to the spacecraft. Then, the spacecraft will point its antennas to the Ground Station and wait for commands. To access the NM, the Ground Station needs to send a certain set of telecommands (TC), as is the standard procedure in spacecraft operations. Once in NM, different actions can be performed:

- Orienting the spacecraft’s instrument toward Mars nadir for science operations.
- Orienting toward Mars anti-nadir for instrument calibration.
- Pointing of antenna systems toward Earth for communications.
- Keeping solar arrays pointed toward the Sun vector.
- Orienting spacecraft to optimise thermal management.
- Avoiding “keep-out zones” for the star tracker or PL.

Finally, the OCM will be used during orbital manoeuvres. This mode will be entered and exited through an automated procedure that implements the thrust profile generated by the GNC subsystem.

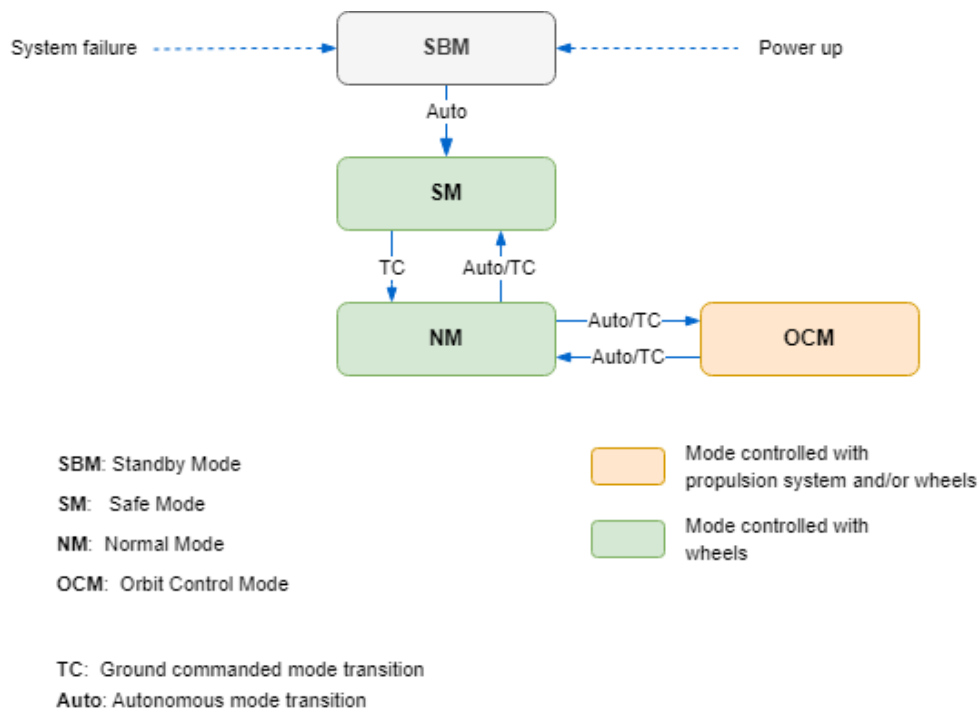


Figure 4.5: State diagram showing the connection between the different ADCS modes.

Disturbance environment

The disturbance environment must be analyzed in order to correctly size the ADCS subsystem. To do so, two cases have been studied: the disturbances just after launch (i.e., at an altitude of 3500 km above Earth) and at Mars PSO (i.e., at an altitude of 250 km above Mars). The main disturbances that have been considered are those coming from solar radiation pressure, atmospheric drag, magnetic field and gravity field. The equations for these torques have been adopted from [72] and can be seen

in Equations 4.6-4.3. A reference area for the satellite of 0.6 m^2 is used, taking into consideration the solar array configuration explained in Subsection 4.1.8. Table 4.4 shows the calculated disturbances and the total momentum storage needed for each case.

$$T_s = \frac{\Phi}{c} A_s (1 + q) (cp_s - cm) \cos \phi \quad (4.3)$$

where T_s is the solar radiation pressure torque, Φ is the solar constant adjusted for actual distance from the Sun (average value: 1366 W/m^2 at 1 AU), c is the speed of light ($3 \times 10^8 \text{ m/s}$), A_s is the sunlit surface area in m^2 , q is the unitless reflectance factor (ranging from 0 for perfect absorption to 1 for perfect reflection), ϕ is the angle of incidence of the Sun, and cp_s and cm are the centers of solar radiation pressure and mass in m.

$$T_a = \frac{1}{2} \rho C_d A_d V^2 (cp_a - cm) \quad (4.4)$$

where T_a is the atmospheric drag torque, ρ is the atmospheric density in kg/m^3 , C_d is the drag coefficient (usually between 2.0 and 2.5 for spacecraft), A_d is the drag reference area in m^2 , V is the spacecraft's orbital velocity in m/s , and cp_a and cm are the centers of aerodynamic pressure and mass in m.

$$T_m = DB = D \left(\frac{M}{R^3} \lambda \right) \quad (4.5)$$

where T_m is the magnetic torque, D is the spacecraft's residual pole moment in Am^2 , B is the magnetic strength in tesla, M is the magnetic moment of Earth or Mars multiplied by the magnetic constant ($M_E = 7.8 \times 10^{15} \text{ tesla m}^3$ and $M_M = 1.35 \times 10^{11} \text{ tesla m}^3$, respectively), R is the distance between the spacecraft and the center of the celestial body in m and λ is the unitless function of the magnetic latitude taken the worst-case scenario of 2 at the magnetic poles.

$$T_g = \frac{3\mu}{2R^3} |I_z - I_y| \sin(2\psi) \quad (4.6)$$

where T_g is the gravity-gradient torque about the X principal axis, μ is the Earth's gravitational constant ($3.986 \times 10^{14} \text{ m}^3/\text{s}^2$), R is the distance between the center of the celestial body in m, ψ is the angle between the local vertical and the X principal axis, and I_y and I_z are the moments of inertia about the Y and Z axis in kg m^2 .

Disturbance	Earth escape	Mars PSO
Solar Radiation Pressure [N · m]	$4.37 \cdot 10^{-7}$	$1.89 \cdot 10^{-7}$
Atmospheric Drag [N · m]	$6.15 \cdot 10^{-11}$	$2.35 \cdot 10^{-7}$
Magnetic Field [N · m]	$8.09 \cdot 10^{-6}$	$2.80 \cdot 10^{-8}$
Gravity Gradient [N · m]	$-2.90 \cdot 10^{-8}$	$-6.22 \cdot 10^{-8}$
Needed momentum storage [N · m · s]	$1.53 \cdot 10^{-2}$	$2.60 \cdot 10^{-3}$

Table 4.4: Overview of the main disturbances at Earth escape and Mars PSO.

The total momentum storage has been calculated by adding the absolute values of the perturbations for each case and integrating them for a certain amount of time. For Earth escape, 30 minutes have been assumed, and for Mars PSO, a full orbit around the Red Planet assuming a circular orbit at an altitude of 250 km. As can be seen, the limiting case is Earth's escape with a total needed momentum storage in the order of 10^{-2} Nms. In this case, the perturbation with the highest contribution is that of Earth's magnetic field.

ADCS requirements

As explained in the ConOps, this mission requires a wide range of spacecraft attitudes during manoeuvres or science operations. Therefore, 3-axis stabilization is needed. On top of that, the analysis performed in the previous section provides the requirements for needed torque capabilities and momentum storage for the ADCS: 10^{-5} Nm and 16 mNms, respectively. The payload drives the attitude knowledge and control requirements for the ADCS to 0.01 deg and 0.1 deg, respectively [16]. Moreover, the ADCS must comply with the attitude modes established in the previous sections.

Therefore, the full list of ADCS requirements is:

- SR-ADCS-01: The ADCS shall provide 3-axis stabilization.
- SR-ADCS-02: The ADCS shall provide a torque of at least 10^{-5} Nm.
- RS-ADCS-03: The ADCS shall provide momentum storage of at least 16 mNms.
- SR-ADCS-04: The ADCS shall achieve attitude knowledge better than 0.01 deg (1σ).
- SR-ADCS-05: The ADCS shall achieve attitude control better than 0.1 deg (1σ).
- SR-ADCS-06: The ADCS shall implement all the modes established above.

COTS selection

As established in the ConOps, the spacecraft has the need for a high number of pointing options: transfer orbit manoeuvres, orbit insertion, PL pointing, antenna pointing, etc. Therefore, the ADCS solution shall provide 3-axis stabilization. On top of that, the selected payload introduces high attitude accuracy requirements (i.e., lower than 0.1 deg). To reach that accuracy knowledge, both star trackers and sun sensors will be used. The star trackers will be used to determine the precise absolute attitude. On the other hand, the sun sensors will be used to acquire initial attitude information relative to the Sun and general coarse attitude data. In terms of actuators, a set of 3 or 4 reaction wheels can provide 3-axis stabilization within the required accuracy. The propulsion system shall be used complementarily to the ADCS system in order to de-saturate the reaction wheels.

The most straightforward solution for ADCS is an integrated COTS system that includes the selected combination of sensors and actuators. With a focus on heritage, the best commercial option is the XACT family of integrated ADCS systems [74] developed by Blue Canyon Technologies. Their XACT-15 was used in relevant interplanetary CubeSat missions such as MarCO or Lunar IceCube. However, this model would not perform sufficiently when used in a 12U configuration. Therefore, the higher-tier XACT-50 system, shown in Figure 4.6, has been chosen, which provides a 1-sigma pointing accuracy of 0.007 deg. This system provides up to 50 mNms of momentum storage and a maximum torque of 0.006 Nm. These values clearly comply with the established requirements, so the XACT-50 will be used as the reference ADCS for the mission.



Figure 4.6: Blue Canyon Technologies XACT-50 integrated attitude control system. [74]

4.1.4. Guidance, navigation and control

GNC requirements

One of the main goals of the mission is for the spacecraft to perform a stand-alone Earth-Mars transfer. To do so, it shall transfer to Mars, perform orbital insertion into the PSO and maintain its orbit during science operations. The most critical stage of the transfer is the orbital insertion around Mars. Therefore, the position of the spacecraft needs to be known with a high degree of accuracy during this phase. In the case of the Mars Reconnaissance Orbiter, a position accuracy of 50 km was set as a requirement during orbital insertion [36]. However, advancements in the field of navigation have allowed for improved position knowledge of interplanetary spacecraft. Therefore, the position accuracy requirement is set at 1 km [19]. In terms of velocity knowledge, modern navigation techniques offer accuracies in the order of 1 mm/s [19].

Therefore, the list of GNC requirements is as follows:

- SR-GNC-01: The GNC system shall provide a position accuracy in the order of 1 km (1σ) in all three axes.
- SR-GNC-02: The GNC system shall provide a velocity accuracy in the order of 1 mm/s (1σ) in all three axes.

GNC solution

The standard approach to estimating the position of interplanetary spacecraft is using radiometric tracking data. This includes range, Doppler, and Delta-DOR measurements. While the range and Doppler data are suitable for line-of-sight coordinates, they have a weakness in determining the spacecraft declination component. In the past decades, Earth's deep space ground stations have been developing capabilities for long baseline interferometry measurements. This Delta-DOR technique provides data close to one-nanoradian accuracy with a reliability of 98% [19]. This would translate to an accuracy of around 300 m at Mars distance. To enable these measurements, the spacecraft needs to integrate a phase-coherent radio architecture that can input certain special navigational tones in

the spacecraft carrier. This will be delved into in Subsection 4.1.7.

As in other missions that used electric propulsion systems, such as BepiColombo, navigation procedures take place at the ground station [27]. During each contact with the spacecraft, radiometric data is gathered. Then, the state of the spacecraft is calculated and its trajectory is estimated. This allows the generation of updated thrust profiles, which are uploaded to the spacecraft and carried out using the propulsion system and ADCS. This is done to compensate for any deviations from the nominal trajectory. In the case of BepiColombo, two weeks of electric propulsion operations are uplinked every week, starting immediately at the end of the pass in which the commands are uplinked. This is done to ensure the spacecraft can continue its transfer orbit even if one or more contacts with the ground segment cannot be performed due to ground station issues. Figure 4.7 shows a diagram of the GNC strategy for this mission following the aforementioned procedure.

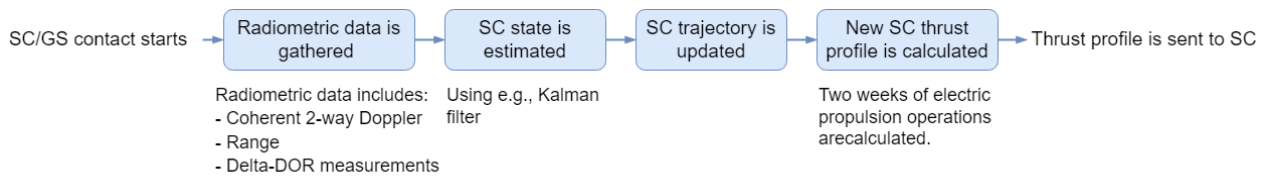


Figure 4.7: GNC strategy for the mission.

Usually, Delta-DOR sessions are considerably longer (and therefore more expensive) than Doppler/range passes. Therefore, Delta-DOR measurements will be performed more sparsely, while Doppler/range sessions will be performed during each spacecraft contact. Using MarCO’s navigation strategy [52] as a reference, a tracking schedule has been generated for this mission. As can be seen in Table 4.5, Doppler/range and Delta-DOR passes will have different sequences depending on the phase of the mission. In the most critical phases, such as Mars Orbit Insertion (MOI), the number of passes will be higher to reduce the risk. A more extensive explanation of the spacecraft contact schedule will be provided in Subsection 4.2.1.

Start	End	Doppler/Range Passes	Δ DOR Sessions
Launch	Launch + 15 days	Daily	1 per week
Launch + 15 days	MOI - 28 days	1 per week	1 per week
MOI - 28 days	MOI - 14 days	2 per week	1 per week
MOI - 14 days	MOI	Daily	2 per week
MOI	PSO	2 per week	1 per week
PSO	PSO + 60 days	Daily	1 per week

Table 4.5: Tracking schedule for the mission.

To add robustness to the spacecraft’s GNC, the imaging payload can also be used to provide higher autonomy to the spacecraft. Using the images taken by the CMOS Camera, optical stellar navigation can be performed. This can be done through full-disk optical navigation near target bodies and celestial triangulation during deep-space cruises [26]. In a celestial object’s vicinity, images of nearly spherical objects can be used to estimate the spacecraft’s position to an accuracy in the order of 100 km. In interplanetary space, the processing of line-of-sight directions to certain visible targets can

enable accuracies in position estimation of 1000 km. Even though these techniques do not comply with the established requirements, they can reduce the costs of navigation and operating the mission. These costs are still considerable compared to other mission costs that scale down with spacecraft size. Therefore, they could be used in parts of the mission where the state knowledge accuracy is not as demanding as those for orbital insertion around Mars (e.g., intermediate stages of the Earth-Mars transfer).

4.1.5. Avionics stack

Avionics stack requirements

CubeSat avionics usually follow a “stack” design, where circuit boards are stacked on top of one another while sharing a common header bus. This allows for simple designs with fewer cables that can be placed with more freedom inside a CubeSat. More specifically, the DLR technologies to be used have been designed with a backplane-based avionics stack configuration in mind. Moreover, these technologies use CPCI Serial Space mechanical interfaces.

Therefore, the requirements for the avionics stack are as follows:

- SR-AVI-01: The avionics stack shall use a backplane-based configuration.
- SR-AVI-02: The avionics stack shall be mechanically compatible with CPCI Serial Space.

Avionics stack solution

The DLR ICA developed in-house is considered for the avionics stack. A model of the ICA can be seen in Figure 4.8. It provides an interface to the avionic domains of onboard data handling, power, communication and software. The ICA was designed using a backplane-based configuration to be mechanically compatible with CPCI Serial Space but tailored to fit into a 3U CubeSat. Thus, the main advantage of ICA is its scalability for different applications and spacecraft classes, including CubeSats. It also implements a wireless intra-spacecraft communication system. This allows a simplification of harness design and routing, which can be used to reduce cables and the mass of the spacecraft.

Compared to other avionics frameworks such as PC104, this configuration has several advantages, especially on CubeSats. Firstly, the backplane enables more connections and makes higher data rates feasible. Secondly, the use of dedicated mounting frames for the boards improves the thermal connection of the board to the primary structure. And lastly, the usable area per board is about 125 cm². Compared to the overall board area of 85 cm² for PC104 this enables the use of larger components, and more complex designs and reduces the overhead needed for connectors. Although mainly intended to demonstrate the ICA for later application in larger systems, the application in a CubeSat environment may be of interest for science missions with challenging requirements. These characteristics comply with the requirements stated above. Therefore, the DLR ICA is selected as the avionics interface for this mission.

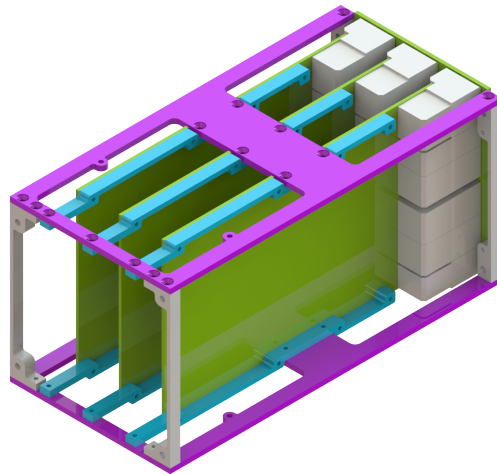


Figure 4.8: Render of the ICA physical interface.

4.1.6. On-board computer

OBC requirements

The computing performance requirements are mainly driven by the data throughput of the Atmospheric Payload. Thus, the OBC must be able to handle ~ 0.5 kBps during science operations [50]. This amounts to an average of 2 MB per orbit at an altitude of 250 km above Mars. This produces a volume of ~ 200 MB of scientific data per week. Assuming that the gravity and imager payloads produce the same amount of data combined, a total of 400 MB of storage would be needed per week. While spacecraft contacts occur daily during science operations, a safety storage margin is needed. Therefore, the spacecraft shall be equipped with at least 400 MB of data storage so that it can store all the scientific data produced during one week. Since most of the computationally demanding tasks are performed on the ground (e.g., GNC), engineering data is orders of magnitude lower, so it can be disregarded. Moreover, the OBC shall implement some form of redundancy for fault tolerance during deep space operations. Finally, the OBC shall implement serial communication interfaces with the other subsystems. A serial communication interface such as RS422 is convenient for this type of mission [11].

Therefore, the requirements for the OBC are as follows:

- SR-OBC-01: The OBC system shall handle data rates of up to 0.5 kBps.
- SR-OBC-02: The OBC shall be equipped with at least 400 MB of memory to store the nanosatellite telemetry data.
- SR-OBC-03: The OBC shall implement dual modular redundancy.
- SR-OBC-04: The OBC shall implement RS422 interfaces for communication with the rest of the SC.

OBC solution

Given the above-mentioned requirements, the DLR in-house developed Scalable On-board Computing for Space Avionics (ScOSA) is considered for the spacecraft's OBC. The ScOSA consists of several computing nodes that are interconnected via a switched SpaceWire network. These computing nodes are reliable space-qualified or high-performance COTS components. The nodes are operated in a worker-monitor redundancy concept, where the functionality of the "worker" is supervised by the "monitor". On the one hand, reliable computing nodes (RCN) are space-qualified and radiation-hardened, which makes them suitable for interplanetary space missions. On the other hand, high-performance nodes (HPN) are COTS-based processing modules for application acceleration. The OBC interfaces to all subsystems and payloads using a selection of standard interfaces like RS422/RS485 serial, CAN, SpaceWire, and discrete I/O

For this mission, a simple application of a single RCN and HPN is implemented. The RCN is the LEON3FT fault and radiation tolerant processing module used in the MASCOT mission [31]. This board provides up to 160 DMIPS/160 MFLOPS of performance. It also includes 128 MiB of RAM and 4 GiB of NAND flash memory. Having been previously used by DLR, the implementation process of this board into the system will be more straightforward. The HPN is a COTS-based processing module with a higher performance of 8660 DMIPS/410 MFLOPS. This board includes 1 GiB of RAM and 4 GiB of NAND flash memory. Given the higher performance of the HPN, the spacecraft capabilities can be extended to include higher autonomy or more advanced data processing. These characteristics comply with the requirements mentioned above. Therefore, the DLR ScOSA is an excellent choice for the spacecraft's OBC.

Software

The ScOSA implements DLR's Open modular software Platform for Spacecraft (OUTPOST) [21]. This flight software is independent of the operating system and the hardware it runs on so that it can be used in different stages of the mission design. OUTPOST includes several capabilities, including modules with Packet Utilization Standard (PUS) services, internal and external communication protocols, sparse logging, ground parsing and other mission control software. Altogether, the flight software implements the following functions:

- Autonomy algorithms.
- Failure Detection Isolation and Recovery (FDIR).
- Acquisition and compression of scientific and housekeeping data.
- Storing of housekeeping and scientific data.
- Reception and transmission to the ground station via the TT&C system.

While other modules need to be developed for the mission, the OUTPOST platform will serve as the cornerstone of the mission flight software.

4.1.7. Telemetry, tracking and command

TT&C requirements

First of all, interplanetary CubeSats have limited capabilities in terms of power and communications. This means that feasible communications at Mars distance with data rates in the order of 1 kbps

can only be achieved using X-band (i.e., 8-12 GHz) [11]. More specifically, NEA Scout is set to achieve this data rate at a distance of 1 AU, while MarCO achieved communications at 8 kbps at Mars distance. Therefore, a first estimate of the needed data rate will be a conservative 2 kbps at a worst-case Mars distance of 1.5 AU. In terms of Bit Error Rate (BER), a value of 10^{-5} is deemed appropriate for an interplanetary mission [72]. Moreover, the ConOps imposes the requirement for the spacecraft to be able to communicate with the Ground Station during LEOP. Therefore, the spacecraft shall be able to maintain X-band communications without the use of deployable antennas. As discussed in Subsection 4.1.4, the TT&C shall also enable navigation through radiometric measurements, including two-way Ranging and Doppler and Delta-DOR data. On top of that, the system shall be capable of acquiring radiometric data while simultaneously sending telemetry and receiving telecommands. Finally, the TT&C shall comply with the applicable ESA ECSS telecommunication standards, as established by the mission requirements.

Therefore, the TT&C requirements are as follows:

- SR-TT&C-01: The TT&C subsystem shall establish communication using X-Band for uplink and downlink during all mission phases.
- SR-TT&C-02: The TT&C subsystem shall be able to establish communication using X-Band without the need for deployables.
- SR-TT&C-03: The TT&C subsystem shall support a downlink data rate of 2 kbps at a distance of 1.5 AU.
- SR-TT&C-04: The TT&C subsystem shall have a downlink BER lower than 10^{-5} .
- SR-TT&C-05: The TT&C subsystem shall support two-way Ranging and Doppler measurements of the SC throughout all mission phases.
- SR-TT&C-06: The TT&C subsystem shall support Delta-DOR measurements of the SC throughout all mission phases.
- SR-TT&C-07: The TT&C subsystem shall be capable of simultaneously handling telemetry, ranging and telecommands.
- SR-TT&C-08: The TT&C subsystem shall comply with ESA ECSS telecommunication standards.

TT&C architecture

A TT&C architecture that complies with the requirements stated above is presented in Figure 4.9. As can be seen, the OBC is connected to the TT&C system through the transceiver. This component transforms the data into RF signals and vice-versa. A power amplifier is used at the exit of the transceiver to increase the transmit power. Then, the diplexer allows for simultaneous receive and transmit procedures. Finally, the diplexer is connected to the antennas through the RF network.

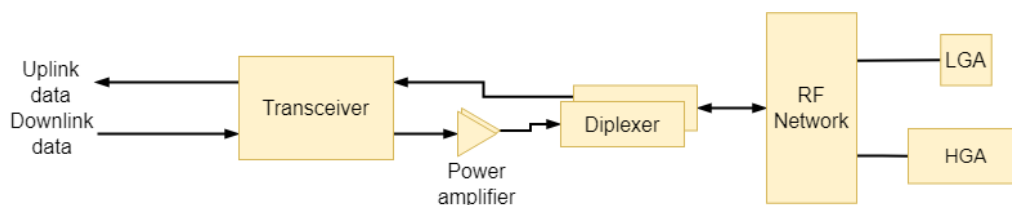


Figure 4.9: TT&C architecture for the mission.

Transceiver solution

The proposed transceiver is the Generic Software Defined Radio (GSDR) developed by DLR. The GSDR allows the operation of multi-band RF applications in the harsh environment of space, being designed with a notable focus on its radiation hardening [9]. Figure 4.10 shows the GSDR prototype board during a TID test. This system is built around the concept of Software Defined Radio (SDR). The basic principle of SDR systems is to perform most parts of the signal processing through software, which has led to systems with much simpler and less heavy and costly hardware. This also means its functionalities are easily updated and upgraded through simple re-programming while using the same hardware. All these features make it an ideal option for a CubeSat spacecraft.

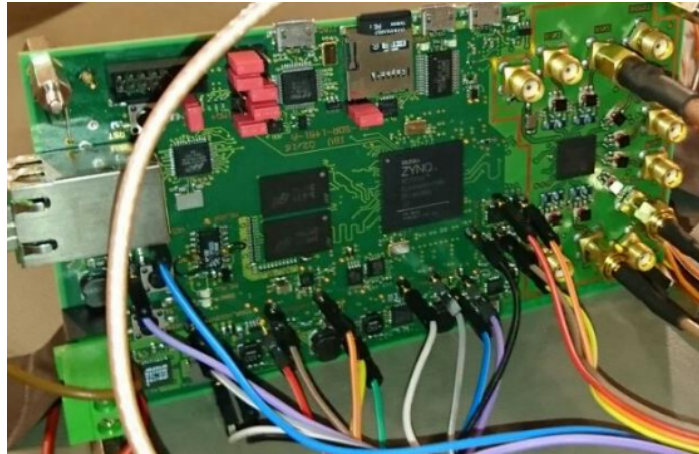


Figure 4.10: GSDR prototype board during a TID test. [9]

At the current point of development, the GSDR offers operation in the RF range of up to 6 GHz. However, interplanetary CubeSats need to operate in X-Band (i.e., 8-12 GHz) in order to achieve feasible communications with Earth. On that note, there are current studies at DLR in order to improve the RF range of the GSDR up to K_a-Band [8]. This can be done through an add-on to the GSDR which has been designed with small satellite missions in mind. In terms of output power, the base design can reach 500 mW. This value stands at one order of magnitude lower than the transceiver used for the MarCO and the secondary payloads of the Artemis 1 missions, which operated in a similar environment [41]. The Avionics Systems Department of the DLR has also been working on a power amplifier module for the GSDR that could bridge the gap to that power output requirement. This would come at an efficiency cost of $\sim 30\%$.

As discussed in Subsection 4.1.4, this transceiver also needs to enable the radiometric measurements to perform spacecraft navigation. To do that, it needs to receive and transmit simultaneously on different frequencies in support of coherent Doppler and range measurements. This can be achieved with the GSDR since it implements a 4-receive and 4-transmit channel design for multiple input, and multiple output applications. For the Delta-DOR technique, the spacecraft transmitter needs to modulate a high-frequency signal onto the carrier (usually around 19 MHz) measured on the ground station. This functionality, as well as others, can be easily implemented in the GSDR through software. Therefore, the GSDR capabilities can be extended to enable radiometric navigation. At the current point of development, the GSDR transceiver doesn't comply with the frequency band and radiometric measurement requirements. However, it can be readily upgraded to comply with the requirements stated above, so it is deemed an adequate choice for this mission.

Antenna solution

Given the requirements of the mission, at least two sets of antennas are needed for the mission. First, a set of Low Gain Antennas (LGA) is needed for LEOP and contingency operations. These antennas should be nondeployable so that they can be used to establish first contact with the ground station after launch. Since these antennas shall only be used to send and receive engineering data and commands, a high gain is not needed. On top of that, a high-gain antenna (HGA) system is needed to account for the large free space losses at Mars distance. For a CubeSat system, this can be achieved through different antenna configurations, including patch arrays, reflectarrays and mesh reflectors [12].

Regarding the LGA, the most viable option is a patch antenna. These antennas consist of a radiating patch that can be placed on the surface of a CubeSat. Therefore, they offer reduced dimensions and mass compared to other types of antennas. A quick glance at NASA’s Small Spacecraft Technology State-of-the-Art Report [33] shows two main options for X-band patch antennas: EnduroSat’s X-Band 4x4 Patch Antenna Array and Syrlinks’ SPAN-X-T3. As can be seen in Table 4.6, EnduroSat’s antenna has better overall capabilities than Syrlinks’: it provides higher gain at a lower mass. Therefore, EnduroSat’s X-Band 4x4 Patch Antenna, which can be seen in Figure 4.11, is chosen as the reference LGA. Since the spacecraft requires full coverage using LGAs, two patch antennas are needed: one on the front and one on the back.

Antenna	Endurosat	Syrlinks
Type	Patch	Patch
Frequency band [MHz]	8025-8400	8025-8400
Gain [dBi]	16	11.5
Polarization	RHCP	RHCP
Mass [g]	53	65
Dimensions [mm]	98x83x3	73x73x11
Flight heritage	Yes	Yes

Table 4.6: LGA overview. [33]

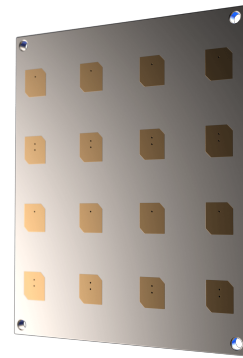


Figure 4.11: EnduroSat X-Band 4x4 Patch Antenna. [25]

The choice for the HGA is not as straightforward as for the LGA. As mentioned above, there are three types of antenna configurations that are considered feasible for such an interplanetary CubeSat mission. An overview of these types can be seen in Figure 4.12 [32]. First, patch antennas have also been built to satisfy high-gain requirements. For example, NEA Scout used an 8 x 8 circularly polarised patch array providing more than 23.4 dBic. However, this gain is still not enough to close the link at Mars distance. Then, preliminary designs have been presented for high-gain mesh reflector antennas [13] that could be used for satellite communications. The main disadvantages of these antennas are their large stowage volume and complex deployment mechanisms. Finally, the reflectarray antenna, such as the one used for MarCO, presents itself as the most viable option for the HGA. Its reflecting surfaces rely on a simple mechanical deployment with spring-loaded hinges so that it can be folded against the spacecraft body at launch. This leads to an antenna that only consumes $\sim 2\%$ of the usable spacecraft volume (for a 12U CubeSat) with a mass of less than 1 kg [32].

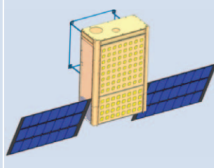
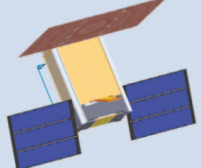
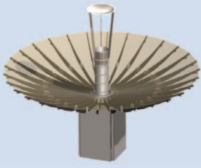
	Patch Array	Reflectarray	Mesh Reflector
			
Max. Aperture 6U Bus	20 cm × 34 cm 680 cm ²	60 cm × 34 cm 2,040 cm ²	0.5 cm Diameter 1,964 cm ²
Gain	24 dB	>28 dB	>28 dB
23° Pointing	Yes	Yes	No
Bandwidth	Medium, < 10%	Low-Medium, < 5%	Large (Feed Limit)
Sidelobes	Controllable	Low	Medium High
Stowage	Small (~0.1 U)	Small (~0.1 U)	Large (~1.5 U)
Deployment Complexity	None	Simple Hinge + Flip-Out Feed	30 Folding Ribs + Deploy Feed and Sub
Reliability	No Deployment	No Lifetime Issues	Mesh Snags, etc.
Mass	Low, <2 kg (est)	Low, <1 kg	Low, 1.4 kg
Cost	Low	Low	Medium

Figure 4.12: Overview of HGA antenna design options. [32]

The European Space Agency has been working on developing a reflectarray antenna to be used in its CubeSat missions through the GSTP Develop programme [71]. This design, led by TICRA, shall achieve a transmit gain of 28.5 dBi and a receive gain of 24 dBi. This is quite an advance compared to the MarCO HGA since it only allowed for RF transmitting. This design will be demonstrated in the GOMX-5 mission to be launched in late 2023. This will take the design to a target TRL of 7, making it a great candidate for this mission. Therefore, the TICRA reflectarray will be used as the reference HGA. Figure 4.13 shows the TICRA reflectarray design, which as of May 2023 has already completed Engineering Qualification Model (EQM) testing [71].

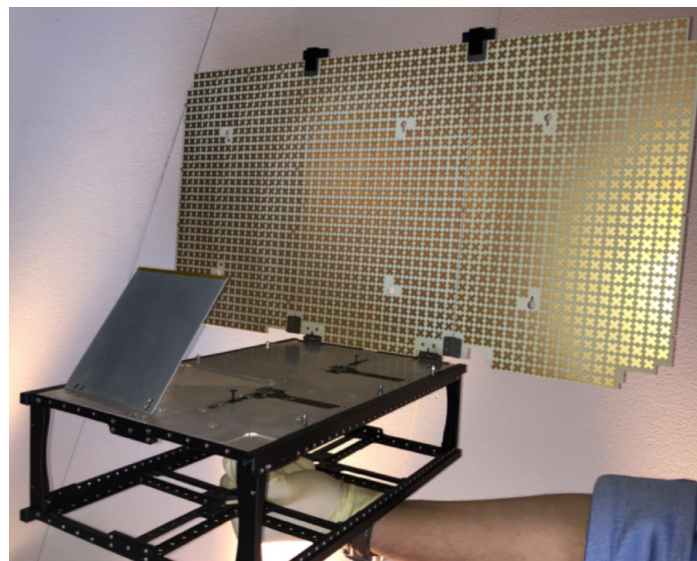


Figure 4.13: TICRA reflectarray EQM. [71]

Link budget

Given the selection of the transceiver and HGA, a preliminary link budget calculation has been performed and can be seen in Table 4.7. This analysis, adapted from [72], focuses on the downlink since it is the most restrictive case in terms of transmit power and antenna gain. This analysis has been done using an RF frequency of 8.4 GHz (i.e., X-Band), a distance to the ground station of 1.5 AU (i.e., the average distance from Earth to Mars), a phase modulation index of 1.2 and an information bit rate of 2 kbps.

A bit rate of 2 kbps has been chosen in order to close the link with a 3 dB margin using a 34-m Deep Space Network dish [45]. Assuming that the atmospheric payload gathers data during a third of its orbit, the spacecraft would need daily 8-hour contacts with the ground station in order to downlink all the scientific data. Note that this is a first estimate since compression or filtering algorithms can be used to reduce the amount of data to be downlinked. If a higher bit rate is needed, the link can also be closed using a 70 m DSN dish (with a gain of 74.6 dBic) and a bit rate of up to 8 kbps. However, this would greatly increase operational costs.

Parameter	Value	Notes
Transmit Power (dBm)	37	Equates to 5 W
Transmit Passive Loss (dB)	-2	Between transmitter and antenna
Transmit Antenna Gain (dBic)	29	Reflectarray HGA
EIRP (dBm)	63.99	
Path Loss (dB)	-278.0	
Atmospheric Loss	-0.3	No rain
Ground Antenna Gain (dBic)	68.2	34-m DSN dish
Total Received Power (dBm)	-146.1	
Data-to-Total Power (dB)	-0.6	
System Noise Density (dBm/Hz)	-184.6	Ts = 25 K
Received Eb/No (dB)	4.9	
Required Eb/No (dB)	1	Rate 1/6 Turbo coding for deep space
Receiver System Loss	-1	Relative to theory
Link Margin (dB)	2.9	

Table 4.7: Downlink margin calculation for the mission.

4.1.8. Electrical power

Power budget

In order to calculate a power budget, the power consumption of each of the spacecraft subsystems has been grouped in Table 4.8. Several things should be taken into account from this table. First, the TT&C system has different entries. COM-HGA includes the power consumption of the GSDR at high power output, the power amplifier, and the HGA. These components consume 9.5, 16.5 and 10 W, respectively. Similarly, COM-LGA includes the power consumption of the GSDR at low power output, the power amplifier, and the HGA, which consume 4.5, 16.5 and 3 W respectively. COM-R is the communications receive mode, which only includes the GSDR in low power mode. TCS includes the needed heater power as calculated in Subsection 4.1.9. Finally, MECH refers to the power consumption of the solar array orientation actuators.

Subsystem	Power consumption [W]
PL-ATM	25
PL-GRA	0.5
PL-IMG	5
EPS	1
COM-HGA	36
COM-LGA	24
COM-R	9.5
OBC	2
ADCS	10
PROP	56.0 - 75.0
TCS	35
MECH	1

Table 4.8: Overview of the power consumption of the main spacecraft subsystems.

The power consumption of each of these subsystems has been grouped into different power operational modes that comply with the ConOps. These modes are shown in Table 4.9, together with the active systems for each mode and its total power consumption. As can be seen, the most demanding power mode is the Maneuver Mode (MAN), which consumes between 70 and 89 W. The power consumption for this mode depends on the needed thrust level during orbital maneuvers and therefore the input power to the propulsion system.

Power Mode	Code	Active systems	Power consumption [W]
Comissioning	CMS	EPS, OBC, ADCS, GNC, COM-LGA, MECH	38.17
Cruise Mode	CRU	EPS, OBC, ADCS, GNC, MECH	14.00
Communication Mode	CRC	EPS, OBC, ADCS, GNC, COM-HGA, MECH	50.17
Maneuver Mode	MAN	EPS, OBC, ADCS, GNC, PROP, MECH	70.00 - 89.00
Science Mode	SCI	EPS, OBC, ADCS, GNC, PL, MECH	39.50
Safe Mode	SFM	EPS, OBC, ADCS, GNC, COM-LGA, MECH	38.17
Eclipse Mode	ECL	EPS, OBC, ADCS, GNC, MECH, TCS	49.00

Table 4.9: Overview of the spacecraft power operational modes and their power consumption.

EPS requirements

First, the EPS system shall provide power to the spacecraft using solar arrays. In order to enable the generation of power using solar arrays, they shall be able to point towards the Sun autonomously. On top of that, as explained in the previous section, the Maneuver Mode drives the power generation requirement at Mars distance to 90 W. During Mars eclipse, the EPS shall provide at least 49 W of power.

Therefore, the EPS requirements are as follows:

- SR-EPS-01: The EPS shall have Sun-pointing capabilities.
- SR-EPS-02: The EPS shall provide at least 90 W to other subsystems at a distance of 1.5 AU from the Sun.
- SR-EPS-03: The EPS shall provide at least 49 W of power during eclipse.

Solar array solution

The solar arrays have been sized using the most demanding power mode, the Maneuver Mode, which has a power consumption in the range of 70 to 89 W. These solar arrays will be designed using Azur Space 32% Triple Junction 3G30C Solar Cells, as used on DLR's PLUTO mission [4]. Every individual solar cell, measuring 7 x 4 cm, has the capability to generate a maximum power output of 1.07 W at the Beginning Of Life (BOL) when situated at Earth's distance from the Sun. However, the system shall be sized using the power generation at End Of Life (EOL) at Mars distance from the Sun. By assuming a 5% decrease in performance at EOL, 5° cosine losses and 5% power conditioning and distribution losses, the EOL net power generation of an individual solar cell at Mars distance is 0.41 W. Therefore, to meet the power demand of 89 W necessary for the full-range Maneuver Mode, a total of 218 solar cells are needed.

With the dimensions of the 12U CubeSat configuration in mind, it is possible to distribute 24 solar cells across panels that match the size of the spacecraft's rectangular side. A linear distribution of these panels can be used to design the solar arrays. For this study, two 4-panel solar arrays will be assumed, which can allocate 192 solar cells. These solar arrays shall be equipped with Sun-orientation mechanisms to increase their efficiency. This configuration, which can be seen in Figure 4.19, would ensure a net power generation of 79 W. The remaining 10 W can be gathered using body-mounted solar cells. Assuming that body-mounted solar cells have an efficiency loss of 20% [72], 30 additional solar cells shall be placed on the surface of the spacecraft. The distribution of these cells will be specified in later stages of the mission design.

PCDU solution

The PCDU used for DLR's PLUTO CubeSat is a candidate for this mission. This PCDU is designed to handle the 100 W generated by its foldable solar panel [4]. It implements two array power regulators (APRs) that handle the tracking of the maximum power point and convert the input voltage down to battery voltage. These APRs are based on GaN transistors in order to minimise the conversion losses in the PCDU. This system will need to be redesigned in order to account for the power generated by the solar arrays at BOL and Earth's distance from the Sun (i.e., > 200 W). In addition, the PCDU will encompass a range of voltage converters to accommodate various system requirements. Particularly, the BIT-3 propulsion system necessitates a 28 V interface, while the XACT-50 ADCS relies on a 12 V interface. Furthermore, the imager payload is designed with a 5 V interface.

The energy storage needed for the batteries can be calculated using the worst-case scenario for the Mars eclipse. Using the procedure explained in [49] for a low Mars PSO, the spacecraft will remain in Mars' shadow for 0.7 h. Using the Eclipse Mode power consumption and accounting for a 5% loss for power conditioning and distribution, along with a depth of discharge of 60%, the required battery capacity is approximately 60 Wh. Notably, the PLUTO PCDU integrates a 100 Wh battery comprised of commercial 18650 Li-Ion Cells. These cells are arranged in a 4s2p configuration, consisting of four cells connected in series to increase voltage and two sets of these series-connected cells connected in parallel to increase capacity. Although the battery's storage capacity exceeds the requirements, maintaining its current configuration is preferred to provide a safety margin and simplify the design process. Therefore, PLUTO's PCDU is a valuable choice for the mission.

4.1.9. Thermal control

Subsystem functional temperatures

First, the operational and survival temperatures of each of the primary subsystem components have been gathered. In the cases where no data about the survival temperatures have been found, they are assumed to be 10 °C lower than the lower bound and 10 °C higher than the higher bound of the operational temperatures. These values can be seen in Table 4.10. As can be seen, the most demanding component in terms of operational temperature is the atmospheric payload detector. However, the BIRCHES spectrometer already features a cryocooler capable of maintaining the detector and optics box at the required temperatures. Regarding the survival temperature, the most critical component is the BIT-3 propulsion system, as it needs to be kept at a temperature range of -25 to 55 °C.

Subsystem	Component	Operational Temp. [°C]	Survival Temp. [°C]
PL-ATM	Optics	-10 to +40	-45 to +85
	Detector	-163.15 to -268.15	up to +70
	Cryocooler	-34 to +71	-44 to +81
PL-IMG	Sensor	-40 to +70	-50 to +80
PROP		-15 to +45	-25 to +55
ADCS		-20 to +60	-30 to +70
OBC		-24 to +61	-40 to +61
TT&C	GSDR	-20 to +50	-30 to +60
	HGA	-55 to +80	-65 to +90
	LGA	-50 to +125	-50 to +125
EPS	Solar array	-40 to +125	-50 to +135
	PCDU	-40 to +85	-50 to +95
	Batteries	Charge: 0 to +50 Discharge: -20 to +75	-30 to +85

Table 4.10: Overview of the main subsystem components' operational and survival temperatures. The most critical component is highlighted.

TCS requirements

Given the operational and survival temperatures presented above, the TCS requirements are as follows:

- SR-TCS-01: The TCS shall preserve all other subsystems within their operational temperature limits during all phases of the mission.
- SR-TCS-02: The TCS shall never allow any subsystem to go outside of its survival temperature range.

Preliminary thermal analysis

A preliminary analysis will be carried out for the hot and cold cases of the mission. This will provide a first approximation of the need for radiators and heaters in the spacecraft. The hot case will be evaluated just after launch since this is the closest the spacecraft will be to the Sun. On the other hand, the cold case will be evaluated during Mars eclipse since no direct sunlight will hit the spacecraft.

Hot case

To determine the required radiator area for this 12U CubeSat, a heat balance analysis will be performed after launch. This analysis leads to the following equation [11], which can be used to calculate the needed radiator area assuming the radiators don't receive any external heat as they are pointed towards deep space:

$$A = \frac{Q_{int} + Q_{backload}}{\epsilon \sigma T_{max}^4} \quad (4.7)$$

where $Q_{int} = 100 \cdot 0.4 = 40$ W is the internal heat generated by the spacecraft (with an assumed efficiency of 40%), $\epsilon = 0.8$ is the radiator emissivity, $\sigma = 5.67 \cdot 10^{-8}$ W/M²K is the Stefan-Boltzmann constant, $T_{max} = 315$ K is the maximum radiator temperature, and $Q_{backload}$ is the external heat load on the spacecraft surfaces.

The $Q_{backload}$ will be calculated in the worst case, in which the rectangular surface of the 12U CubeSat (i.e., Y panel) is in direct sunlight and the 2x2 surface (i.e., Z panel) is facing the Earth, as can be seen in Figure 4.14.

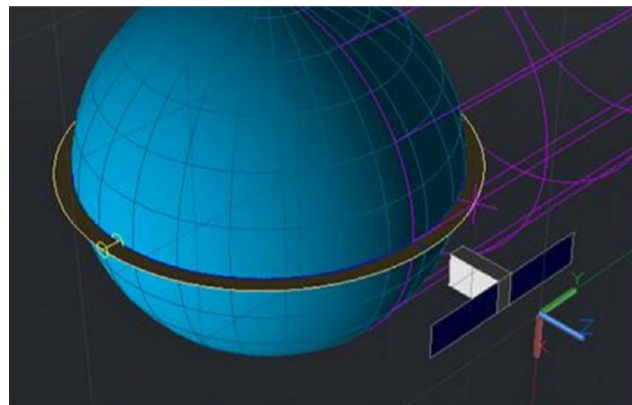


Figure 4.14: Worst-case scenario for the mission hot case. [11]

Therefore, assuming the spacecraft has an absorptivity of $\alpha = 0.2$:

$$Q_{backload, -Y} = A_Y \cdot \alpha \cdot q_{solar} = 0.3 \cdot 0.2 \cdot 0.2 \cdot 1370 = 16.44 \text{ W} \quad (4.8)$$

$$Q_{backload, Z, albedo} = 0.3 \cdot Q_{backload, Z, solar} = 0.3 \cdot A_Z \cdot \alpha \cdot q_{solar} = 0.3 \cdot 0.2 \cdot 0.2 \cdot 0.2 \cdot 1370 = 3.29 \text{ W} \quad (4.9)$$

$$Q_{backload, Z, EarthIR} = A_Z \cdot q_{EarthIR} = 0.2 \cdot 0.2 \cdot 240 = 9.6 \text{ W} \quad (4.10)$$

Then, the total external heat load can be computed as $Q_{backload} = 16.44 + 3.29 + 9.6 = 29.45 \text{ W}$. With this value, the needed radiator area can be found using Equation 4.7:

$$A = \frac{40 + 29.45}{0.8 \cdot 5.67 \cdot 10^{-8} \cdot 315^4} = 0.16 \text{ m}^2 \quad (4.11)$$

This area could be achieved with radiators on three of the rectangular surfaces of the CubeSat, with a margin of 0.02 m^2 . These radiators need to have a low solar absorptivity and a high IR emissivity. The most efficient way to implement these radiators in terms of mass is using radiator films. For example, the Sheldahl Aluminum Coated FEP film can be used [66]. These FEP films are coated in aluminium on one side so that they can be used as second surface mirrors. For the 5-micron thickness option, this film offers an absorptivity of less than 0.15 and an emissivity higher than 0.85. For the needed amount of film, this would translate to a mass of 50 g.

In case more heat needs to be radiated, another patch of radiator film could be added to one of the squared surfaces of the CubeSat. On top of that, the radiator temperature could be increased, which would improve the efficiency of the radiators. This can be done by assigning different radiators to different components depending on their heat generation. Thermal strips could be used to achieve these thermal connections.

Cold case

The cold case will be evaluated in order to analyze the need for heaters in certain components during Mars eclipse. Here, the thermal balance equations can be used to evaluate the spacecraft temperature [11]:

$$T = \sqrt[4]{\frac{Q_{int} + Q_{backload}}{\epsilon \sigma A}} = \sqrt[4]{\frac{5.6 + 9.6}{0.8 \cdot 5.67 \cdot 10^{-8} \cdot 0.28}} = 186 \text{ K} = -87.2 \text{ }^\circ\text{C} \quad (4.12)$$

Where $Q_{int} = 14 \cdot 0.4 = 5.6 \text{ W}$ is the internal heat generated by the spacecraft during eclipse without the contribution of the TCS, $Q_{backload} = 0.2 \cdot 0.2 \cdot 240 = 9.6 \text{ W}$, and $A = 0.2 \cdot 0.2 + 4 \cdot 0.2 \cdot 0.3 = 0.28 \text{ m}^2$. As mentioned above, the highest lower bound survival temperature for any component is $-25 \text{ }^\circ\text{C}$ or 248 K . Therefore, a cold case temperature of $-87.2 \text{ }^\circ\text{C}$ would damage most of the spacecraft components. It should be noted that this is an unrealistically low temperature, since this analysis assumes a steady state and does not take into account the time that the spacecraft will spend in Mars eclipse. However, to solve this issue, heaters need to be placed on the most thermally sensitive components. A suitable option could be the Minco Satellite All-Polyimide Thermofilm Heater [62]. These thin

and lightweight heaters are constructed from entirely low-outgassing materials, incorporate pressure-sensitive mounting adhesive, and are fabricated in compliance with NASA GSFC S-311-P-841. By adding heaters that output a total of 35 W to the heat generated by the spacecraft in Equation 4.12, the spacecraft temperature during Mars eclipse can be brought to -22 °C. This temperature would ensure the survivability of all the spacecraft components.

4.1.10. Structure

Structure requirements

As presented in the mission requirements, the spacecraft shall use a 12U CubeSat configuration. The dimensions and other spatial requirements are established in the CDS [18]. On top of that, the structure shall allow the different instruments to have a direct line of sight with the exterior of the spacecraft. Therefore, the spacecraft shall accommodate openings using the configuration presented in Subsection 4.1.11. Finally, as explained in Section 2.2, one of the main reliability concerns in interplanetary CubeSat missions is their radiation tolerance. In order to increase the spacecraft's radiation tolerance, the structure shall also shield the necessary subsystems from radiation.

Therefore, the structure requirements are as follows:

- SR-STR-01: The structure shall be in compliance with the 12U CubeSat standard established in the CDS [18].
- SR-STR-02: The structure shall accommodate openings for the necessary subsystems as established in Subsection 4.1.11.
- SR-STR-03: The structure shall shield the necessary subsystems from radiation.

Primary structure solution

The primary structure in a CubeSat has two main objectives: mechanically supporting and protecting all spacecraft subsystems and providing a mechanical interface to the deployer system. These primary structures are highly standardized so that they can be acquired as COTS components. Most of these options are machined from aluminium alloy 6061 or 7075 and are designed with several mounting locations for components to increase flexibility in spacecraft configuration.

The main manufacturers of 12U CubeSat structures are EnduroSat, ISISPACE, Spacemind and C3S Electronics Development LLC. All these options offer compliance with the CubeSat standard and similar features in terms of mass and materials. Nevertheless, the EnduroSat 12U XL CubeSat Structure comes with a full campaign of tests at qualification level following ESA standard ECSS-E-ST-10-03C and GEVS standard GSFC-STD-7000A. This campaign contains the following tests:

- Random vibration
- Sinusoidal vibration
- Pyroshock test
- Thermal cycling
- Thermal vacuum

On top of that, the PLUTO mission being developed at the Institute of Space Systems of the DLR

is planned to use a 6U structure from EnduroSat. The fact that a communication channel has already been opened between the DLR and EnduroSat provides yet another benefit from this option. Therefore, the EnduroSat 12U XL CubeSat Structure is chosen as the primary structure for the mission [24]. This structure is manufactured using Aluminium 6082, has a mass of 2 kg and its dimensions are 226.3 x 226.3 x 366 mm. Figure 4.15 shows the structure in Basic Configuration 2, which includes six mounted rings to ease the distribution of subsystems. This configuration shall be modified to include an opening in the central part of the structure that enables the allocation of the propulsion system's thruster, as will be explained in Subsection 4.1.11.

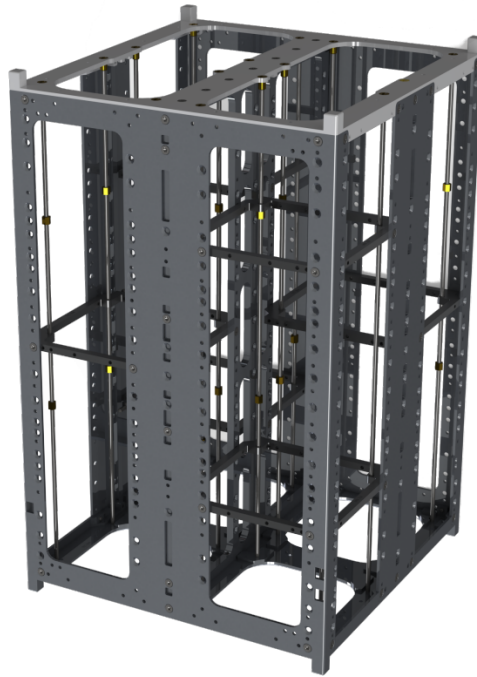


Figure 4.15: EnduroSat 12U XL CubeSat Structure in Basic Configuration 2. [24]

Radiation shielding

One of the main concerns about the first interplanetary CubeSats was their tolerance to radiation. In the end, single-event upset rates were lower than expected since interplanetary radiation environments are generally more benign than those in GEO. For a 1-year mission from Earth to Mars, the expected ionizing dose is approximately <1 krad, 1-3 krad, and 7-16 krad at confidence levels of 50.0%, 84.1% and 97.7%, respectively [75]. As Table 4.11 shows, the majority of subsystem electronics have a higher TID than expected or implement some sort of radiation tolerant feature.

Subsystem	Radiation tolerance
PL-ATM	Radiation tolerant miniaturized low-cost micro cryocooler electronics developed for the US Air Force.
PL-IMG	TID >40 krad.
PROP	Power processing unit with radiation-tolerant components.
ADCS	TID >40 krad.
OBC	Fault and radiation tolerant architecture with RCN and HPN.
TT&C	TID >25 krad.
EPS	Early in development.

Table 4.11: Overview of subsystem radiation tolerance for the mission.

Since the PCDU is early in its development, its strength against radiation is still not clear. In this case, ad hoc shielding is the simplest method to reduce both a system's ratio of total ionizing dose to displacement damage dose accumulation and the rate at which single event upsets occur. New technologies are under development, including multiple-layer graded-Z technology, that show promise for radiation shielding. Therefore, the PCDU shall be protected using a multiple-layer shield in order to increase its radiation tolerance.

4.1.11. Configuration and budgets

Mass budget

After a thorough analysis of all the subsystems of the space segment, a mass budget is presented in Table 4.12. Different safety margins have been incorporated based on the developmental stage of each component. For example, a 5% margin has been allotted to most of COTS components due to their low mass uncertainty. Specific COTS components that are under additional development, such as the BIT-3 propulsion system that requires an expanded propellant tank, are assigned a 10% margin. Similarly, in-house technologies that are under active development or under further enhancement (e.g., GSDR, ScOSA) also bear a 10% margin. Lastly, a 15% margin is reserved for in-house developed technologies demanding substantial development efforts, such as the gravimeter or the solar arrays. After both system and launch margins, the total mass of the spacecraft is 20.01 kg, which complies with the mass requirement outlined by the CDS of 24 kg.

Configuration

There are two main configuration alternatives that comply with the ConOps and the mission requirements. Figure 4.16 shows these two configurations, with the Z-axis pointing in the forward-moving direction. Figure 4.16a shows Configuration A, with the longer side of the CubeSat aligned with the Y-axis. The main advantage of this configuration is that the propulsion system (i.e., the red subsystem) is located in a central position in the CubeSat. Since this is one of the heaviest subsystems, it will make it easier to place the centre of mass of the spacecraft in its geometric centre. This will allow the thrust vector to be aligned with the centre of mass so that no torque is induced to the spacecraft when the propulsion system is active. The only downside of this configuration is that the effective surface area in the forward-moving direction is slightly higher, which will result in

Sub-system	Component	Mass (kg)	Margin (%)	Total mass (kg)
PAY	IR Spectrometer	2.50	5	2.63
	Gravimeter	0.50	15	0.58
	CMOS Camera	0.12	5	0.13
PROP	BIT-3	1.40	10	1.54
ADCS	XACT-50	1.36	5	1.43
AVI	ICA	0.4	5	0.42
OBC	ScOSA	0.25	10	0.28
TT&C	GSDR	0.50	10	0.55
	LGA	0.05	5	0.05
	HGA	1.00	10	1.10
STR	12U XL Structure	2.00	5	2.10
TCS	Heaters	0.03	5	0.03
	Thermal Coating	0.05	5	0.05
EPS	PCDU	0.20	10	0.22
	Battery	0.50	10	0.55
	Solar arrays	2.00	15	2.30
Other	Harness	0.10	10	0.11
SC dry				14.06
SC dry w/ System margin				5
SC propellant				4.3
SC wet				19.06
Launch mass			5	20.01

Table 4.12: Mass budget for the mission.

marginally higher drag in lower altitudes at Mars. On the other hand, Configuration B is shown in Figure 4.16b. Although the effective drag surface area is lower in this configuration, the propulsion system is placed towards the $-Y$ and $-Z$ axis. The propellant contributes considerably to the mass budget ($\sim 25\%$). As it gets depleted along the mission, the centre of gravity will move towards the Y direction. In addition, since the centre of gravity and the thrust vector will not be aligned, a torque will be created that will have to be constantly mitigated by the ADCS. For this reason, Configuration A is preferred.

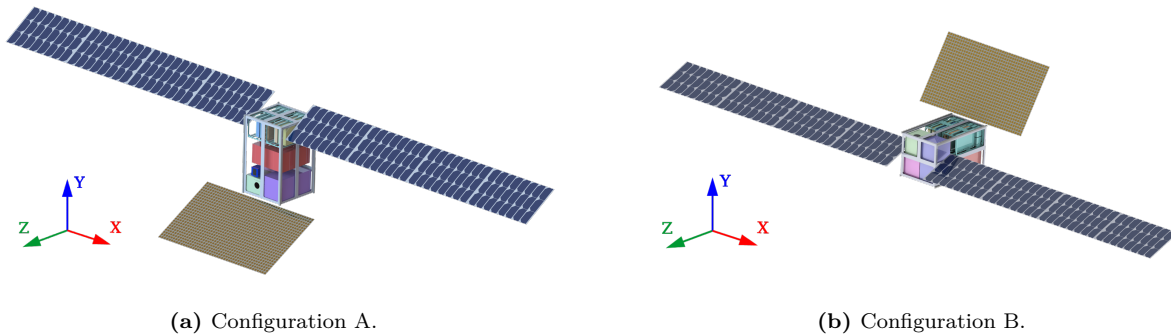


Figure 4.16: ConOps-compliant configurations to be assessed

The distribution of the various subsystems in Configuration A is mainly driven by the ConOps. Figure 4.17 shows the space segment interior as seen from the $-X$, $-Y$ and $+Z$ sides. The subsystem configuration will be explained from ‘top’ (i.e., side $+Y$) to ‘bottom’ (i.e., side $-Y$). First of all, both ICA stacks are located at the top, which include the GSDR, the battery, the PCDU, and the ScOSA OBC. The BIT-3 Propulsion System is located at the centre of the spacecraft, with its thruster pointing towards the $-Z$ direction. The payloads are located in the lower region of the spacecraft. The atmospheric payload is positioned adjacent to the $+X$ side, orientated in such a way that its sensor faces the $-Y$ side. Consequently, while conducting science operations, the nadir will point towards the $-Y$ direction. Both the imager and the gravimeter payloads are adjacent to the spectrometer. The sensor of the imager payload is aligned with the forward-moving direction so that it can easily be used for navigation purposes. Finally, the XACT-50 ADCS is situated between the imager payload and side $-Y$, with its star tracker pointing towards the $+Z$ face. This enables the ADCS to have a direct line-of-sight to outer space during science operations. This also allows for the reflectarray antenna to block incoming radiation from Mars, which could interfere with the star tracker.

A render of the back of the spacecraft can be seen in Figure 4.18. This model shows the need for modifications in the back panel of the structure to accommodate the thruster. As can be seen, there is space available in the spacecraft to accommodate a larger propellant tank. This can be helpful in case the mission analysis (Chapter 5) indicates that more Delta-V than expected is needed for the mission.

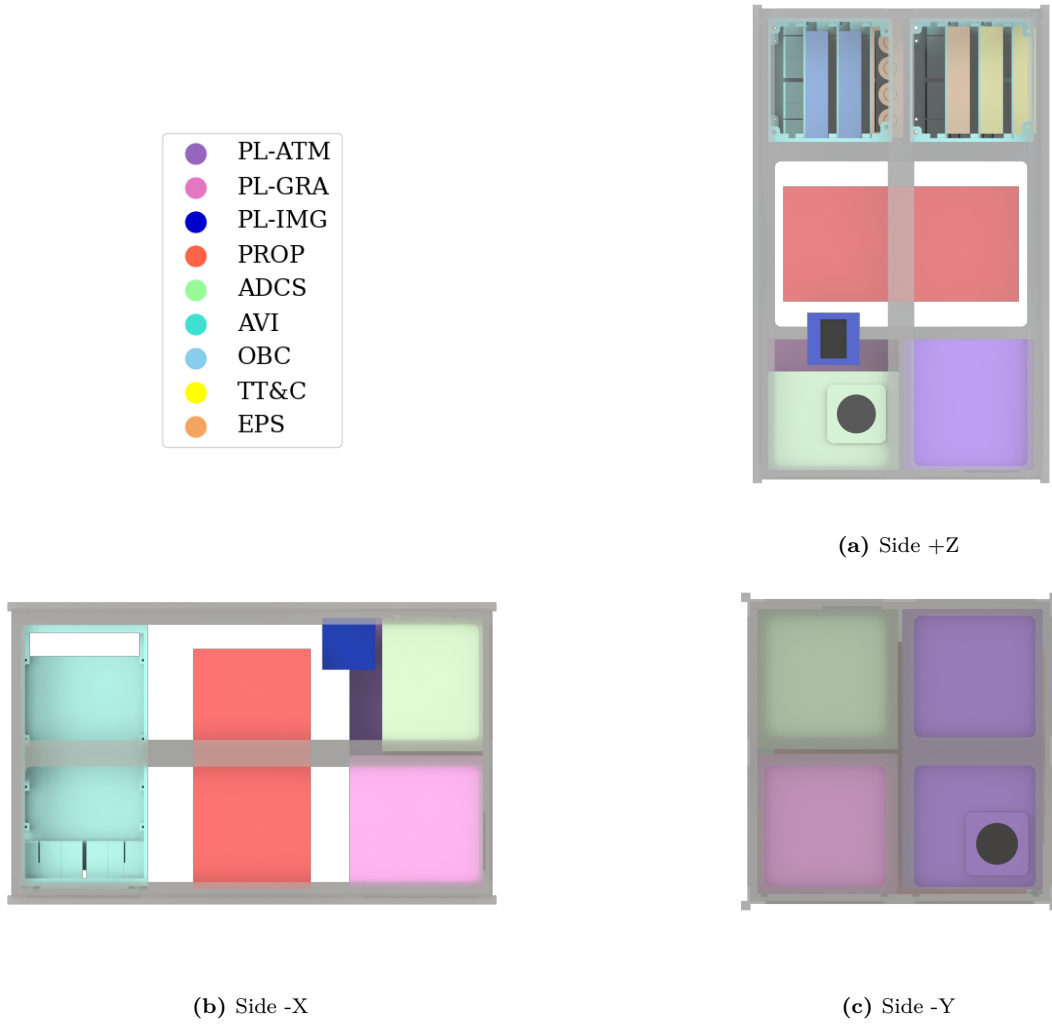


Figure 4.17: Subsystem configuration inside the space segment as seen from sides -X, -Y and +Z.



Figure 4.18: Spacecraft as seen from the back showing the modified back panel and the propulsion system thruster.

4.1.12. Space segment overview

The space segment consists of a 12U CubeSat, which can be seen in Figure 4.19. The spacecraft has a wet mass of 20 kg, a manoeuvrability of 5.1 km/s, and can generate up to 90 W of power at Mars using deployable solar panels. Its main payloads are a 2U infrared spectrometer, a 1U gravimeter and a 12 Mpx CMOS camera. The DLR ICA stack will be used, which combines multiple avionics systems (i.e., onboard computer, communications, and power) into a single unit. The DLR ScOSA onboard computer will be used, which integrates two computing nodes to ensure robustness. The reliable computing node comprises the OBC used on the MASCOT lander developed by DLR [31]. The high-performance computing node consists of a COTS-based processing module for application acceleration. The spacecraft uses the radiofrequency X-band in order to communicate with its ground segment. The in-house developed GSDR is used as a transceiver. The system also features a main reflectarray antenna as used by MarCO [32] and secondary patch antennas. Electrical power is generated using two linear solar arrays with 32% efficiency triple junction solar cells developed by Azur Space. The power control and distribution unit, as well as the batteries, will be adapted from those used by the DLR PLUTO mission [4].

For other subsystems, COTS components have been chosen that satisfy the needs of the mission. The propulsion system is a Busek BIT-3 gridded-ion engine as used in the Lunar IceCube and LunaH-Map missions [69]. This system features an expanded tank to accommodate the needed 4.3 kg of propellant. The XACT-50 developed by Blue Canyon Technologies is used as the integrated attitude control and determination system [74]. Thermal coating and heaters are used for thermal management. All of these systems are housed in an EnduroSat 12U XL main structure [24].

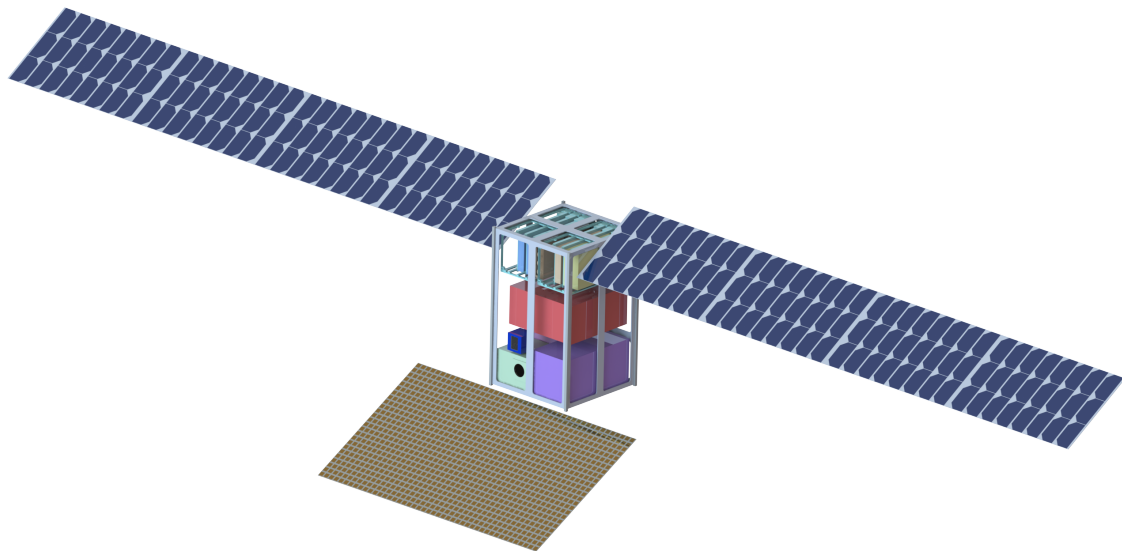


Figure 4.19: Space segment using a 12U CubeSat configuration.

4.2. Ground segment

The following sections provide a comprehensive analysis of the ground segment subsystems, including the ground station and operations.

4.2.1. Ground station

Several ground station networks on Earth offer the necessary capabilities to operate interplanetary spacecraft on the X-band. NASA's Deep Space Network, ESA's European Space Tracking (ESTRACK) network, and DLR's ground stations stand out as the most appealing choices. The DSN is distributed among three key locations: the United States (California), Spain (Madrid), and Australia (Canberra). This allocation allows uninterrupted view of a distant spacecraft by at least one of the stations. The DSN stations are equipped with 34- and 70-m dishes that operate on the S-, X- and K-bands. They provide the full range of radiometric measurements needed for spacecraft navigation, including Doppler tracking, ranging, and Delta-DOR measurements. The ESTRACK network offers similar characteristics. However, their ground stations in Australia, Spain and Argentina are only equipped with 35-m dishes, resulting in diminished transmitting and receiving performance. Finally, the DLR ground station in Weilheim is classified both as a Deep Space Network and a Non-Deep Space Network (Near Earth Network) and can support space missions in the L, S, X, Ku, and Ka frequency bands. This station features a 30-m dish designed for solar and deep space missions. While the antenna supports navigational radiometric data, it does not have transmitting capabilities.

All three options offer different advantages and disadvantages. On the one hand, the DSN and ESTRACK provide high availability and communication capabilities; however, they come with a substantial cost. On the other hand, the DLR ground station can only be used to receive telemetry signals and gather radiometric data. Nevertheless, the operational costs would be considerably lower, as it would be managed by one of the main customers. Therefore, a combination of the three ground station networks shall be used in order to balance the communication performance and its underlying operational costs. During LEO, interplanetary transfer and MOI phases, the DSN and ESTRACK networks will be used due to their availability and transmitting capabilities. The DLR ground station will also be used during the interplanetary transfer to perform health checks and assess the need for transmitting contacts. Separately, during science operations, the DLR network will be used to downlink the scientific data. During this phase, the DSN and ESTRACK ground stations will be used when command uplink is required. Therefore, the ground station shall acquire the pertinent ITU radio frequency licenses to operate on the three different networks.

Figure 4.20 shows the proposed ground station architecture. As can be seen, the different network antennas are connected to RF down- and upconverters that transform the 8 GHz signal into a medium frequency of 70 MHz, or vice-versa. Then, the combiners and splitters allow the antennas to operate using different signals. These are connected to baseband equipment (BBE), which acts as the interface between the RF and the digital domains. A router is then used to send data between the different BBEs and the Mission Control System (MCS). The operations team oversees the MCS, collecting all telemetry data and issuing commands to the spacecraft.

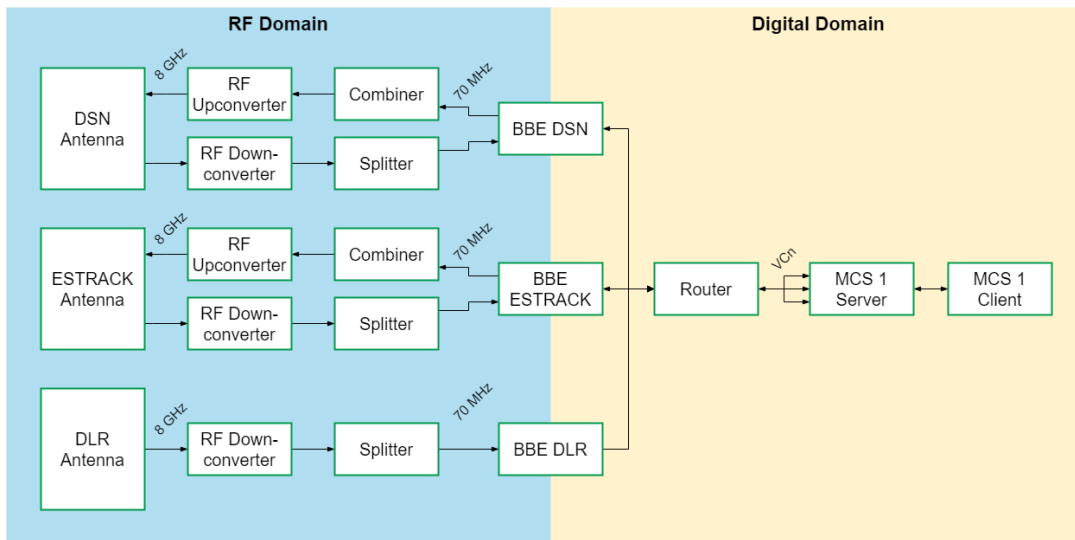


Figure 4.20: Ground station architecture for the mission.

4.2.2. Operations

The operations team shall be located at DLR’s GSOC. The team is mainly responsible for planning the spacecraft contact schedule, gathering all the necessary telemetry, and commanding the spacecraft. As explained in Subsection 4.1.4, the operations team is also in charge of the guidance and navigation of the spacecraft. Therefore, the team shall use the radiometric data available from the spacecraft contacts in order to estimate its state, simulate possible trajectories and calculate updated thrust profiles. Figure 4.21 shows the interrelations between the different operational actors. The operations team shall have a direct communication channel to both the station operators and the systems engineering team. This is mostly convenient for contingency operations or during malfunctions on the spacecraft or the ground station. As explained in the previous section, the MCS will be connected to the different ground stations through a router. The MCS shall also be connected to an internal database. This database will then be open to academia in order to promote research using the scientific data acquired by the spacecraft.

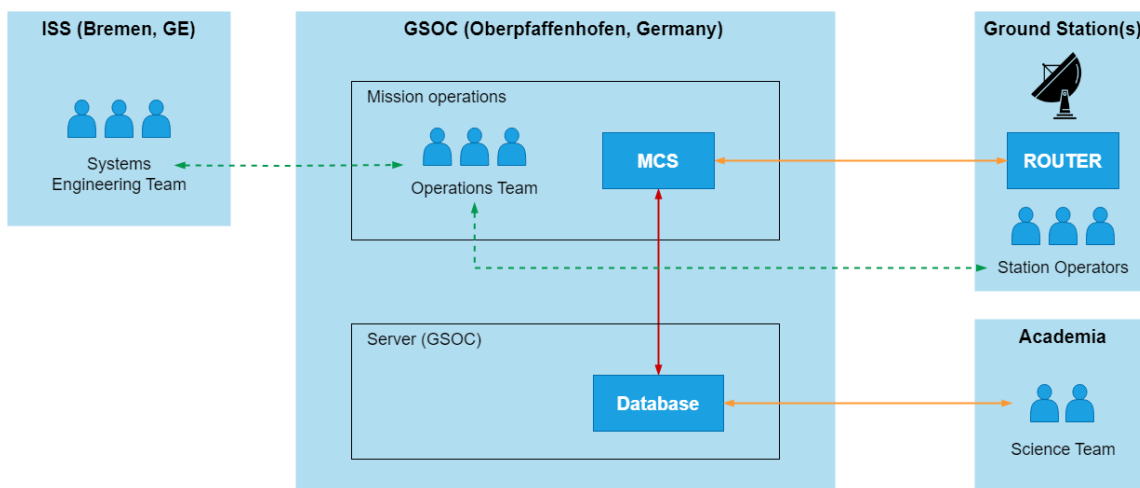


Figure 4.21: Operations architecture for the mission.

A preliminary contact schedule has been generated taking MarCO's requirements as a reference [52]. This contact plan coincides with the tracking schedule for Doppler and ranging passes presented in Subsection 4.1.4. This is due to the collection of radiometric data being scheduled for every contact with the spacecraft. Table 4.13 shows the proposed spacecraft contact schedule. It is important to observe that these contacts will have different lengths depending on the phase of the mission. On the one hand, passes during the interplanetary transfer will be shorter since the data to be sent to the ground will mainly be composed of engineering data. On the other hand, passes during science operations will be substantially longer, as the volume of scientific data to be sent is orders of magnitude higher than the engineering data. This should not be a problem considering that downlinks during science operations can be performed using DLR's ground station network at a reduced cost.

Start	End	Spacecraft Contacts
Launch	Launch + 15 days	Daily
Launch + 15 days	MOI - 28 days	1 per week
MOI - 28 days	MOI - 14 days	2 per week
MOI - 14 days	MOI	Daily
MOI	PSO	2 per week
PSO	PSO + 60 days	Daily

Table 4.13: Spacecraft contact schedule for the mission.

4.3. Launch segment

The following sections provide a comprehensive analysis of the launch segment subsystems, including the possible launchers and CubeSat deployers.

4.3.1. Launcher

Three main options are considered in order to launch this mission. First of all, the last set of interplanetary CubeSats were launched as secondary payloads of the Artemis 1 mission. NASA's CubeSat Launch Initiative also sought proposals in 2019 to fly 6- and 12U CubeSat missions as secondary payloads of Artemis 2. However, all mission proposals were dropped in October 2021. Four more Artemis missions are planned in the next decade, which could open similar calls for proposals. While these calls have been limited to U.S. institutions and companies, the planned delivery of the I-HAB developed by ESA and JAXA on the Artemis 4 mission could be leveraged to include European institutions in the call. The main downside of this alternative is that an Earth-Mars transfer may not be feasible on these launches.

Next, the spacecraft could piggyback on another Mars-bound mission. Table 4.14 shows the planned missions to Mars in the next decade and their planned launch vehicles. The launchers used on missions headed for Mars usually provide launch energies up to $C_3 = 16 \text{ km}^2/\text{s}^2$ [34]. For example, NASA's Perseverance mission was launched using an Atlas V-541 with an excess energy of $15 \text{ km}^2/\text{s}^2$ [2]. This excess energy could contribute to the low-thrust Earth-Mars transfer by reducing the necessary Delta-V and increasing the feasibility of the mission. However, including a piggyback secondary

mission could increase risks on the main mission. This could be an issue when negotiating with the project management team for these missions.

Mission	Developer(s)	Launcher	Planned launch date
EscaPADE	NASA	New Glenn	2024
Mars Orbiter Mission 2	ISRO	LVM3	2024
Starship Cargo	SpaceX	Starship	2024
ExoMars	ESA	Atlas V	2028
Tianwen-3	CNSA	Long March 5	2030
Starship Crew	SpaceX	Starship	2030
Mars Sample Return	NASA, ESA	Falcon 9/Atlas V	2033

Table 4.14: Planned Mars missions for the next decade.

Finally, internal studies at DLR show a peculiar method for upper-stage disposal that could be potentially used to launch the mission. It has been observed that certain high-orbit launchers reach GEO with substantial excess Delta-V. In order to dispose of the upper stage, a final burn is performed in order to thrust it into deep space. The aforementioned studies show that this is a common practice with launchers such as the Atlas V, the Delta II and the Falcon 9. These launches happen regularly, which would be an advantage in terms of departure date flexibility. Thus, the CubeSat could be piggybacked on a launcher to GEO and launched into interplanetary space with a certain excess velocity during the disposal manoeuvre.

4.3.2. Deployer

Several companies offer deployers for the 12U CubeSat standard. One of the most interesting options is the Canisterized Satellite Dispensed (CSD) developed by Planetary Systems Corporation. This deployer was used for the secondary payload CubeSats on board the Artemis 1 mission. Figure 4.22 shows the 6U CSDs on the Orion MPCV Stage Adapter. While the 12U model has not been used to deploy CubeSats into deep space, it does have flight heritage, which grants it a TRL 9. This model also offers an ejection Delta-V of ~ 1.5 m/s which produces an expected one-sigma rotation rate of 10 degrees per second per axis. Moreover, it features a tab constraint system that provides an invariant load path and constrains the spacecraft motion in the X, Y and Z axes. It should be noted that these dispensers impose requirements in terms of tabs, dimensions and deployables that supersede those of the CDS. These should be taken into account in a later iteration of the mission design.

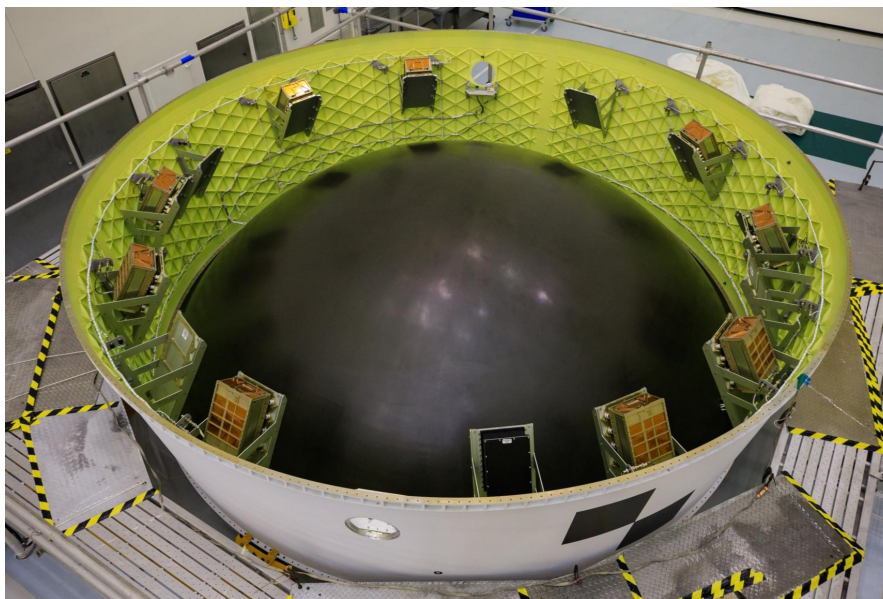


Figure 4.22: 6U CSD integrated into the Artemis 1 Orion MPCV Stage Adapter. [56]

4.4. Development, integration and testing

SR-SYS-03 states that the system shall be ready for launch in less than 4 years. To reach that goal, a plan for the further development of the mission, its integration and testing is presented.

4.4.1. Development

A preliminary plan is needed for the future development of the mission. In that regard, Table 4.15 presents the needed development effort for the main subsystem components. As this table shows, there are a certain set of components that do not need any modifications and can be used as they are acquired from the vendor (e.g., XACT-50) or at their current state of development (e.g., ICA).

Another set of components needs certain modifications to be feasible for the mission. As discussed in Subsection 4.1.2, the BIT-3 propulsion system needs an expanded propellant tank as the needed Delta-V for the mission is higher than the one that the standard model provides. Regarding the GSDR, developments are needed in order to extend its frequency range and increase its power output. On top of that, the selected HGA is still being developed and has just undergone EQM testing. The ScOSA OBC, the PCDU and the batteries are still in development for the PLUTO mission, but will be used as they are designed for that mission.

Finally, two components will require slightly more development effort. First, it is necessary to fully develop the solar arrays. However, having developed PLUTO's deployable solar array, the DLR has considerable experience in this regard. Furthermore, the solar arrays in this preliminary design integrate the same solar cells as the ones used for PLUTO, which would alleviate the needed effort. Second, the gravimeter shall be developed completely in-house. While the operating principle of such a gravimeter has already been studied by academia, it would be a new development at DLR. Therefore, it will present the highest developmental burden.

Sub-system	Component	Development/ Manufacturing	Development effort
PAY	IR Spectrometer	External	None
	Gravimeter	In-house	High
	CMOS Camera	COTS	None
PROP	BIT-3	COTS	Low
ADCS	XACT-50	COTS	None
AVI	ICA	In-house	None
OBC	ScOSA	In-house	Low
TT&C	GSDR	In-house	Low
	LGA	COTS	None
	HGA	COTS	Low
STR	12U XL Structure	COTS	None
TCS	Heaters	COTS	None
	Thermal Coating	COTS	None
EPS	PCDU	In-house	Low
	Battery	In-house	Low
	Solar arrays	In-house	Medium
Other	Harness	COTS	None

Table 4.15: Needed development effort for the main subsystem components. The term “in-house” is used for the DLR-developed components.

4.4.2. Integration

The integration of the space segment will be completely performed at the Institute of Space Systems of DLR, in Bremen, Germany [44]. The Institute has a 250 m² integration laboratory that operates as a class ISO-8 clean room. This clean room enables the integration of spacecraft under Planetary Protection guidelines. Missions such as MASCOT, AISat, Eu:CROPIS and InSight have been successfully integrated in this laboratory. The laboratory is also equipped with various testing facilities, including among others:

- Pyroshock test facilities
- 11- and 89-kN vibration tables
- A 17 m³ Solar-thermal-vacuum chamber
- A complex irradiation facility
- An ultra-high-vacuum laboratory

The integration will be performed using a test-as-you-build philosophy. This will result in various development models, on which testing will be performed continuously from the initial integration stages. At least, the integration process will be performed on a flat-sat, qualification and flight models.

4.4.3. Testing

Figure 4.23 shows the test flow that will be applied to these integration models. This diagram has been adapted from the CDS. As can be seen, testing will be performed at two levels: qualification and acceptance. First, a qualification unit will be built which will undergo qualification testing. The qualification level is usually more demanding than acceptance testing. The information collected by the qualification testing will then be used to build a flight unit. This unit will undergo acceptance testing by itself and while integrated into its deployer. Then, the flight unit will be deemed fit for flight.

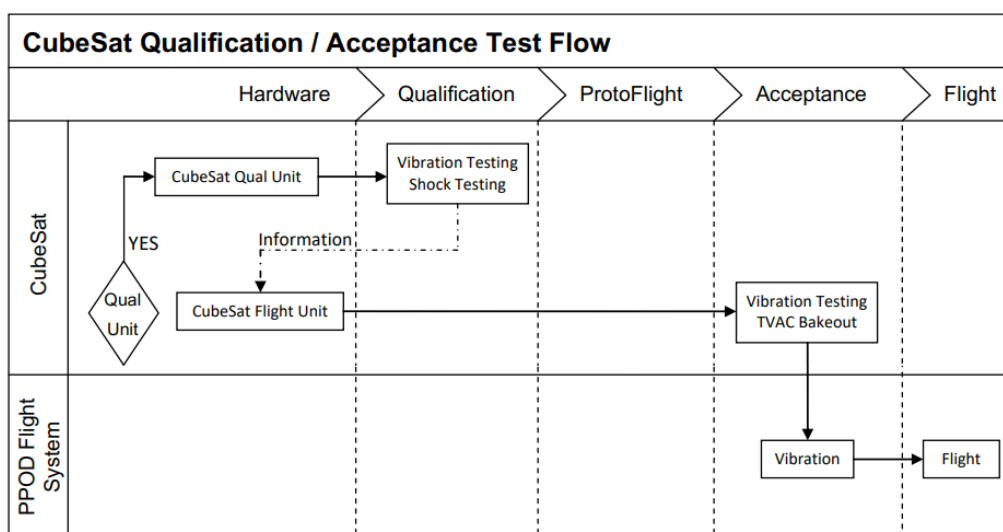


Figure 4.23: Qualification/acceptance test flow for the mission. Adapted from [18].

Testing will be performed to meet the General Environment Verification Standard (GEVS, GSFC-STD-7000A) [28] according to the CDS. Once the launcher and deployer are known, their testing requirements (i.e., test type, level, and duration) will supersede those from the standards. At this point of development, the tests shown in Table 4.16 shall be considered, using the most demanding test levels from publicly available launcher data [37]:

Test	Qualification level	Acceptance level
Structural static loads	1.25 x 9.0 g / 1 min.	1.0 x 9.0 g / 30 sec.
Random vibration	$G_{\text{rms}} = 2.0 \times 4 / 2 \text{ min.}$	$G_{\text{rms}} = 1.0 \times 4 / 1 \text{ min.}$
Thermal-vacuum bakeout	0 to +70 °C	+5 to 65 °C
Thermal cycling	-15 to +85 °C	-10 to 80 °C

Table 4.16: Main tests to be performed on the CubeSat with their respective level and/or duration. [37]

On top of these, several other tests can be performed, which will need to be added to the test flow shown in Figure 4.23 in later stages of the mission design:

- System Electromagnetic Compatibility (EMC) testing is designed to demonstrate the spacecraft's compatibility with the self-induced electromagnetic environment. This becomes important during the reception of uplink data, for errors in sensor data or electric propulsion-induced noise.
- Radiation testing will be needed at the subsystem level if its components have not undergone TID tests, as is the case with the PCDU.
- Deployment testing verifies that the deployment mechanisms, such as antennas and solar panels, can function according to the design requirements.
- Ground station compatibility testing demonstrates the correct functioning of both uplink and downlink.
- Deployer interface testing involves inserting the assembled CubeSat into the deployer to see whether it can fit in it and exit smoothly when the deployer mechanism is activated.
- Visual inspection of the CubeSat and measurement of critical areas will be performed per the CubeSat Inspection and Fit-Check Procedure [18].

4.5. Risk management

A solution for the design of the system and its subsystems has been provided in the previous sections. Each of the specified subsystems has inherent risks that need to be acknowledged and mitigated as efficiently as possible to ensure the continuity of the mission. Therefore, the main risks for each of the space segment subsystems have been identified, and are shown in Table 4.17. Each of the risks has been assigned a likelihood and severity ranging from 1 to 5. A likelihood of 5 is given if a risk is bound to happen with full certainty during the mission. Similarly, a severity rating of 5 is assigned when a risk results in a loss of mission. By multiplying these parameters, a risk rating can be calculated for each item on the list.

Figure 4.24 shows a likelihood/severity matrix, where each of the identified risks has been placed based on their likelihood and severity ratings. The orange area of the matrix is the most important, as it shows the risks with higher severity and likelihood. As can be seen, the two risks that appear in this area are related to the propulsion system. These are important as they have a precedent on the LunaH-Map mission launched as a secondary payload of the Artemis 1 mission [30]. Due to the long wait from the spacecraft delivery to its launch, the propulsion system on LunaH-Map did not ignite. If this were to occur, it would render two of the mission's key goals unattainable. Therefore, it is essential to implement mitigation strategies aimed at minimizing these risks.

For each of the identified risks, a mitigation strategy is presented in Table 4.18. Updated likelihood and severity scores have been presented for the mitigated risks. By calculating the risk score for the whole set of mitigated risks, a reduction of nearly 65% can be attained when compared to the scores shown in Table 4.17. The mitigated risks are presented in the matrix shown in Figure 4.25. As can be seen, the mitigation strategies should relocate the risks in the orange area, making it safe to accept them.

Subsystem	Code	Description	Likelihood	Severity	Risk
PL	R-PL-01	Cryocooler is not able to keep PL-ATM within operational limits.	1	3	3
PROP	R-PROP-01	Propellant valve might get stuck due to long storage periods.	4	4	16
	R-PROP-02	Difficulty in raising tank and valve temperature.	4	4	16
ADCS	R-ADCS-01	Malfunction in a reaction wheel.	2	2	4
GNC	R-GNC-01	Entering an impact trajectory with Mars.	2	5	10
	R-GNC-02	Malfunction or failure of sensors or actuators used for navigation and control.	2	2	4
	R-GNC-03	Errors in state estimation.	2	3	6
OBC	R-OBC-01	Difficulty in ensuring the proper functioning of all subsystems and maintaining system-wide synchronization.	2	3	6
	R-OBC-02	Data loss or corruption due to hardware or software failure.	2	2	4
COM	R-COM-01	Data rate not being enough to send all science data to Earth.	1	2	2
	R-COM-02	Failure of the High Gain Antenna.	2	4	8
TCS	R-TCS-01	Damaging the CubeSats or subsystems due to extreme temperatures.	1	3	3
EPS	R-EPS-01	Damaging to the power system due to exposure to the space environment.	2	4	8
	R-EPS-02	Batteries may go below their operational temperature while in Mars eclipse.	4	3	12
	R-EPS-03	Power generation is insufficient.	1	3	3
	R-EPS-04	Battery degradation is higher than expected.	2	3	6
STR	R-STR-01	Failure of primary structure due to fatigue from launch or repeated thermal cycles.	2	5	10
MECH	R-MECH-01	Malfunction of deployable mechanisms.	3	4	12
TOTAL					133

Table 4.17: Identified risks for each of the mission subsystems.

Subsystem	Code	Mitigation strategy	New likelihood	New severity	New risk
PL	R-PL-01	Reinforced local thermal shielding.	1	2	2
PROP	R-PROP-01	Demand extended testing from manufacturer.	3	2	6
	R-PROP-02	Perform extended testing.	2	2	4
ADCS	R-ADCS-01	Add redundancy.	1	1	1
GNC	R-GNC-01	Add automation layer for collision avoidance.	1	4	4
	R-GNC-02	Add redundancy.	1	2	2
	R-GNC-03	Include more SC contacts in the schedule, correlate data between different GS.	1	2	2
OBC	R-OBC-01	Extended testing on flat-sat during integration.	1	2	2
	R-OBC-02	Reinforced local radiation shielding on OBC.	1	1	1
COM	R-COM-01	Use data compression strategies and data filtering.	2	1	2
	R-COM-02	Add redundancy through patch antenna.	2	2	4
TCS	R-TCS-01	Adding insulation in critical parts.	2	2	4
EPS	R-EPS-01	Extended radiation testing.	1	1	1
	R-EPS-02	Adding heaters.	2	2	4
	R-EPS-03	Adding body-mounted solar cells where possible.	2	1	2
	R-EPS-04	Adding redundant batteries.	1	1	1
STR	R-STR-01	Extended thermal-vacuum and random vibration testing.	1	2	2
MECH	R-MECH-01	Extended deployable testing.	1	3	3
TOTAL					47

Table 4.18: Mitigation strategy applicable to each identified risk for the mission.

Likelihood	5					
	4			R-EPS-02	R-PROP-01, R-PROP-02	
	3	R-COM-01			R-MECH-01	
	2		R-ADCS-01, R-GNC-02, R-OBC-02	R-OBC-01, R-EPS-04, R-GNC-03	R-COM-02, R-EPS-01	R-GNC-01, R-STR-01
	1			R-PL-01, R-TCS-01, R-EPS-03		
		1	2	3	4	5
Severity						

Figure 4.24: Likelihood/severity matrix for the identified risks.

Likelihood	5					
	4	R-GNC-01				
	3		R-PROP-01			
	2	R-COM-01, R-EPS-03	R-PROP-02, R-COM-02, R-TCS-01, R-EPS-02			
	1	R-ADCS-01, R-OBC-02, R-EPS-01, R-EPS-04	R-PL-01, R-GNC-02, R-GNC-03, R-OBC-01, R-STR-01	R-MECH-01		
		1	2	3	4	5
Severity						

Figure 4.25: Likelihood/severity matrix for the mitigated risks.

4.6. Requirement compliance

The compliance of the proposed system solution with the mission, system and subsystem requirements can be consulted in Appendix A, Appendix B and Appendix C, respectively. By following an appropriate system engineering process, the presented system solution complies with the majority of requirements. Since the mission is in a very early stage of design, there are some requirements the compliance of which cannot be assessed yet. Thus, their compliance is indicated with a '-' symbol. This is the case for MR-02 and SR-SYS-02, which establish the maximum cost of the mission. In this case, it is difficult to find the cost of the COTS components, which is usually acquired through a non-disclosure agreement with the respective companies. On top of that, a big percentage of the cost might come from the launch provider, which is very uncertain at this point of the study. All in all, the solution does not comply with the following requirements:

- MR-18, SR-SYS-23, SR-TT&C-01, SR-TT&C-02: The GSDR cannot operate on the X-band at the current point of development so the system would not be able to establish communications during every phase of the mission.
- MR-25, SR-SYS-29, SR-GNC-01, SR-GNC-02, SR-TT&C-05, SR-TT&C-06: The GSDR does not have the capabilities to process radiometric data so that state estimation cannot be performed at the required level.

Both of these sets of non-compliances arise from the current state of development of the GSDR. However, as explained in Subsection 4.1.7, ongoing development efforts aim to enhance the capabilities of the GSDR. On the one hand, there are current studies at DLR in order to improve the RF range of the GSDR up to K_a-Band [8]. On the other hand, the operating principle of software-defined radios makes it easy to implement the processing of radiometric data through software reconfigurations. Thus, the system can be expected to comply with both sets of requirements in the near future.

5

Mission analysis

As shown in the previous chapters, a system has been designed that can accomplish the proposed ConOps and therefore achieve the projected goals and objectives. In this chapter, the Mission Analysis is performed in order to study the feasibility of the designed system in the context of its trajectory design from the Earth to Mars. The hodographic-shaping method will be used to calculate this low-thrust trajectory. An orbit insertion strategy is proposed. Finally, the characteristics of the Mars PSO will be studied.

5.1. Earth-Mars transfer

This section presents an analysis of the Earth-Mars transfer trajectory for the mission using the hodographic-shaping method. First, the available launch windows are established. Then, an optimization procedure is performed to study the optimal trajectories in terms of Delta-V. The feasibility of the designed system is then assessed.

5.1.1. Hodographic-shaping method

The hodographic-shaping method [29] is the main tool used to calculate the low-thrust Earth-Mars transfer trajectory for the mission. This method designs orbital trajectories by shaping the velocity components along the transfer. To do so, the velocity behaviour of the low-thrust trajectory is modelled using the shape of its velocity hodograph. This velocity profile is then integrated to find the change in position and the resulting trajectory. Figure 5.1 shows such a trajectory and its associated velocity hodograph.

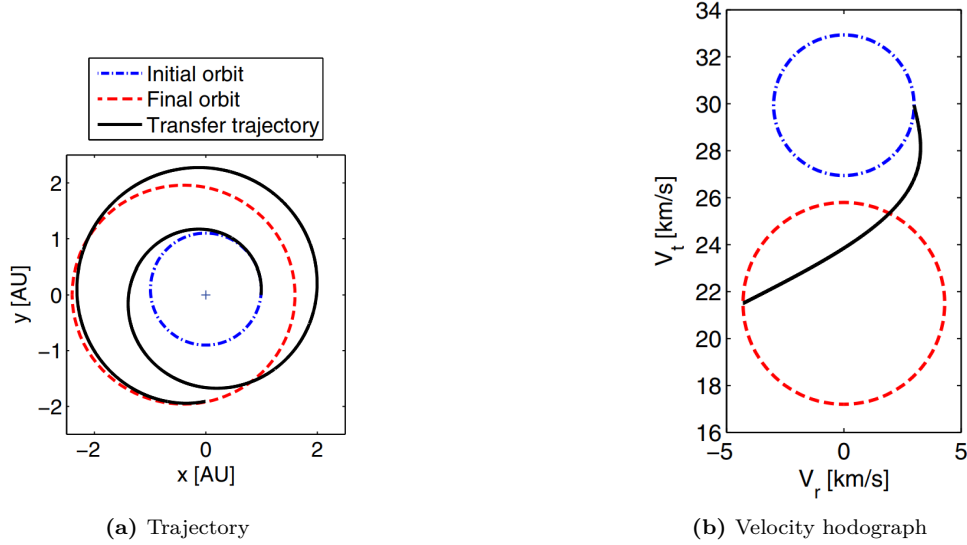


Figure 5.1: Low-thrust transfer trajectory with its initial and final orbits and their corresponding velocity hodographs. [29]

The cylindrical coordinates r , θ and z are used to shape the velocity in three dimensions, resulting in a radial, transverse and axial velocity. The equations of motion in cylindrical coordinates are the following:

$$\ddot{r} - r\dot{\theta}^2 + \frac{\mu}{s^3}r = f_r \quad (5.1)$$

$$r\ddot{\theta} + 2\dot{r}\dot{\theta} = f_\theta \quad (5.2)$$

$$\ddot{z} + \frac{\mu}{s^3}z = f_z \quad (5.3)$$

where the dotted variables represent the first (one dot) and second (two dots) time derivatives, $s = \sqrt{r^2 + z^2}$ is the distance from the central body and f_r , f_θ and f_z are the low-thrust accelerations generated by the spacecraft. This method uses a two-body formulation, where the only considered gravitational acceleration is that due to the central body; in this case, the Sun.

The trajectory can then be computed by integrating the radial, transverse and axial velocities (V_r , V_θ and V_z , respectively). While the polar angle requires numerical integration, the radial and axial distances can be integrated analytically if their corresponding velocity functions are simple. Therefore, these velocity functions are made up of base functions, which are a sum of polynomial, trigonometric, and exponential terms. At least three base functions for each velocity component are needed to satisfy three boundary conditions: mainly on initial and final velocity and on the difference between the initial and final position. However, more base functions can be added to improve the hodographic solutions. These will result in extra degrees of freedom and their corresponding coefficients, which can be optimized to find (near-)optimal trajectories. For this study, the base functions recommended by Gondelach and Noomen [29] for a similar transfer problem will be used: CPowPow2PSin05PCos05 for the radial component, CPowPow2PSin05PCos05 for the transverse component, and Cos25P3SinR5P3CosR5P4CosR5P4SinR5 for the axial component. This means that, apart

from three base functions for each component to satisfy their corresponding boundary conditions, two more base functions are added to each component. These last base functions are known as higher-order functions, which will result in a total of six free parameters that enable an optimization of the problem.

By substituting V_r , V_θ and V_z and their derivatives and integrals into the aforementioned equations of motion, the needed thrust acceleration in each direction can be computed. Then, the total thrust acceleration can be computed as:

$$f = \sqrt{f_r^2 + f_\theta^2 + f_z^2} \quad (5.4)$$

And finally, the required Delta-V can be obtained by numerically integrating this thrust acceleration over time:

$$\Delta V = \int_0^{t_f} f dt \quad (5.5)$$

5.1.2. Simulation

The Mission Analysis is performed using the Tudat Python library. This library supports astrodynamics and space research by implementing a wide range of functionalities, including the aforementioned hodographic-shaping method. For the calculations herein, Cartesian coordinates are used, with the reference frame origin located at the Solar System barycenter and the ‘ECLIPJ2000’ inertial frame orientation. ‘ECLIPJ2000’ is a right-handed inertial frame which has its x-axis oriented towards the vernal equinox and its z-axis oriented perpendicular to the ecliptic, at the J2000 epoch. While the hodographic shaping method uses cylindrical coordinates, the necessary reference frame transformations are implemented in lower levels of the applicable functionalities. On another note, the pre-defined ephemerides and rotation models of Solar System bodies used in Tudat are derived from so-called Spice kernels. Spice is a toolkit developed by NASA’s Navigation and Ancillary Information Facility (NAIF) and is used throughout the space industry for the design and analysis of planetary missions. The first step in any Tudat simulation is always to define a system of bodies and retrieve their information using the `get_default_body_settings()` function. The vehicle and its properties (e.g., mass, specific impulse of its thrusters) can also be added to this system of bodies.

Three different types of formulations will be used to describe the interplanetary trajectories dealt with in this section. First of all, Lambert’s problem will be used to constrain the launch dates to be analyzed in further steps. This analytical formulation is used to compute ballistic orbital trajectories. It is based on Keplerian orbital motion, which assumes a two-body problem where the mass of one body is infinitesimal. Lambert’s theorem states that the transfer time of a body moving between two points on a conic trajectory is a function only of the sum of the distances of the two points from the origin of the force, the linear distance between the points, and the semi-major axis of the conic [57]. In Tudat, the `get_lambert_problem_result()` function can be used to calculate a trajectory between two Solar System bodies by providing the initial and target bodies and departure and arrival epochs. However, these calculations assume impulsive thrust manoeuvres at the start and at the end of the transfer to escape and enter the orbits of each respective body. Thus, Lambert’s problem is not applicable to the low-thrust trajectories to be studied for the mission and will only be used for the preliminary departure date analysis.

The simulation of the low-thrust trajectories will mainly be performed using the hodographic-shaping method. In this case, given the departure and target bodies, a departure date, a TOF and a number of revolutions around the central body (N), a low-thrust trajectory can be computed using the shape of its velocity hodograph. As explained in Subsection 5.1.1, two higher-order base functions are used in each of the velocity components. Therefore, a total of six free coefficients can be specified as inputs to the trajectory, which will be used to optimize the results in a later stage. The `trajectory_design` module in Tudat includes functionalities for the definition of these shaping functions, which can then be passed on as parameters of the `hodographic_shaping_leg()` function to specify the trajectory (i.e., leg of the transfer) settings. Initial and final orbits around the departure and target bodies (that is, nodes of the transfer) can also be specified using the `departure_node()` and `capture_node()` functions. Using these settings, and specifying the departure, target and central bodies, the `create_transfer_trajectory()` function can then be used to create a trajectory object. This object can be evaluated by specifying departure and arrival epochs to obtain, among other information, the states of the spacecraft along the trajectory, its thrust acceleration profile, and the total needed Delta-V.

The final trajectory calculation method comprises a numerical propagation of the trajectory. Using this approach, the thrust acceleration profile calculated using the hodographic shaping method can be used to propagate the state of the vehicle. While this method is more computationally demanding, the environment models can be extended to include third-body or solar radiation pressure effects, among others. Since the gravitational acceleration of the initial and target bodies will be taken into account, a buffer time needs to be implemented. This way, the propagation can start and finish outside of their sphere of influence and their perturbations are not dominant. Consequently, the initial and final state vectors for the propagation will not exactly match those for the hodographic-shaping method. To perform these simulations, the propagator and integrator settings need to be defined. On the one hand, the propagator settings encompass the different accelerations to be considered during the propagation and translational state representation type. On top of that, the mass of the spacecraft can also be propagated taking into account the hodographic thrust profile, which results in more realistic Delta-V and thrust calculations. On the other hand, the integrator type needs to be selected along with its corresponding settings. The `create_dynamics_simulator()` function from the `numerical_simulation` module is used to propagate the trajectory and retrieve the spacecraft state history.

Both the hodographic-shaping and propagation methods can be used to calculate the low-thrust Earth-Mars trajectories with particular advantages. While the hodographic shaping method offers reduced computational power, the propagation method offers more realistic results. As the optimization process will entail a significant computational load, an analysis is needed to gauge if a more realistic propagation method that accounts for perturbations along the trajectory is truly needed.

Environment analysis

For this propagation analysis, a position accuracy requirement of 1 km is chosen, as established by SR-GNC-01 presented in Subsection 4.1.4. For the numerical model requirement, an accuracy three orders of magnitude lower will be used [20]. This results in a numerical model requirement of 1 m. A time step for the propagation needs to be found that satisfies this numerical model requirement. To do so, an error analysis is performed by propagating the same unperturbed trajectory (i.e., only gravitational acceleration from the Sun) using an 8th-order Runge-Kutta integrator for an array of time steps. For each time step, the error is calculated by comparing the associated state history with the resulting state history using the next time step in the array. This gives the order of magnitude of the associated error for a certain time step [20]. The Cowell formulation is used, which uses Cartesian

elements as the propagated states. Figure 5.2 shows the maximum position error for each evaluated time step. As can be seen, the numerical model requirement is met with time steps lower than five days. For time steps below two days, truncation errors dominate so that the error behaviour cannot be estimated. Therefore, a numerical model time step of three days is chosen for the following step of the analysis.

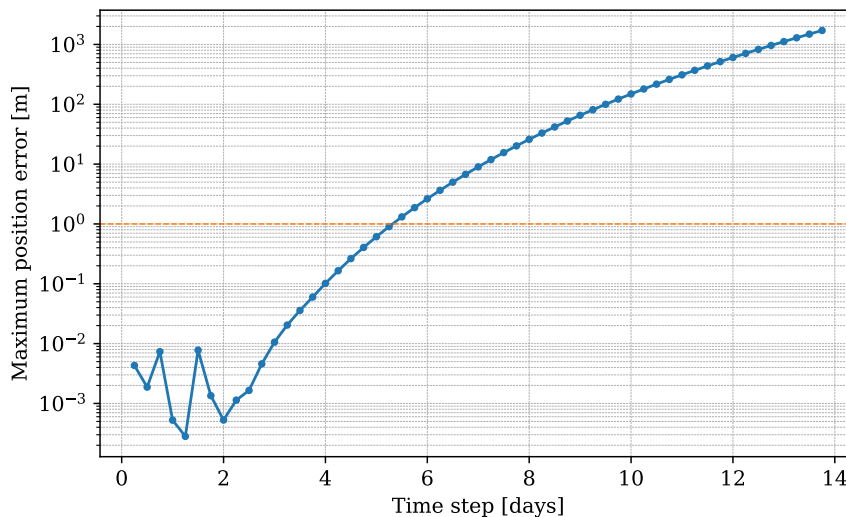


Figure 5.2: Maximum position error for different time steps.

Then, a perturbed trajectory can be simulated. Tudat offers different environment models that can be used for this type of simulation. For this analysis, the following perturbations are used: the point-mass third-body perturbations of all planets in the Solar System and the Moon; the spherical harmonic J_2 term third-body perturbations of the Earth, the Moon and Mars; the solar radiation pressure effect and the relativistic perturbations of the Sun. The effect of each of these types of perturbations on the trajectory has been analyzed. Figure 5.3 shows the position error due to each different type of perturbation along the trajectory. Here, the perturbed propagations are compared against the (unperturbed) benchmark. As can be seen, all these perturbations lead to a position error higher than the position accuracy requirement. Therefore, all the following perturbations will need to be taken into account:

- Third-body point mass perturbations of all planets in the Solar System and the Moon.
- Third-body spherical harmonic J_2 term for the Earth, the Moon and Mars.
- Solar radiation pressure with a reference area of 0.6 m^2 and a $C_R = 1.2$.
- Schwarzschild relativistic correction for the Sun.

Finally, a set of simulations has been performed including all the aforementioned perturbations. However, the hodographic solution starts and ends at the centers of the departure and target bodies. Therefore, a time buffer at the start and at the end of the simulation has been added so that the propagation starts and ends outside of the sphere of influence of the departure and target bodies. This means that the initial state of the propagation will not be at the center of the Earth, but in a state from the hodographic solution outside of Earth's sphere of influence. This ensures that the third-body perturbations of these bodies (including Earth and Mars) are not dominant. Through this analysis, the magnitude of the perturbation forces can be compared to the magnitude of the hodographic

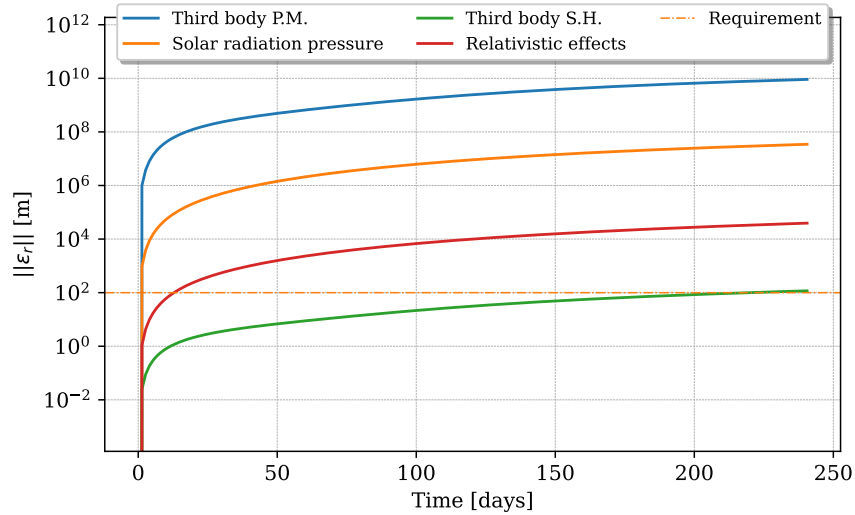


Figure 5.3: Position error due to different perturbations along the trajectory.

thrust. As a result, the total perturbation forces have been observed to be consistently around two orders of magnitude lower than the thrust that follows from the hodographic solution. Figure 5.4 shows the perturbation forces and the hodographic thrust profiles along a test case trajectory, where this behaviour can be seen. This test case has been selected randomly from the optimized trajectories shown in Figure 5.6, with a departure date on 2028-11-02, a TOF of 290 days (corresponding to zero revolutions around the Sun) and a Delta-V of 8.5 km/s. A buffer of ~ 15 days is applied to the propagation for the reasons stated above.

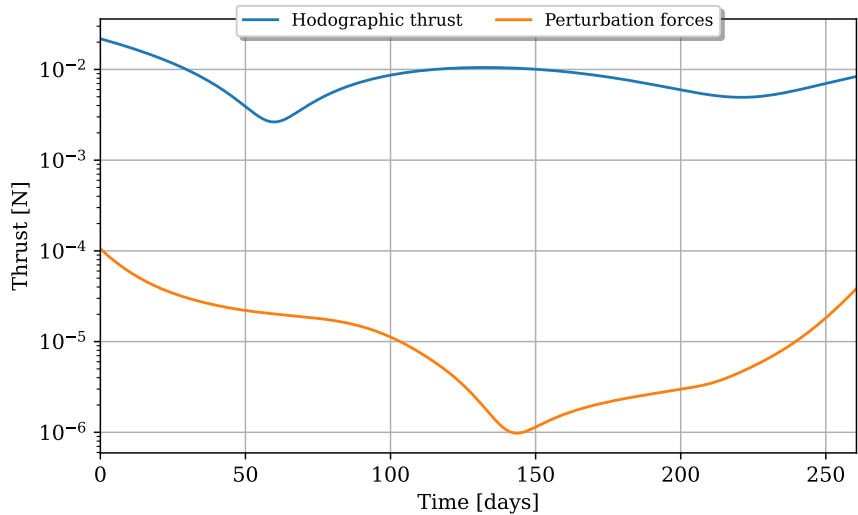


Figure 5.4: Hodographic thrust and perturbation force profiles acting during the trajectory.

Consequently, if a simulation were performed that accounted for the perturbation forces in the thrust profile, it would not lead to a significant change in the resulting Delta-V for the transfer and therefore the feasibility of the mission. While a perturbed simulation would show a more realistic representation, it is deemed out of the scope of this preliminary study. On top of that, the perturbed propagation regularly takes up to 10 times more computation time than the hodographic-shaping

method. This can be critical in the context of an optimization analysis, where the number of trajectory calculations goes up to the millions. Therefore, a two-body formulation perturbed by thrust only (such as the hodographic-shaping method) is considered to provide the best tradeoff between computational load and accuracy of results, and will be used for the optimization procedure.

5.1.3. Departure date analysis

As explained in Section 4.3, one of the most interesting options to launch the mission is to piggyback on another Mars-bound launch. These missions usually perform ballistic transfer trajectories to Mars using launchers that provide excess energies of $C_3 \sim 15 \text{ km}^2/\text{s}^2$. Lambert's problem can be used to locate the launch windows that correspond to such excess energy. While the CubeSat will perform a low-thrust trajectory, its departure date will be tied to these 'Lambert solution' windows. In this way, the departure dates can be constrained for the next steps of the Mission Analysis.

Given an initial and final position, together with a time of flight, Lambert's problem can be used to determine the connecting orbit. This method uses a two-body formulation, which can be solved analytically by Keplerian orbital motion. By comparing the velocities in the transfer orbit and the planet's orbits, the excess velocity of the spacecraft at the start and the end of the trajectory can be found. This velocity difference at the start of the trajectory can be linked to the launch energy as $C_3 = V_\infty^2$. By performing a grid search over a defined set of departure dates and Times of Flight (TOF), the launch energy can be represented in a so-called 'Porkchop Plot'.

According to established requirements presented in Section 3.1, the mission shall be ready for launch in less than four years. Therefore, the first two launch windows after 2027 will be analyzed. Figure 5.5 shows a porkchop plot for each launch window. The contours in these plots represent combinations of departure date and TOF that result in Keplerian trajectories with the same launch energy. In this case, the interest lies in the areas with a C_3 equal or lower than $15 \text{ km}^2/\text{s}^2$. These regions have been filled in, effectively defining the departure date range for the next steps of the Mission Analysis. In this case, the TOF is irrelevant, since the trajectories to be performed by the mission are not ballistic, but rather low-thrust. A month has been added to each end of these departure date sets as a margin. Therefore, the two departure date search spaces to be analyzed are: for the 2028/2029 launch window, from 2028-10-15 to 2029-05-01; and for the 2030/2031 launch window, from 2030-11-01 to 2031-06-15.

5.1.4. Optimization

The goal of this optimization analysis is to assess if low-thrust Earth-Mars trajectories can be found that ensure the success of the mission. The total trajectory Delta-V and the maximum thrust along the trajectory will be studied for the launch windows established in Subsection 5.1.3 to check if they comply with the requirements of the mission. As it stands, the designed CubeSat offers up to 4.8 km/s of Delta-V for the Earth-Mars transfer and can provide up to 1.25 mN of thrust, as presented in Subsection 4.1.2.

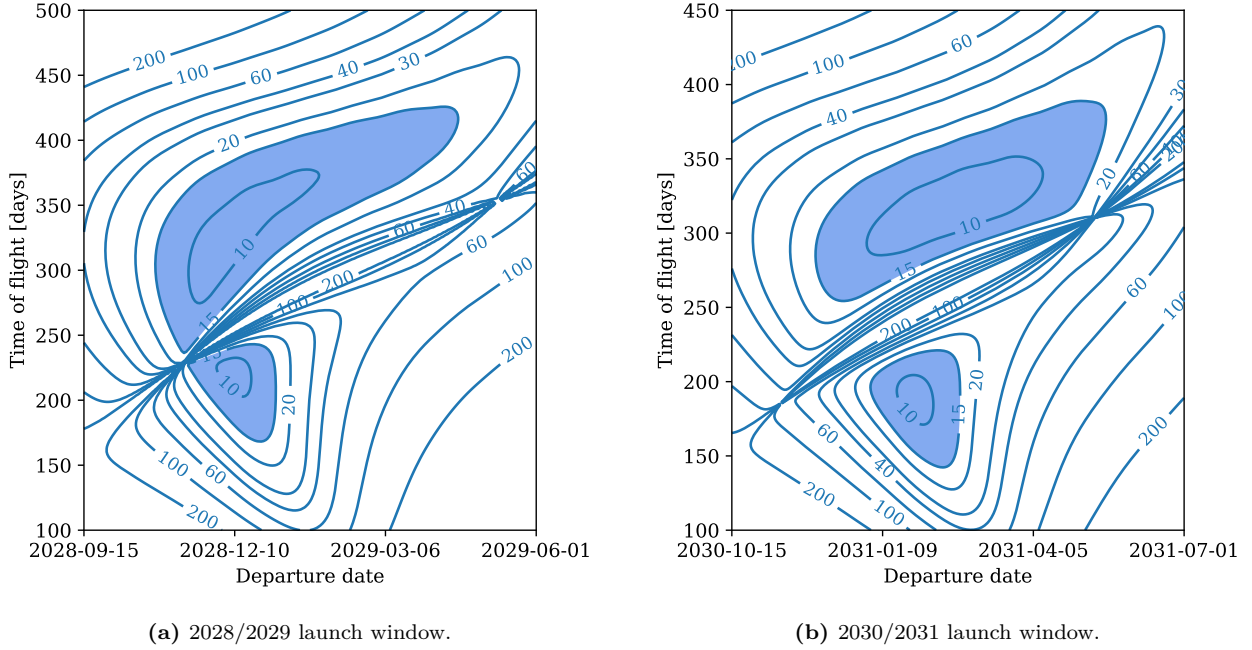


Figure 5.5: Porkchop plots of C_3 for the next two possible Earth-Mars launch windows. The coloured area represents trajectories with $C_3 \leq 15 \text{ km}^2/\text{s}^2$.

Methodology

The main parameter to be optimized in this analysis is the total low-thrust Delta-V for the trajectory. On top of that, the maximum thrust along the trajectory will also be studied and will be used as a constraint to establish feasibility. The complete list of decision variables is as follows:

- **Departure time** (t_0): it will influence the initial state.
- **Time-of-flight** (TOF): it will vary the final time and thus the shaping of the trajectory and the arrival conditions.
- **Number of revolutions** around the Sun (N): the higher this number, the greater ToF. These two variables are strongly related and only certain combinations make the transfer feasible.
- The **six free parameters** for radial, normal and axial shaping functions ($c_{r,1}, c_{r,2}, c_{n,1}, c_{n,2}, c_{a,1}, c_{a,2}$): they will change the shape of the transfer trajectory and the thrust profile.

These decision variables will serve distinct roles within the optimization process. A grid search will be performed using the departure date, TOF and number of revolutions around the Sun. Then, for each combination of departure date, TOF and number of revolutions around the Sun, an optimization of the hodographic free parameters will be performed to find the best solution in terms of Delta-V. The optimization procedure will be performed for both launch windows discussed in the previous section. Therefore, the decision variable design space is shown in Table 5.1.

Launch window	Departure dates	TOF [days]	N. revs.	Free parameters
2028/2029	2028-10-15 to 2029-05-01	150 to 1400	0 to 2	-10000 to 10000
2030/2031	2030-11-01 to 2031-06-15	150 to 1400	0 to 2	-10000 to 10000

Table 5.1: Decision variable design space for the optimization.

The optimization of the free parameters will be performed using the `Pygmo` library in Python. While this library offers a variety of single-objective optimization algorithms, many studies point towards differential evolution (DE) algorithms being the most appropriate for interplanetary trajectory optimization [59]. This algorithm works by using a particular scheme to generate vectors of design variables: new vectors are generated by adding the weighted difference vector between two population members to a third member [55]. As they only require a few robust control variables, DE algorithms are user-friendly and straightforward to implement. However, they have their limitations, as they are susceptible to instability and getting trapped into local optima [61]. The risk for this to occur is strongly reduced by implementing a grid search on three decision variables. In conclusion, the DE algorithm will be used for the optimization process.

This optimization procedure is implemented as follows. For each point in the grid search, an initial population is generated with 100 different combinations for the free parameters. The objective (i.e., the Delta-V) for each of these combinations is evaluated and the population is evolved using the DE algorithm. For each generation of the population, the arithmetic average of the objective for each combination is calculated. Finally, the optimization procedure will stop once this average has reached convergence or a maximum number of generations is achieved. A preliminary analysis has been performed, showing that a convergence rate of 1% for 5 consecutive generations and a maximum number of generations of 100 are appropriate for this analysis. The default parameters set by `Pygmo` will be used for the DE algorithm. This means that a weighting factor of 0.8 and a crossover of 0.9 will be applied. An analysis of their impact on the results is reserved for future work. The seed number used for the optimization is 42.

A set of preliminary calculations has been performed to assess the robustness of the optimization given different seed numbers. To do so, the Delta-V has been optimized for a specific departure date, TOF and N using the following seed numbers: 42, 14, 1702, 221018, 300321. The optimum obtained for the first launch window (Figure 5.9) has been selected as a reference, with a departure date on 17-04-2029, a TOF of 1079 days and $N = 2$. Table 5.2 shows the Delta-V obtained in the optimization using the seeds mentioned above, in the specified order. As can be seen, the results have an average of 6.124 km/s, with a standard deviation of 0.101 km/s. For this preliminary study, a standard deviation of an order of magnitude lower than the results will be considered adequate to determine feasibility.

Seed 1	Seed 2	Seed 3	Seed 4	Seed 5	Average	Std. Dev.
5.991	6.225	6.063	6.085	6.257	6.124	0.101

Table 5.2: Optimized Delta-V for departure date on 17-04-2029, a TOF of 1079 days and $N = 2$ using different seed numbers. All the values are in km/s.

Results

A first analysis is performed on a constrained set of departure dates and TOFs in the first launch window for 0 revolutions around the Sun. On the one hand, Figure 5.6a shows the optimized Delta-V for each departure date and TOF combination on a 20 x 20 grid. For each of these optimal trajectories, their maximum thrust is represented in Figure 5.6b. As can be seen, the dynamics of the system result in an optimum Delta-V area where the best trajectories for earlier departure dates are achieved at higher TOFs. This can be explained by studying the relative distance between Earth and Mars, as the closest approach between the two celestial bodies takes place in March 2029. Therefore, the farther away in time the departure date is from that closest approach, the more time will be needed to reach the target body efficiently. These higher TOFs also go hand in hand with a lower maximum thrust. This is logical as the thrust acceleration profile is distributed over an extended trajectory, leading to a reduction in the average acceleration and the occurrence of peak accelerations. There is a certain point (i.e., upper left) in which the TOF is too high for a trajectory that does not complete a full revolution around the Sun.

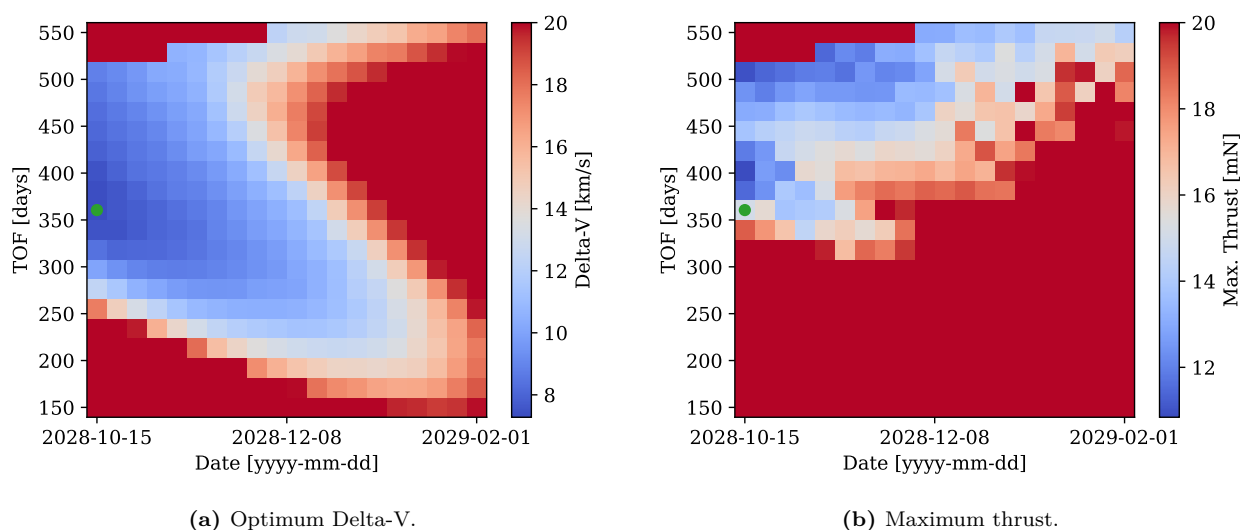


Figure 5.6: Optimum Delta-V and corresponding maximum thrust on a 20 x 20 grid for a constrained set of decision variables with $N = 0$ in the first launch window.

The green dot in Figure 5.6 represents the most optimal trajectory, with a minimum Delta-V of 7.27 km/s and a maximum thrust of 15.08 mN. By numerically propagating this trajectory using its hodographic thrust profile, a more realistic simulation can be performed. This results in a propagation low-thrust Delta-V of 5.86 km/s and a maximum thrust of 9.86 mN. Two primary factors contribute to these significant reductions in Delta-V and maximum thrust. The thrust profiles for the hodographic and the propagated trajectories are shown in Figure 5.7 to exemplify these reasons. First of all, the numerical propagation accounts for the loss of propellant mass along the trajectory, while the hodographic trajectory assumes a constant spacecraft mass. For a given acceleration value at any epoch beyond departure, this translates into a lower value for the required thrust. On top of that, a time buffer of 10 days has been used at the start and at the end of the propagated trajectory so that it is constrained outside the bounds of the SOIs of the Earth and Mars. This propagated trajectory does not reach the center of mass of either Earth or Mars, and is slightly truncated at both ends. Although this results in a Delta-V that could be accommodated with an increased propellant tank, the maximum thrust for this trajectory is still one order of magnitude higher than the propulsion system requirement, rendering it unfeasible. Therefore, this analysis shall be extended to include

trajectories that perform one and two revolutions around the Sun.

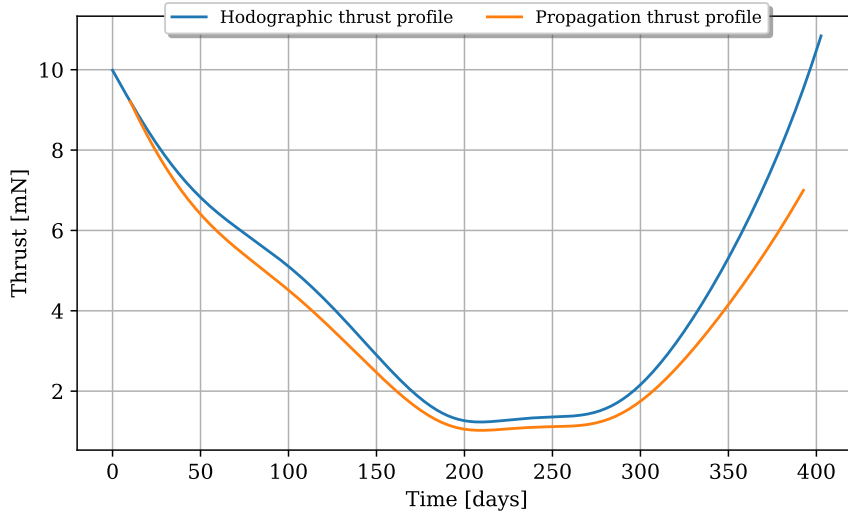


Figure 5.7: Hodographic thrust and propagation thrust profile for the optimum trajectory in Figure 5.6.

The number of revolutions around the Sun cannot be an input to the optimization procedure. Therefore, the results for different values of N shall be computed independently for the same grid. Figure 5.8 shows the optimum Delta-V for the same grid using zero, one and two revolutions around the Sun. As can be seen, optimal trajectories can be found in different regions of the search space for different values of N . It is reasonable that trajectories involving a greater number of orbits around the Sun will inherently require a longer duration of flight. In order to provide a full picture of the search space, the plots for different values of N can be combined by finding the best Delta-V value for each combination of departure date and TOF among them.

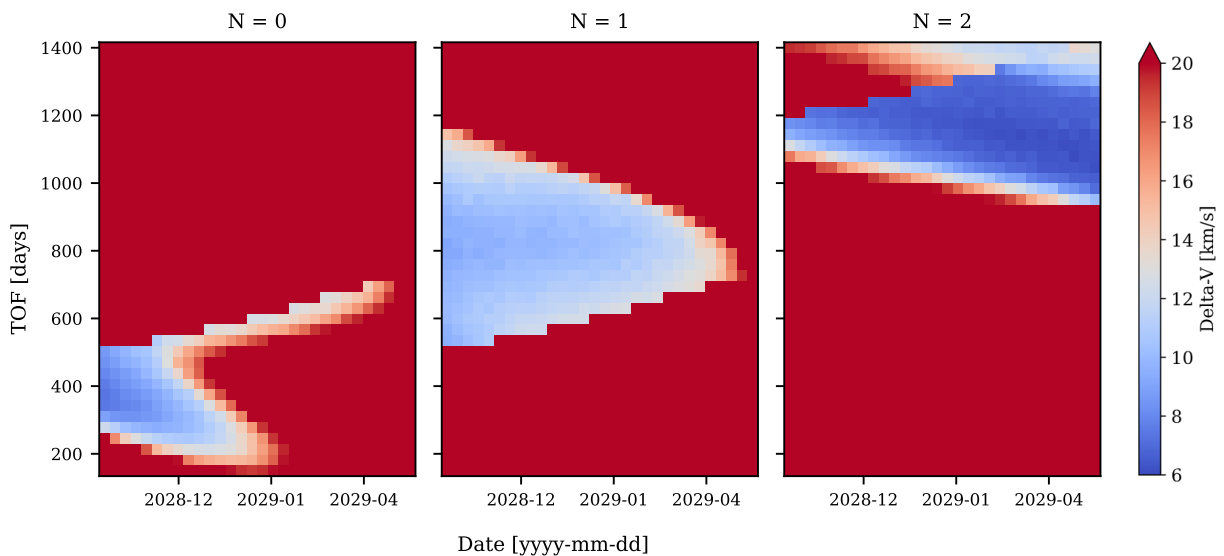


Figure 5.8: Optimum Delta-V for a 30 x 40 grid for the first launch window using different number of revolutions around the Sun (N).

2028/2029 launch window

The optimization procedure is performed on the complete design space allocated for the 2028/2029 launch window. Figure 5.9 shows the combined results of the optimization procedure for $N = 0-2$. On the one hand, Figure 5.9a shows the optimum values of Delta-V. As explained previously, three local minimum areas can be recognized, each originating from distinct values of N . The area that shows the most promising results is that corresponding to $N = 2$, which is consistent with the results presented by Gondelach and Noomen in a similar study [29]. This area shows great potential in Delta-V, with values around 6-7 km/s throughout the departure date range. Additionally, peak thrust values in this region decrease to 2 mN, a notable improvement over the results mentioned above for $N = 0$.

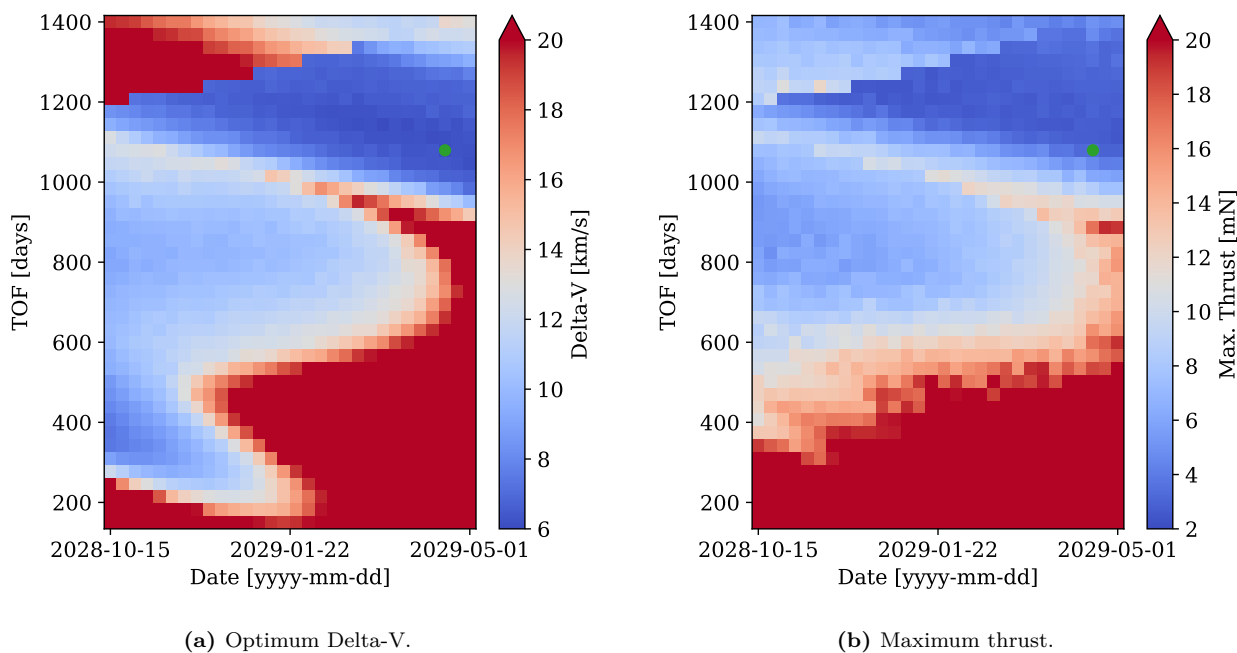


Figure 5.9: Optimum Delta-V and corresponding maximum thrust on a 30 x 40 grid for the first launch window with $N = 0-2$. The green dot shows the most optimal trajectory in terms of Delta-V.

In this analysis, the best trajectory is indicated by the green dot. It departs on 2029-04-17 and has a TOF of 1079.5 days. This solution yields a total Delta-V of 5.99 km/s and a maximum thrust of 3.28 mN. By numerically propagating this trajectory, the Delta-V and maximum thrust go down to 5.07 km/s and 2.56 mN, respectively. This trajectory is located in the local optima region with higher TOF (i.e., 900-1400 days) for $N = 2$. A local refinement analysis is performed in this area with increased resolution to check for better solutions. Figure 5.10 shows a local refinement analysis on the $N = 2$ optimum region. As can be seen, the best trajectory coincides with the one obtained with the full analysis. However, when comparing the most optimum solution for each departure date for the full analysis and local refinement, the local refinement provides improvements in the order of 0.1 km/s for certain departure dates. It can then be concluded that limited optimization can be achieved using a finer mesh.

To assess the feasibility of these trajectories across the launch window, the best trajectory in the local refinement region for each of the analyzed departure dates is numerically propagated. The Delta-V and maximum thrust for each of these optimum propagations are shown in Figure 5.11. This figure clearly shows a downward trend in Delta-V as the departure is pushed to later dates. As this trend seems to continue into future departure dates, a lower Delta-V could be achieved if the launch window

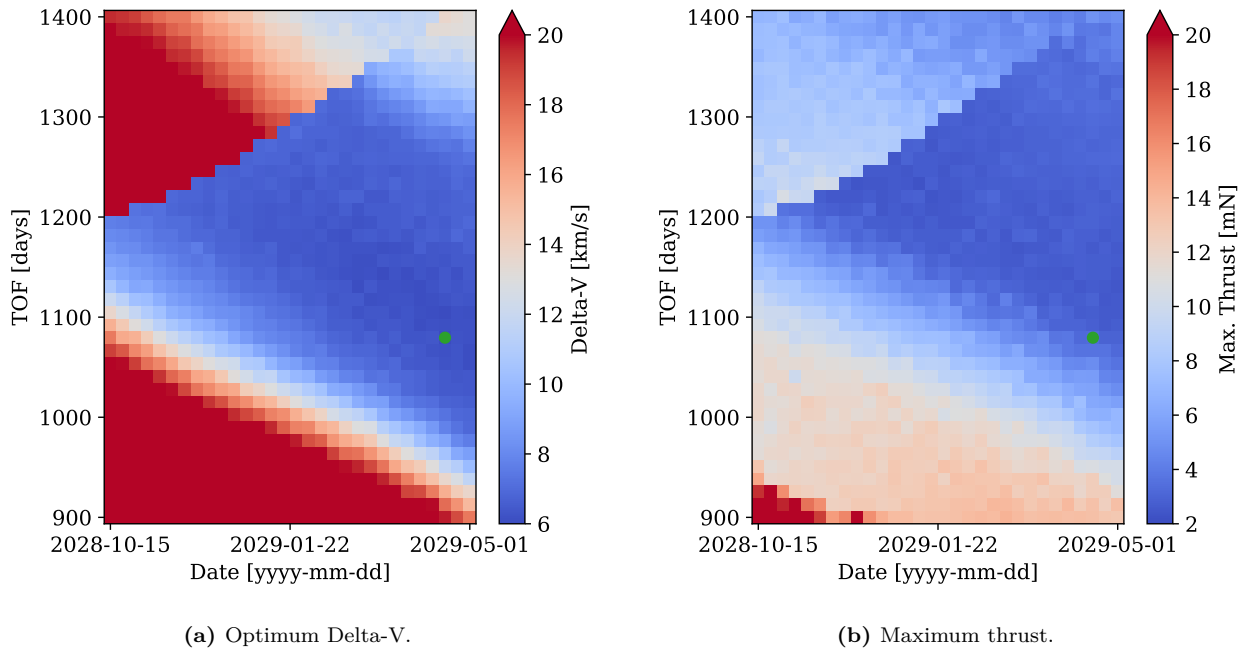


Figure 5.10: Optimum Delta-V and corresponding maximum thrust on a 30 x 40 grid for the local optima region with $N = 2$ for the first launch window. The green dot shows the most optimal trajectory in terms of Delta-V.

was widened using the other launch methods discussed in Section 4.3. However, the required Delta-V is higher than the requirement established in Subsection 4.1.2 for all the analyzed departure dates. One possible solution is to raise the Delta-V requirement by 1 km/s since the system can allocate more propellant. This change would result in viable trajectories in terms of Delta-V for over 75% of the proposed departure dates.

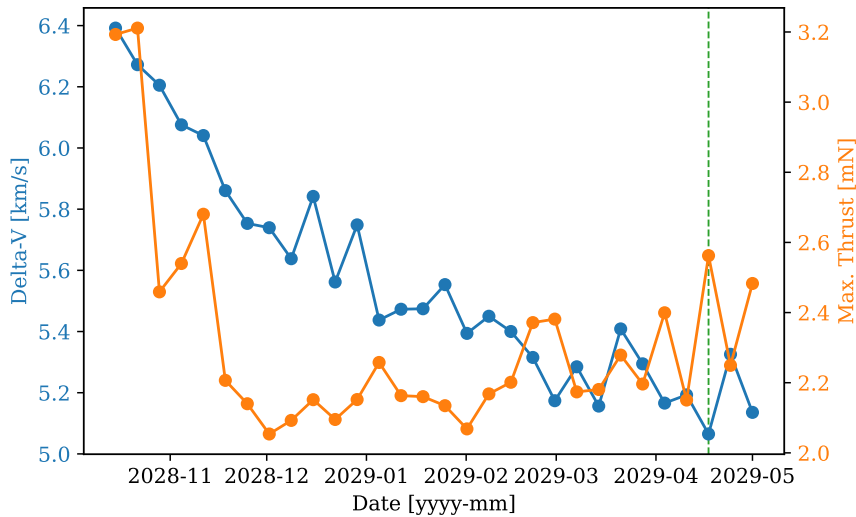


Figure 5.11: Delta-V and maximum thrust for the propagated optimum trajectory for each of the analyzed departure dates in the first launch window. The green dashed line shows the epoch of the best solution in Figure 5.10.

Regarding the behaviour of the maximum thrust, Figure 5.11 shows a significant drop to 2 mN after the 15th of November. For the following departure dates, a slight upward trend is observed, reaching

~ 2.5 mN at the end of the launch window. Therefore, there is a trade-off to be made: an earlier departure date requires a lower maximum thrust, whereas a later departure date is preferable in terms of Delta-V. In the context of this mission, the most critical requirement is for the maximum thrust, making an earlier departure date preferable. Still, the lowest maximum thrust in this analysis is 2 mN, which is an increase of 60% over the requirement of 1.25 mN. Therefore, a strategy is necessary to further reduce this number. Figure 5.12 shows the thrust profile of the best trajectory in terms of the maximum thrust in Figure 5.11. As can be seen, more than 60% of the trajectory complies with the maximum thrust requirement of 1.25 mN. However, there is a high thrust region in the later stages of the transfer that has been observed in all other trajectories of Figure 5.11. Further analysis of these trajectories shows that the average thrust of all the optimum propagations is below 1.25 mN. This means that the thrust of these trajectories could in principle be distributed over the length of the trajectory to mitigate these peaks.

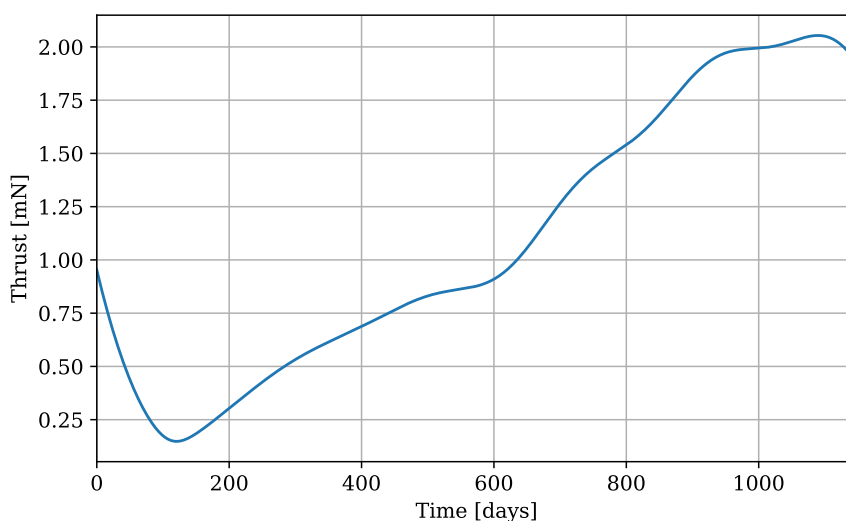


Figure 5.12: Thrust profile along the trajectory for the optimum trajectory with departure date on 2028-12-01 shown in Figure 5.11.

An additional analysis is conducted within the local optima region for the case of $N = 2$. In this analysis, the maximum thrust is optimized instead of the Delta-V. In this manner, the minimum bound for the maximum thrust can be determined. The results for the Delta-V and maximum thrust of this analysis are shown in Figure 5.13. Using the hodographic method, the trajectory that offers the lowest maximum thrust departs on 2028-12-15 and has a TOF of 1244.8 days. This trajectory uses a combined Delta-V of 8.83 km/s with a maximum thrust of 2.18 mN. The propagated trajectory offers a reduced Delta-V and a maximum thrust of 7.76 km/s and 1.6 mN, respectively. These findings are encouraging as the optimization process produces maximum thrust values that exceed the requirement only by 30%, a significant improvement over the 60% in the previous analysis. However, this comes at the cost of a considerable increase in Delta-V. As a result, one can infer that a multi-objective optimization process could provide a trade-off between both objectives.

Before moving on to study the second launch window, the effects of launch excess velocity will be considered. Up to this point, it has been assumed that the spacecraft starts its Earth-Mars transfer with the same heliocentric velocity as the Earth so that the excess velocity is $V_\infty = 0$ km/s. Thus, the spacecraft departs on a parabolic trajectory. However, a gain in Delta-V needed for transfer could potentially be achieved if the spacecraft used all the excess energy that the launch vehicle can provide (i.e., $C_3 = 15$ km²/s²). In that case, an excess velocity of up to ~ 4 km/s can be achieved.

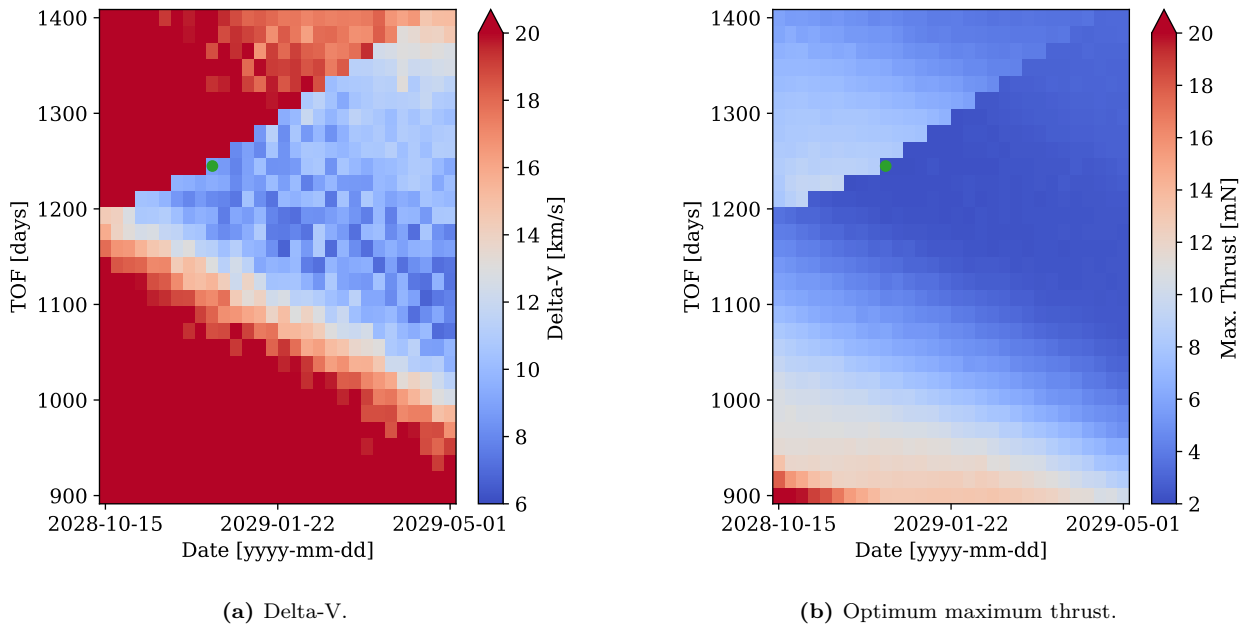


Figure 5.13: Optimum maximum thrust and corresponding Delta-V on a 30 x 30 grid for the local optima region with $N = 2$. The green dot shows the most optimal trajectory in terms of maximum thrust.

A Delta-V optimization study over the full range of decision variables is performed again for the 2028/2029 launch window, but this time considering an excess velocity of $V_\infty = 4$ km/s. The results of this analysis are shown in Figure 5.14. As can be seen in Figure 5.14a, this analysis only produces an interesting local optima region for low TOF and $N = 0$. This behaviour can be explained by the fact that these trajectories resemble the Kepler trajectories with the same departure date, TOF and with an excess velocity of 4 km/s. In regions of the search space where the low-thrust trajectories are considerably different from their ballistic counterpart, an excess velocity leads to worse results.

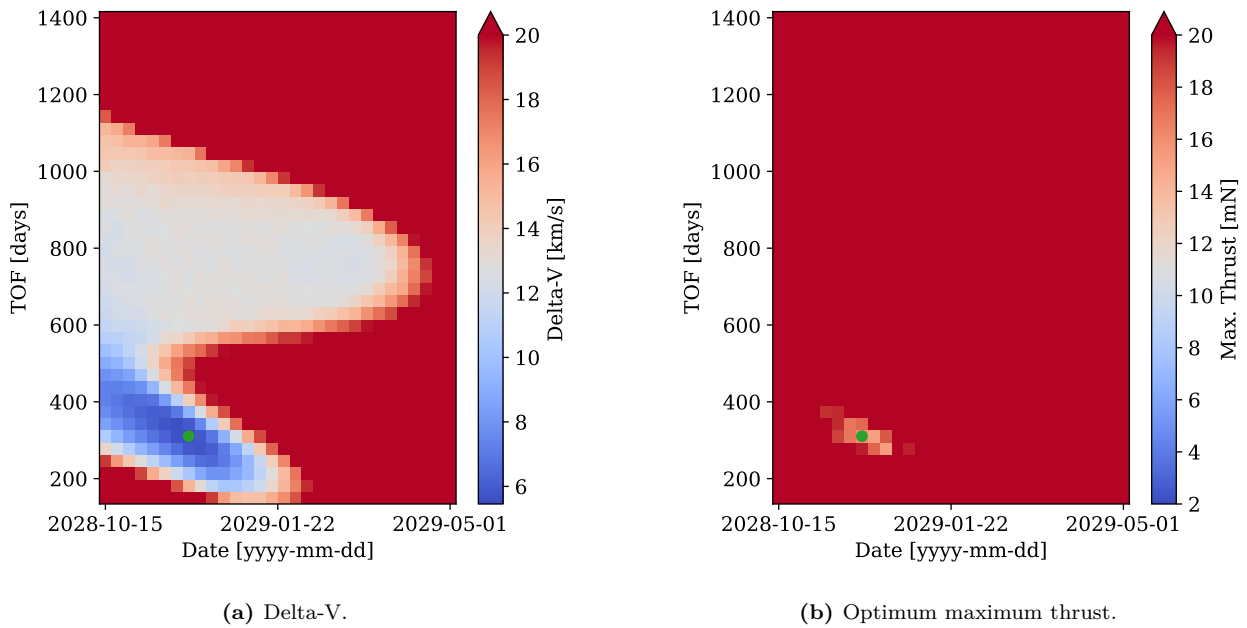


Figure 5.14: Optimum Delta-V and corresponding maximum thrust on a 30 x 40 grid for the first launch window with $N = 0-2$ and excess velocity of $V_\infty = 4$ km/s. The green dot shows the optimal trajectory in terms of Delta-V.

For the trajectories in the optima region corresponding to $N = 0$, better Delta-V results are achieved when compared to the analysis for zero excess velocity. However, the addition of the initial velocity induces a substantial increase in the maximum thrust for these trajectories, as can be seen in Figure 5.14b. For example, the optimum trajectory is performed with a Delta-V of 5.5 km/s. However, the maximum thrust for this trajectory is 16.61 mN, which is an order of magnitude higher than the requirement, and therefore unfeasible. Propagating the trajectory does not improve the feasibility, as the maximum thrust only drops to 11.92 mN. Therefore, it can be concluded that an excess velocity will only be favourable for a low-thrust trajectory in terms of Delta-V when this trajectory resembles the ballistic trajectory with the same departure date and time of flight, so it will not be considered further.

2030/2031 launch window

A similar analysis is performed on the 2030/2031 launch window. First, a full-grid analysis is performed on the full range of the specified decision variable design space. The results are shown in Figure 5.15. The outcome of this analysis is comparable to the results for the 2028/2029 launch window shown in Figure 5.9. The Delta-V optima regions are again distributed in three distinct zones, each corresponding to a specific number of revolutions around the Sun. As was the case with the 2028/2029 launch window, the most favourable areas in terms of Delta-V are the ones corresponding to $N = 0$ and $N = 2$. However, the $N = 0$ region is populated with trajectories characterized by excessive maximum thrust values. This is the case with the overall optimum, which is now located in this region. Although this trajectory offers a favourable Delta-V of 6.13 km/s, its maximum thrust is 8.84 mN, rendering it unfeasible. It should be noted that the optimum is located at the boundary of the departure date search space. This means that a better optimum could be achieved if the search space was expanded.

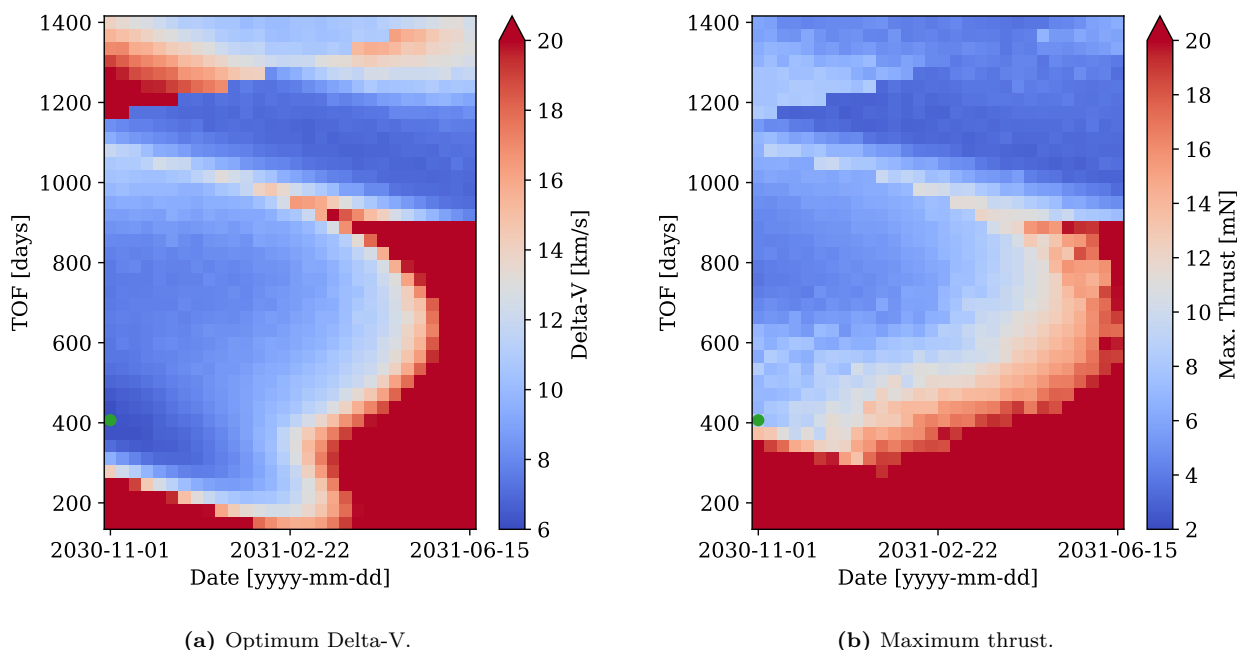


Figure 5.15: Optimum Delta-V and corresponding maximum thrust on a 30 x 40 grid for the second launch window with $N = 0-2$. The green dot shows the most optimal trajectory in terms of Delta-V.

A local refinement analysis provides a better picture of the feasibility of the trajectories in the second launch window. Figure 5.16 shows the results for $N = 2$ and TOF from 850 to 1300 days. The outcome

of this analysis, though not as promising as for the 2028/2029 launch window shown in Figure 5.10, is still optimistic. The local optimum offers a Delta-V and a maximum thrust of 6.71 km/s and 3.17 mN, respectively. These values go down to 5.97 km/s and 2.72 mN when numerically propagating the trajectory. As was the case for the 2028/2029 launch window, this refinement analysis improves the Delta-V of the optimum solutions for certain departure dates in the order of 0.1 km/s.

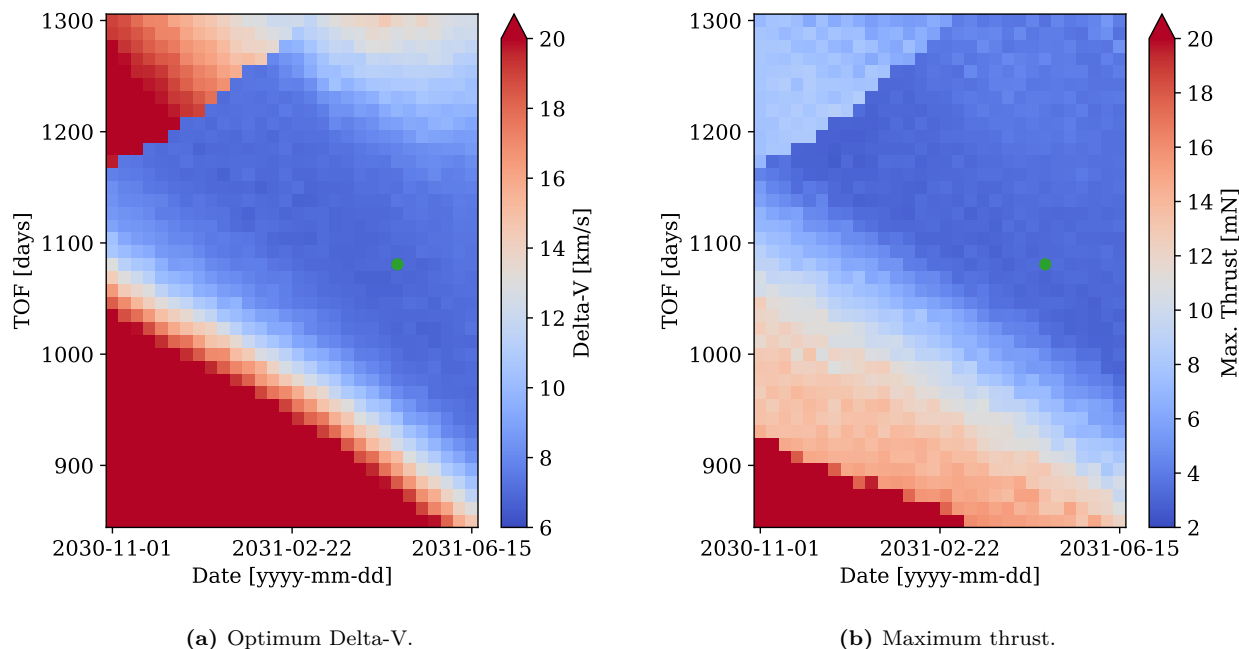


Figure 5.16: Optimum Delta-V and corresponding maximum thrust on a 30 x 40 grid for the local optima region with $N = 2$ for the second launch window. The green dot shows the most optimal trajectory in terms of Delta-V.

For this local optima region, the optimum trajectories for each departure date are numerically propagated. Their corresponding Delta-V and maximum thrust are shown in Figure 5.17. The behaviour of the optimum trajectories is similar to the ones obtained for the first launch window. On the one hand, Delta-V is reduced in the first half of departure dates and then stabilizes at ~ 6 km/s. On the other hand, the maximum thrust also shows a substantial drop on the first departure dates and then grows as the departure date is pushed further back in time. Concerning the maximum thrust, the optimum trajectories for this launch window favour an earlier departure date. This is consistent with the behaviour of optimum trajectories across the 2028/2029 launch window. By increasing the Delta-V requirement of the mission by 1.2 km/s, 75% of the launch dates could result in feasible trajectories, given the thrust peaks are mitigated. This would entail an increase of $\sim 30\%$ in the Delta-V budget for the Earth-Mars transfer and an increase in propellant mass of ~ 725 g. The updated mass budget for the space segment with the increased propellant tank is 20.77 kg which complies with the upper limit for a 12U CubeSat of 24 kg as per the CDS [18].

All in all, the optimization results for the 2028/2029 and 2030/2031 launch windows exhibit a high degree of similarity. The behaviour of the optima distributions along the departure date and TOF arrays is similar on both launch windows. This consistency in the results provides a first step towards the verification of the procedures. However, the 2030/2031 launch window does not offer higher feasibility than the one two years prior. Generally, the optimal trajectories within the second launch window require slightly greater Delta-V and maximum thrust compared to those in the initial window. The optimum (propagated) trajectory for the first and second launch windows are 5.07 and

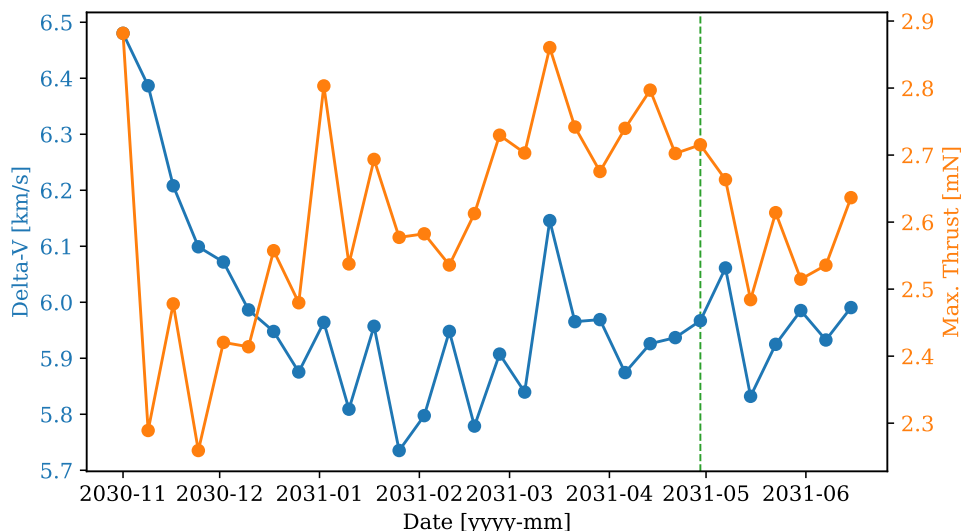


Figure 5.17: Delta-V and maximum thrust for the propagated optimum trajectory for each of the analyzed departure dates in the second launch window. The green dashed line shows the epoch of the best solution in Figure 5.16.

5.74, respectively. Still, these results do not diminish the feasibility of the mission if it were to be launched during the second launch window. As discussed above, the propellant tank can potentially be expanded to increase the Delta-V capabilities of the propulsion system. As was the case for the previous launch window, all these trajectories have an average thrust below 1.25 mN. Therefore, the spikes in maximum thrust can potentially be mitigated by spreading the thrust over the trajectory. It should be noted that in this case, the propagated trajectories result in a different optimum than the one obtained in Figure 5.16. This implies that the propagation method might produce different optima in the studied search space. While it is outside the scope of this work, the optimization procedure should be performed using the propagation method in later stages of the mission design.

Takeaways

As explained above, the initial estimation for the Delta-V needed for the low-thrust Earth-Mars transfer (i.e., 4.8 km/s) is not feasible for the mission. Therefore, the Delta-V requirement for the Earth-Mars transfer shall be increased by 1.2 km/s to a total of $4.8 + 1.2 = 6$ km/s. This will allow feasible trajectories for 80% of the departure dates studied with TOFs in the range of 1000 to 1400 days. As explained, this number of feasible departure dates could be increased by extending the launch windows using other launch strategies. The time of flight of these trajectories is substantially higher than the initial estimations, which accounted for Earth-Mars transfers lasting up to 450 days. This increased mission lifetime of ~ 4 years will have implications for most of the design aspects of the spacecraft in the following iterations, including the mission operations and the durability of the system. However, an increase in the total ionising dose should not be a concern from the radiation tolerance analysis performed in Section 1.3.

By adding the Delta-V required to place the spacecraft in a graveyard orbit at end-of-life to the value stated above, the updated total Delta-V for the system is 6.3 km/s. This increased Delta-V will result in a total propellant mass of 5 kg. Therefore, the final spacecraft launch mass is 20.77 kg, which complies with the upper limit for a 12U CubeSat of 24 kg established by the CDS [18]. Expanding the propellant tank will result in new dimensions for the propulsion system, measuring 88x180x180

mm. Using the spacecraft configuration presented in Subsection 4.1.11, this new volume can also be accommodated. It is worth mentioning that the maximum thrust achieved by these trajectories still exceeds the 1.25 mN requirement by approximately twice the amount. Since the average thrust along these trajectories is lower than the maximum thrust requirement, a strategy can potentially be implemented to distribute this peak in thrust over the entire trajectory. Therefore, the following requirements shall be updated for the next iteration of the system design:

- MR-07: The mission lifetime shall be no more than **4** years including the Earth-Mars transfer.
- SR-SYS-04: The system shall be operational for a maximum of **4** years.
- SR-SYS-10: The SC shall perform a stand-alone Earth-Mars transfer in less than **40** months.
- SR-PROP-01: The propulsion system shall provide at least **6.3** km/s of Delta-V.

In order to comply with these requirements, an updated system is proposed. The updated space segment will have a total Delta-V budget of 6.3 km/s. This will increase the propellant mass compared to the initial estimations by 0.725 kg. Therefore, the wet mass budget of the updated space segment will be 20.77 kg. The new dimensions for the propulsion system are 88x180x180 mm. On top of that, the Earth-Mars transfer will have an increased duration of ~ 40 months. This will lead to an extended mission lifetime of ~ 4 years. All other aspects of the system will remain unchanged.

All in all, the trajectory shown in Figure 5.18 stands out as the optimal choice in terms of Delta-V. This trajectory departs on 2029-04-17, has a TOF of 1079.49 days, and executes two revolutions around the Sun before reaching Mars. Using the hodographic shaping method, the Delta-V and maximum thrust of this transfer are 5.99 km/s and 3.28 mN, respectively. If this trajectory is numerically propagated, which yields more realistic results, this trajectory experiences a reduction in Delta-V to 5.07 km/s, and the maximum thrust diminishes to 2.56 mN.

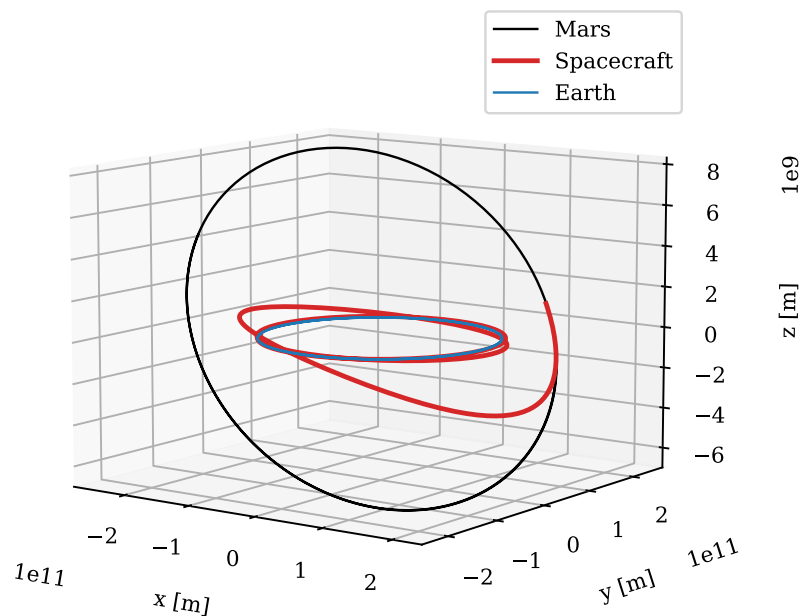


Figure 5.18: Trajectory of the best solution for a low-thrust Earth-Mars transfer for the mission.

5.1.5. Verification

To verify the results obtained here, they must be compared with independent results from other studies. First, the results reported by Gondelach and Noomen in the original hodographic shaping method study [29] are used. On top of that, results from studies that analyze other shaping methods [58], such as spherical-shaping or pseudo-equinoctial-shaping techniques, are included in the analysis. Finally, the results given by DITAN are taken into account. DITAN is a trajectory optimization tool and can be considered as state of the art for low-thrust interplanetary trajectory design. The characteristics of the minimum-Delta-V trajectories found using the aforementioned methods can be seen in Table 5.3.

Method	ΔV [km/s]	f_{max} [10^{-4} m/s ²]
Hohmann	5.50	-
Hodographic - Mars CubeSat	5.99	1.6
Hodographic - Gondelach [29]	5.77	1.5
Spherical [58]	5.74	2.2
Pseudo-equinoctial [58]	5.83	1.6
DITAN [58]	5.66	1.5

Table 5.3: Required Delta-V and maximum thrust acceleration corresponding to minimum-Delta-V trajectory found by different methods for a low-thrust Mars mission.

Table 5.3 shows that the results here perform well compared to other methods. The study conducted using the hodographic method by Gondelach can be seen to provide slightly better results in terms of both Delta-V and maximum thrust acceleration. However, it should be noted that the analysis performed in the original hodographic-shaping method study spans over a substantially wider range of departure dates and uses higher resolution than the optimization presented here. Therefore, it is not unexpected for the study by Gondelach to provide more optimal results. The behaviour of the optimal trajectories examined indicates the possibility of achieving lower Delta-V values by extending the departure date ranges. However, this is reserved for later iterations of the mission analysis. Compared with the spherical-shaping and pseudo-equinoctial methods, the results presented here show good performance. Although the resulting Delta-V for this study is marginally higher, the maximum thrust acceleration is lower than or equal to those obtained with other shaping methods. Hence, the mission analysis results presented here can be considered verified, as they demonstrate strong alignment with both analogous and distinct methods for calculating low-thrust trajectories.

5.2. Mars orbit insertion

Through the shape-based low-thrust transfer presented above, the spacecraft reaches Mars with zero hyperbolic excess velocity. Hence, executing an orbital insertion around Mars requires significantly lower Delta-V compared to a ballistic transfer trajectory. The insertion orbit is assumed to be a highly elliptical 2-sol orbit with a peri- and apoapsis of 300 and 57826 km, respectively. The insertion Delta-V into such an orbit can be calculated using the Tudat functions presented in Section 5.1. For the trajectory shown in Figure 5.18, an insertion Delta-V of 43 m/s is required. This impulsive Delta-V could be achieved using an auxiliary chemical propulsion system. A compact auxiliary propulsion

system could be accommodated given the mass and volume budgets of the spacecraft in this stage of the mission design.

Nevertheless, techniques like ballistic capture could be used, potentially reducing the insertion Delta-V to zero. This is a phenomenon through which the spacecraft is captured into a temporary stable orbit about Mars, only by virtue of the natural attractions of the target body and the Sun [67]. This phenomenon was first exploited in 1990, when the Hiten spacecraft was redirected toward the Moon using a low-propellant trajectory that benefited from the gravitational pull of the natural satellite. Figure 5.19 shows a schematic of a ballistic capture around Mars. The spacecraft enters a highly irregular orbit about Mars after ballistic capture, and some energy needs to be dissipated to stabilise it. This could be done using a low-thrust propulsion system or through some other method for mechanical energy dissipation, such as aerobraking.

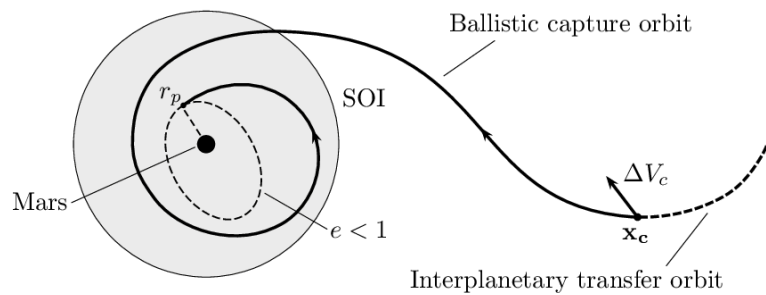


Figure 5.19: Schematic of a ballistic capture around Mars [67].

Aerobraking is a manoeuvre used to slow down or adjust the trajectory of a spacecraft by utilizing a planet's atmosphere to create drag. This technique involves intentionally descending into the atmosphere of a celestial body, typically a planet, at a shallow angle. The resulting friction and air resistance gradually decelerate the spacecraft, allowing it to lower its orbit, change its trajectory, or even enter orbit around the body. Several Mars missions used aerobraking to attain their science orbits, including Mars Odyssey [63] and Mars Reconnaissance Orbiter [48], among others. This technique could be used to lower the altitude and circularize the orbit after ballistic capture to reach the PSO.

5.3. Mars science orbit

As explained in Section 3.1, the main scientific objectives of the mission around Mars' orbit are performing remote sensing on its atmosphere, conducting measurements of its gravity field and carrying out observational analysis of the Red Planet. This would be especially interesting in the lower regions of the atmosphere, where the characterization of the dynamics, thermal structure and distributions of dust, water and carbon dioxide pose a substantial knowledge gap [54]. An appropriate PSO around Mars shall be studied that could enable these science operations.

In their article, Xiaodong Liu et al. [46] identify five special types of orbits around Mars that could be applicable for a remote sensing Mars mission: Sun-Synchronous Orbits (SSO), orbits at critical inclination, frozen orbits, repeating ground-track orbits, and stationary orbits. The SSO has been the most popular type of orbit for Mars exploration, being used for the Mars Global Surveyor, Mars Odyssey and Mars Reconnaissance Orbiter missions. These orbits are chosen at an altitude and inclination where the precession rate of the orbital plane due to Mars' flattening is equal to the precession rate of Mars around the Sun. This means that the object in orbit will

have near-constant Sun directional angles, which has implications for power generation and payload illumination. Essentially, the satellite will always overpass a certain location at the same local time, making it appropriate to examine seasonal variations on Mars. The SSO inclinations for different altitudes on Earth and on Mars can be seen in Figure 5.20. As can be seen, these orbits have a high inclination, giving the spacecraft access to all latitudes. This would enable remote sensing of the Martian poles to study the water cycle, the CO₂ cycle, the dust cycle, and the polar atmospheric dynamics. This figure also shows that at a given altitude, the required inclination of SSOs on Mars will always be smaller than that on Earth.

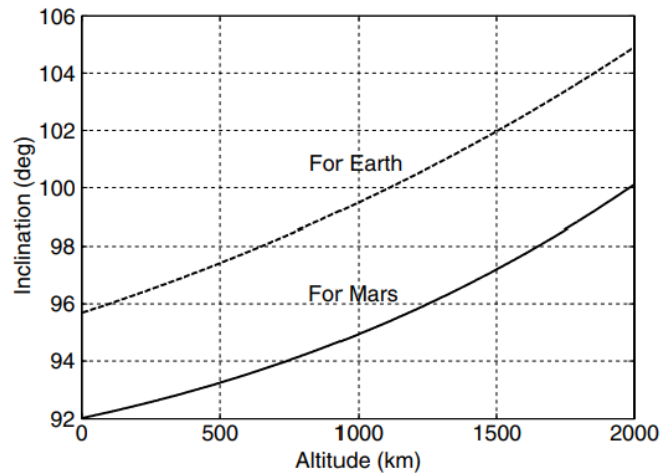


Figure 5.20: Sun-synchronous altitude vs inclination for circular orbits [46].

The scientific objectives for the mission point the PSO design toward a low-altitude orbit. This requires a trade-off since a lower orbit will require a higher amount of propellant to sustain the altitude due to Mars' atmospheric drag. Although Mars' atmosphere is thinner than Earth's, its drag effect should still be taken into account. Furthermore, orbiters around Mars cannot be placed in an orbit that is too low as they are subject to COSPAR's Planetary Protection policies [17]. This means that these orbiters have to meet orbital lifetime or bioburden requirements. On the one hand, the orbital lifetime is defined as 20 years after launch at greater than or equal to 99% probability and 50 years after launch at greater than or equal to 95% probability. Thus, additional propellant is required to exit the orbit to a safe altitude for planetary quarantine [3]. On the other hand, Mars orbiters will not be required to meet these orbital lifetime requirements if bioburden levels are lower than $5 \cdot 10^5$ spores.

Due to the zonal harmonics of Mars' gravity field, the orbital elements of these orbits experience secular and periodic variations. However, by choosing an appropriate combination of eccentricity and argument of periapsis so that the even and odd zonal harmonics cancel each other, these variations can be made to nearly zero. This results in a so-called frozen orbit, with virtually constant shape and orientation. This can be achieved by placing the orbital periapsis near the South Pole ($\omega_o = 270^\circ$) and selecting the appropriate eccentricity [36]. Increasing this eccentricity for a given altitude and inclination will cause the periapsis to move, leading to changes in eccentricity. Therefore, frozen orbits have an important design characteristic: the total altitude variation between periapsis and apoapsis is around 70 km, which is lower than that of a nonfrozen orbit. Thus, a frozen orbit represents the most circular orbit achievable at lower altitudes around Mars.

The final consideration in the orbit selection is the desired ground-track pattern, which is mainly

defined by the semi-major axis of the orbit and consequently, the orbital period, combined with the rotational period of Mars itself. First, the desired ground-track repeat time and the time to achieve global coverage must be established. Once the scientific objectives have been clearly defined and the payload has been characterized, the required ground-track spacing can be calculated. That spacing will be dependent on the number of days in which it is required for the repeat to take place, the length of the Mars day, and the semi-major axis of the orbit.

One relevant case study is that of the Mars Reconnaissance Orbiter (MRO). The science orbit for this mission was designed to provide global access to Mars and satisfy its science and mission objectives while considering effects such as atmospheric drag. The orbital parameters for this orbit, shown in Table 5.4, produced a Sun-synchronous ascending node at 3:00 pm local mean solar time; a periapsis altitude around 250 km; an apoapsis altitude near 320 km; a near-polar inclination and a combination of eccentricity and argument of periapsis that resulted in a frozen orbit. Since the MRO science orbit could enable the scientific objectives for our mission, it will be taken as the reference PSO in this preliminary study. In successive iterations of the mission design, a thorough analysis shall be carried out concerning the specific Mars science orbit required to achieve the proposed objectives.

Classical Orbital Elements at Apoapsis, Mars centred, equator and equinox of epoch (IAU)		
Orbit Epoch, t_o		
		15-July-2006 01:00:00:00.00 ET
Parameter	Value	Characteristic
Semi-Major Axis, a	3648.5995 km	Consistent with: 16 sol target cycle
Eccentricity, e	0.01218	Consistent with: Frozen Periapsis
Inclination, i	92.6426 deg	Consistent with: Sun-synchronous
Ascending Node, Ω	-10.7004 deg	Consistent with: 3:00 PM +/- 15 mins LMST
Argument of Periapse, ω	-90.0 deg	Frozen: Over South Pole
Mean Anomaly of Epoch	180.0 deg	Variable: 0 to 360 deg
Periapsis Altitude, H_p	251.7529 km	Average: 255 +/- 5 km
Apoapsis Altitude, H_a	316.7893 km	Average: 320 +/- 5 km
Nodal Period	6732.4251 sec	Consistent with: 16 sol target cycle

Table 5.4: Mars Reconnaissance Orbiter Science Orbit Reference Elements to be used as a reference [36].

Conclusions and future work

6.1. Summary

A systems engineering framework has been used to design a stand-alone Mars exploration CubeSat mission that integrates DLR's in-house technologies. First, the stakeholders and their expectations have been analyzed. This has led to the identification of the main goals for the mission: demonstrating DLR's in-house technologies, executing an Earth-Mars transfer and performing science in a Mars orbit. The mission requirements have been formulated, which are the foundation blocks for the ConOps. The ConOps for the mission presents several phases. First, the spacecraft will be launched into a 15-month low-thrust transfer trajectory to Mars. Upon arrival at Mars, the spacecraft will execute a ballistic orbital insertion into a highly elliptical orbit. Once in orbit around the Red Planet, the spacecraft will perform aerobraking to position itself around a PSO at an altitude of 250 km, where the science operations will take place. This PSO will be a frozen and Sun-synchronous orbit in order to take advantage of Mars' gravitational parameters that enable a near-circular orbit. During this phase, the spacecraft will tackle two of the most relevant scientific objectives around Mars: gathering data on its lower atmosphere and gravity field. Finally, the spacecraft will be placed into a quarantine orbit for disposal. This ConOps has been used to translate mission requirements into a set of technical system requirements. In turn, this has enabled the definition of the functional and physical architecture of the system. The system's main functions have been identified using functional flow block diagrams and linked to physical subsystems and components through a physical system diagram.

This has resulted in the design for the space, ground and launch segments. The space segment consists of a 12U CubeSat, which can be seen in Figure 4.19. The spacecraft has a wet mass of 20 kg, a manoeuvrability of 5.1 km/s, and can generate up to 90 W of power at Mars using deployable solar panels. Its main payloads are a 2U infrared spectrometer, a 1U gravimeter and a 12 Mpx CMOS camera. The DLR ICA stack will be used, which combines multiple avionics systems (i.e., onboard computer, communications, and power) into a single unit. The DLR ScOSA onboard computer will be used, which integrates two computing nodes to ensure robustness. The reliable computing node comprises the OBC used on the MASCOT lander developed by DLR [31]. The high-performance computing node consists of a COTS-based processing module for application acceleration. The spacecraft uses the radiofrequency X-band in order to communicate with its ground segment. The in-house developed GSDR is used as a transceiver. The system also features a main reflectarray antenna as used by MarCO [32] and secondary patch antennas. Electrical power is generated using

two linear solar arrays with 32% efficiency triple junction solar cells developed by Azur Space. The power control and distribution unit, as well as the batteries, will be adapted from those used by the DLR PLUTO mission [4]. For other subsystems, COTS components have been chosen that satisfy the needs of the mission. The propulsion system is a Busek BIT-3 gridded-ion engine as used in the Lunar IceCube and LunaH-Map missions [69]. This system features an expanded tank to accommodate the needed 4.3 kg of propellant. The XACT-50 developed by Blue Canyon Technologies is used as the integrated attitude control and determination system [74]. Thermal coating and heaters are used for thermal management; a preliminary thermal analysis is presented that demonstrates their feasibility. All of these systems are housed in an EnduroSat 12U XL main structure [24]. A ground segment architecture has been presented using a combination of DLR's antennas, ESA's ESTRACK infrastructure and NASA's Deep Space Network. These are also used for navigation using ranging, Doppler and Delta-DOR measurements. Different launch opportunities have been studied, favouring a piggyback on another Mars-bound launch.

An orbit analysis has been performed to calculate low-thrust Earth-Mars transfer trajectories using the Tudat library developed at TU Delft. These trajectories have mainly been computed using the hodographic-shaping method. This method uses simple base functions to shape the velocity along the trajectory. This velocity profile is then analytically integrated to find the change in position and the resulting trajectory. The thrust acceleration profile can also be retrieved and used in numerical propagations. Through numerical orbit propagation, the mass of the spacecraft can be propagated, and trajectory perturbations can be incorporated to enhance the realism of the simulation. However, this comes at a high computational cost. These perturbations have been shown to be consistently two orders of magnitude lower than the thrust acceleration, thus rendering their consideration unnecessary in a preliminary study as done here. Therefore, the hodographic-shaping method for trajectory calculation has been deemed the most appropriate in terms of accuracy and computational demands.

In order to assess the feasibility of the system in terms of its propulsion capabilities, an extensive array of trajectories has been examined. The proposed formulation for the hodographic technique offers nine different variables to characterise each trajectory. These include the departure date, the time of flight, the number of revolutions around the Sun, and six free coefficients that arise from the use of additional velocity base functions. Assuming that the mission is launched through a piggyback on a Mars-bound launch (i.e., with excess energy of $15 \text{ km}^2/\text{s}^2$), two main launch windows are considered: one at the end of 2028 and one at the end of 2030. A porkchop plot has been generated for each launch window, effectively constraining the departure dates to be analysed.

A grid search has been implemented for these departure dates and a wide range of TOFs (and their inherent number of revolutions around the Sun). For each combination of departure date and TOF, an optimization procedure has been performed to identify the optimal set of free parameters that yield the most favourable trajectory in terms of Delta-V. An optima region can be found in both launch windows for $N = 2$ and $\text{TOF} = 1000\text{-}1400$ days. This region includes trajectories with promising results in both the consumed Delta-V and the maximum thrust. The most optimal trajectory for each of the departure dates has been numerically propagated to find more realistic values for the Delta-V and maximum thrust. Using this data, it can be concluded that the original Delta-V budget is unfeasible. However, raising the total Delta-V capability of the spacecraft by 1.2 km/s to a total of $4.8 + 0.3 + 1.2 = 6.3 \text{ km/s}$ (including the Delta-V required to place the spacecraft in a graveyard orbit at end-of-life) leads to 80% of the departure dates resulting in feasible trajectories. This would mean an increase in propellant mass of $\sim 725 \text{ g}$, which can definitely be accommodated in the mass and volume budget for the spacecraft. Nevertheless, these trajectories exceed the maximum thrust requirement of 1.25 mN in peaks at the end of the trajectories. Since the average thrust along these trajectories is lower than the requirement, a strategy can potentially be implemented to distribute

this peak in thrust over the entire trajectory. Therefore, an updated space segment is proposed that complies with the updated requirements, with a wet mass of 20.8 kg, a Delta-V budget of 6.3 km/s and an increased mission lifetime of ~ 4 years. The results presented here have been verified against other low-thrust trajectory calculation methods. The mission analysis is completed by defining a strategy for Mars orbital insertion using ballistic capture and defining the PSO around Mars. This PSO will be a frozen and Sun-synchronous orbit to take advantage of Mars' gravitational parameters to enable a near-circular orbit.

6.2. Conclusions

Taking into account the results presented in this study, a re-evaluation of the research questions initially introduced in Chapter 1 is undertaken. Here, these research questions are answered, incorporating the insights acquired from the Mission Analysis.

1. What are the design and performance characteristics that enable a stand-alone interplanetary CubeSat system to Mars?

The resulting 12U CubeSat has a wet mass of 20.77 kg, 6.3 km/s of low-thrust manoeuvring capability, and can generate up to 90 W of power at Mars. It integrates several technologies developed by DLR, including onboard data handling, power, communication and software. These have been combined with other reference COTS or externally developed components for the rest of the subsystems. The spacecraft uses the radiofrequency X-band in order to communicate with its ground segment using a primary high-gain reflectarray antenna.

- 1.1. What is the most feasible timeline for a stand-alone Mars CubeSat mission?

Initially, the spacecraft will be launched into a 3-year low-thrust transfer trajectory to Mars. Upon arrival at Mars, the spacecraft will execute a ballistic insertion into a highly elliptical orbit. Once in orbit around the Red Planet, the spacecraft will perform aerobraking to position itself around a PSO at an altitude of 250 km. During this phase, the spacecraft will perform measurements on its lower atmosphere and gravity field. Finally, the spacecraft will be placed into a quarantine orbit for disposal.

- 1.2. How can DLR's in-house technologies be evaluated and combined with COTS components to provide a solution for the space segment?

Considering minor developments, the DLR in-house technologies have all been deemed feasible for the mission. These include the ICA avionics stack, the ScOSA OBC, the PLUTO PCDU, the GSDR transceiver, the OUTPOST software and the available solar array technology. These have been combined with other reference COTS or externally developed components: a 2U infrared spectrometer, a 1U gravimeter and a 12 Mpx CMOS camera, a BIT-3 electric propulsion system, an integrated XACT-50 ADCS system, a combination of a high-gain reflectarray and medium-gain patch antennas, heaters and thermal coating and an EnduroSat 12U XL main structure.

2. What are the trajectory characteristics of a stand-alone CubeSat mission to Mars?

The orbit design of a stand-alone 20 kg CubeSat is deemed feasible using a state-of-the-art electric propulsion system. In two launch windows for 2028 and 2030, a wide range of departure dates spanning several months leads enables trajectories with an Earth-Mars transfer Delta-V of 6 km/s. These trajectories have a TOF of ~ 3 years and perform 2 revolutions around the

Sun. The average thrust for these trajectories is consistently under 1.25 mN.

2.1. What is the feasibility of a low-thrust CubeSat transfer to Mars and what are the associated requirements?

Using an optimization process, it can be concluded that the original Delta-V budget is unfeasible. However, raising the Delta-V capability of the spacecraft by 1.2 km/s to a total of 6.3 km/s leads to 80% of the departure dates resulting in feasible trajectories. This would mean an increase in propellant mass of ~ 725 g, which can definitely be accommodated in the mass and volume budget for the spacecraft. The average thrust along these trajectories is lower than the maximum thrust requirement. Therefore, a strategy can potentially be implemented to distribute the peaks in thrust over the entire trajectory. These trajectories have a TOF of ~ 40 months, which would lead to an increased mission lifetime of ~ 4 years.

6.3. Future work

This work encompassed two main objectives: designing a CubeSat system to execute a stand-alone mission to Mars and performing a mission analysis to determine the feasibility of the mission. Therefore, the recommendations for future work here presented address both elements:

- The systems design process is an iterative one. The results of the mission analysis have been used to update certain design parameters (e.g., higher propellant load, and extended mission duration). However, these findings should be used to revise each step of the design process, from the mission requirements to the subsystem solutions. On each iteration, the state-of-the-art interplanetary CubeSat technologies should be analysed so as to keep the design up to date with the best technology at the time.
- The optimization procedure can be extended in many ways. First, the analysis presented in this work has been performed on a constrained decision variable space assuming a launch on an independent Mars-bound launcher. If other launch alternatives were to arise (e.g., GEO launch upper stage disposal) that could extend the launch windows, better trajectories may be found. On top of that, the analysis has been performed using the recommended set of base functions given by Gondelach and Noomen. Other combinations of base functions may provide room for optimization of both Delta-V and maximum thrust along the trajectory. Finally, while a single-objective optimization has been performed, both the Delta-V and maximum thrust should be optimised. Many multi-objective optimization approaches are available in the Pygmo Python library that could be used to find a trade-off between the two objectives. A very first glimpse of potential results has been obtained here, by performing an optimization on Delta-V and maximum thrust independently.
- Although the two-body formulation of the hodographic-shaping method has been deemed acceptable for this study, it is not the most realistic approach. Further iterations of the mission analysis shall calculate the trajectories using numerical propagation so that the perturbations in the Solar System can be accounted for. In addition, a procedure should be written to update the hodographic thrust profile with these perturbations, so that the trajectory reaches its target with the desired accuracy.

References

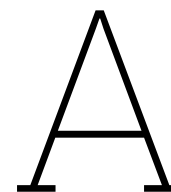
- [1] *12 Megapixels CMOS Space Camera Datasheet*. 3DCM800. 3D Plus. 2023. URL: <https://www.3d-plus.com/products/12-mpx-space-camera-heads/> (visited on 06/15/2023).
- [2] F. Abilleira et al. *Mars 2020 mission design and navigation overview*. Version V1. 2019. DOI: 2014/45974. URL: <https://hdl.handle.net/2014/45974>.
- [3] K. Aggarwal and R. Noomen. “Graveyard orbits for future Mars missions”. In: *Advances in Space Research* (2022). ISSN: 0273-1177. DOI: <https://doi.org/10.1016/j.asr.2022.07.023>. URL: <https://www.sciencedirect.com/science/article/pii/S027311772200624X>.
- [4] N. Aksteiner and F. Eichstaedt. “Increasing the power density of CubeSats - a Demonstration Scenario for deployable Solar Arrays”. 14th IAA Symposium on Small Satellites for Earth System Observation. Berlin, Germany, 2023.
- [5] A. Babuscia et al. “Development of telecommunications systems and ground support for EM-1 interplanetary cubesats missions: Lunar Icecube and LUNAH-Map”. In: *International Astronautical Congress-IAC*. JPL-CL-17-4377. 2017.
- [6] *BIT-3 RF Ion Thruster Datasheet*. Busek. 2023. URL: <https://www.busek.com/bit3> (visited on 04/10/2023).
- [7] J. Budroweit. “Development of a highly integrated and radiation-tolerant software-defined radio platform for multi-band radio applications in space systems”. PhD thesis. Technischen Universität Hamburg, Germany, 2021.
- [8] J. Budroweit, F. Eichstaedt, and F. Stehle. “A Highly Integrated and Software-Controlled L to Ka-Band Front-End for SDRs in space applications”. In: *2023 IEEE Space Hardware and Radio Conference*. Las Vegas, NV, USA, 2023, pp. 12–15. DOI: 10.1109/SHaRC56958.2023.10046258.
- [9] J. Budroweit and A. Koelpin. “Design challenges of a highly integrated SDR platform for multiband spacecraft applications in radiation environments”. In: *2018 IEEE Topical Workshop on Internet of Space (TWIOS)*. Anaheim, CA, USA, 2018, pp. 9–12. DOI: 10.1109/TWIOS.2018.8311399.
- [10] M. Capderou and F. Forget. “Optimal orbits for Mars atmosphere remote sensing”. In: *Planetary and Space Science* 52.9 (2004), pp. 789–798. ISSN: 0032-0633. DOI: <https://doi.org/10.1016/j.pss.2004.03.006>. URL: <https://www.sciencedirect.com/science/article/pii/S0032063304000686>.
- [11] C. Cappelletti, S. Battistini, and B.K. Malphrus. *CubeSat Handbook: From Mission Design to Operations*. Elsevier Science, 2020. ISBN: 9780128178843. URL: <https://books.google.nl/books?id=jGy4yweACAAJ>.
- [12] N. Chahat et al. “Advanced CubeSat Antennas for Deep Space and Earth Science Missions: A review”. In: *IEEE Antennas and Propagation Magazine* 61.5 (2019), pp. 37–46. DOI: 10.1109/MAP.2019.2932608.
- [13] N. Chahat et al. “One-Meter Deployable Mesh Reflector for Deep Space Network Telecommunication at X- and Ka-band”. In: *2019 13th European Conference on Antennas and Propagation (EuCAP)*. Krakow, Poland, 2019, pp. 1–4.

- [14] K. Cheung et al. *Next-Generation Ground Network Architecture for Communications and Tracking of Interplanetary Smallsats*. Jet Propulsion Laboratory, California Institute of Technology, 2015.
- [15] A. Chin et al. “CubeSat: the pico-satellite standard for research and education”. In: *AIAA Space 2008 Conference & Exposition*. San Diego, CA, USA, 2008, p. 7734.
- [16] P. E. Clark et al. “Lunar Ice Cube: ongoing development of first generation deep space CubeSat mission with compact broadband IR spectrometer”. In: *CubeSats and SmallSats for Remote Sensing III*. Ed. by T. S. Pagano, Charles D. Norton, and Sachidananda R. Babu. Vol. 11131. International Society for Optics and Photonics. SPIE, 2019, p. 1113108. DOI: 10.1117/12.2529323. URL: <https://doi.org/10.1117/12.2529323>.
- [17] COSPAR. “COSPAR Policy on Planetary Protection”. In: *Space Research Today* 208 (2020), pp. 10–22. ISSN: 1752-9298. DOI: <https://doi.org/10.1016/j.srt.2020.07.009>. URL: <https://www.sciencedirect.com/science/article/pii/S1752929820300372>.
- [18] Cal Poly. *CubeSat Design Specification (1U – 12U)*. Standard. San Luis Obispo, CA, USA, Feb. 2022.
- [19] D. W. Curkendall and J. S. Border. *Delta-DOR: The One-Nanoradian Navigation Measurement System of the Deep Space Network — History, Architecture, and Componentry*. Jet Propulsion Laboratory, California Institute of Technology, 2013.
- [20] D. Dirx and E. Mooij. *TU Delft AE4866-1: Propagation and Optimisation in Astrodynamics. Lecture notes*. 2022.
- [21] DLR. Institute for Software Technology. *Open modular software Platform for Spacecraft (OUTPOST)*. 2021. URL: <https://github.com/DLR-RY/outpost-core> (visited on 08/23/2023).
- [22] DLR. Institute for Software Technology. *ScOSA On-Board Computer*. 2018. URL: https://www.dlr.de/sc/en/desktopdefault.aspx/tabid-11139/19481_read-45210/ (visited on 05/12/2023).
- [23] M. Drobczyk and A. Lübken. “Novel wireless protocol architecture for intra-spacecraft wireless sensor networks (inspaWSN)”. In: 2018 6th IEEE International Conference on Wireless for Space and Extreme Environments (WiSEE). Huntsville, AL, USA, Dec. 2018. DOI: 10.1109/WiSEE.2018.8637342.
- [24] *EnduroSat 12U XL CubeSat Structure Datasheet*. EnduroSat. 2023. URL: <https://www.endurosat.com/cubesat-store/cubesat-structures/12u-cubesat-structure/> (visited on 06/17/2023).
- [25] *EnduroSat X-Band 4x4 Patch Antenna Array Datasheet*. EnduroSat. 2023. URL: <https://www.endurosat.com/cubesat-store/cubesat-antennas/x-band-4x4-patch-array/> (visited on 06/10/2023).
- [26] V. Franzese, P. Di Lizia, and F. Topputo. “Autonomous Optical Navigation for the Lunar Meteoroid Impacts Observer”. In: *Journal of Guidance, Control, and Dynamics* 42 (Jan. 2019), pp. 1–8. DOI: 10.2514/1.G003999.
- [27] D. Garcia Yarnoz, R. Jehn, and M. Croon. “Interplanetary navigation along the low-thrust trajectory of BepiColombo”. In: *Acta Astronautica* 59.1 (2006). Space for Inspiration of Humankind, Selected Proceedings of the 56th International Astronautical Federation Congress, Fukuoka, Japan, 17-21 October 2005, pp. 284–293. ISSN: 0094-5765. DOI: <https://doi.org/10.1016/j.actaastro.2006.02.028>. URL: <https://www.sciencedirect.com/science/article/pii/S0094576506000890>.
- [28] *General Environmental Verification Standard*. Standard. Goddard Space Flight Center: NASA, Feb. 2019.

- [29] D. J. Gondelach and R. Noomen. “Hodographic-Shaping Method for Low-Thrust Interplanetary Trajectory Design”. In: *Journal of Spacecraft and Rockets* 52 (2015), pp. 728–738.
- [30] C. Hardgrove. “Fly Me To The Moon LunaH-Map: Early Operations, Science Data and Technology Demonstrations”. Inter-Planetary Small Satellite Conference. 2023. URL: <http://www.intersmallsatconference.com/past/2023/>.
- [31] T.M. Ho et al. “MASCOT - The Mobile Asteroid Surface Scout onboard the Hayabusa2 Mission”. In: *Space Science Reviews* 208 (July 2017). DOI: 10.1007/s11214-016-0251-6.
- [32] R. Hodges et al. “A Deployable High-Gain Antenna Bound for Mars: Developing a new folded-panel reflectarray for the first CubeSat mission to Mars”. In: *IEEE Antennas and Propagation Magazine* PP (Feb. 2017), pp. 1–1. DOI: 10.1109/MAP.2017.2655561.
- [33] NASA. Small Spacecraft Systems Virtual Institute. *Small Spacecraft Technology: State of the Art Report*. 2022.
- [34] X. Jiang, B. Yang, and S. Li. “Overview of China’s 2020 Mars Mission Design and Navigation”. In: *Astrodynamics* 1 (July 2017). DOI: 10.1007/s42064-017-0011-8.
- [35] NASA JPL. *Mars Cube One Fact Sheet*. Report. 2014. URL: https://mars.nasa.gov/internal_resources/344/.
- [36] NASA JPL. *Primary Science Orbit Design for the Mars Reconnaissance Orbiter Mission*. Tech. rep. Feb. 2003.
- [37] *JEM Payload Accommodation Handbook*. Interface Control Document. JAXA, July 2020.
- [38] A. Klesh and J. Krajewski. “Marco: Cubesats to Mars in 2016”. In: Proceedings of the 29th Annual AIAA/USU Conference on Small Satellites. Logan, UT, USA, 2015.
- [39] A. Klesh et al. “MarCO: Early operations of the first CubeSats to Mars”. In: (2018).
- [40] A. T. Klesh, J. Baker, and J. Krajewski. “MarCO: Flight Review and Lessons Learned”. In: Proceedings of the 33rd Annual AIAA/USU Conference on Small Satellites. Aug. 2019.
- [41] M. M. Kobayashi et al. “The Iris Deep-Space Transponder for the SLS EM-1 Secondary Payloads”. In: *IEEE Aerospace and Electronic Systems Magazine* 34.9 (2019), pp. 34–44. DOI: 10.1109/MAES.2019.2905923.
- [42] A. S. Konopliv, R. S. Park, and W. M. Folkner. “An improved JPL Mars gravity field and orientation from Mars orbiter and lander tracking data”. In: *Icarus* 274 (2016), pp. 253–260. ISSN: 0019-1035. DOI: <https://doi.org/10.1016/j.icarus.2016.02.052>. URL: <https://www.sciencedirect.com/science/article/pii/S0019103516001305>.
- [43] E. Kulu. *Nanosats Database*. 2022. URL: <https://www.nanosats.eu/> (visited on 04/08/2023).
- [44] *Laboratories and Facilities*. Tech. rep. Institute of Space Systems: DLR, 2023. URL: https://www.dlr.de/irs/en/PortalData/46/Resources/dokumente/27108_Laborbroschu_re_DLR_051021.pdf.
- [45] J. Lazio. *The Deep Space Network Radio Astronomy User Guide*. Jet Propulsion Laboratory, California Institute of Technology, 2021. URL: https://deepspace.jpl.nasa.gov/files/DSN_Radio_Astronomy_Users_Guide.pdf.
- [46] X. Liu, H. Baoyin, and X. Ma. “Five Special Types of Orbits Around Mars”. In: *Journal of Guidance, Control, and Dynamics* 33 (Aug. 2011). DOI: 10.2514/1.48706.
- [47] A. Lund et al. “ScOSA system software: the reliable and scalable middleware for a heterogeneous and distributed on-board computer architecture”. In: *CEAS Space Journal* 14.1 (Jan. 2022), pp. 161–171. ISSN: 1868-2510. DOI: 10.1007/s12567-021-00371-7. URL: <https://doi.org/10.1007/s12567-021-00371-7>.

- [48] D. Lyons. “Mars Reconnaissance Orbiter: Aerobraking Reference Trajectory”. In: *AIAA/AAS Astrodynamics Specialist Conference and Exhibit*. DOI: 10.2514/6.2002-4821. eprint: <https://arc.aiaa.org/doi/pdf/10.2514/6.2002-4821>. URL: <https://arc.aiaa.org/doi/abs/10.2514/6.2002-4821>.
- [49] Sumanth M. “Computation of Eclipse Time for Low-Earth Orbiting Small Satellites”. In: *International Journal of Aviation, Aeronautics, and Aerospace* (Jan. 2019). DOI: 10.15394/ijaaa.2019.1412.
- [50] B. K. Malphrus et al. “The Lunar IceCube EM-1 Mission: Prospecting the Moon for Water Ice”. In: *IEEE Aerospace and Electronic Systems Magazine* 34.4 (2019), pp. 6–14. DOI: 10.1109/MAES.2019.2909384.
- [51] K. Venkatesh Mani. “Combined Chemical–Electric Propulsion Design and Hybrid Trajectories for Stand-Alone Deep-Space CubeSats”. PhD thesis. Politecnico di Milano, 2019.
- [52] T. J. Martin-Mur and B. Young. “Navigating MarCO, the First Interplanetary CubeSats”. In: *Proceedings of the International Symposium on Space Flight Dynamics*. 2019. URL: https://issfd.org/ISSFD_2019/ISSFD_2019_AIAC18_Martin-mur-Tomas.pdf.
- [53] D. M. McIntosh, J. D. Baker, and J. A. Matus. “The NASA Cubesat Missions Flying on Artemis-1”. In: *Proceedings of the 34th Annual AIAA/USU Conference on Small Satellites*. Logan, UT, USA, 2020.
- [54] MEPAG. *Mars Science Goals, Objectives, Investigations, and Priorities: 2020 Version*. Mars Exploration Program Analysis Group (MEPAG), 2020.
- [55] D. R. Myatt et al. “Advanced Global Optimisation Tools for Mission Analysis and Design”. In: *Final Report of ESA Ariadna ITT AO4532/18138/04/NL/MV Call 03/4101* (2004).
- [56] NASA. *Orion Stage Adapter Readied for Ride on Artemis I*. 2021. URL: <https://www.nasa.gov/image-feature/orion-stage-adapter-readied-for-ride-on-artemis-i> (visited on 08/11/2023).
- [57] J. F. Jordan. *The Application of Lambert’s Theorem to the Solution of Interplanetary Transfer Problems*. Tech. rep. Jet Propulsion Laboratory, California Institute of Technology, Feb. 1964.
- [58] D. Novak and M. Vasile. “Improved Shaping Approach to the Preliminary Design of Low-Thrust Trajectories”. In: *Journal of Guidance Control Dynamics* 34 (Dec. 2010), pp. 128–147. DOI: 10.2514/1.50434.
- [59] A. D. Olds, C. A. Kluever, and M. L. Cupples. “Interplanetary Mission Design Using Differential Evolution”. In: *Journal of Spacecraft and Rockets* 44.5 (2007), pp. 1060–1070. DOI: 10.2514/1.27242. eprint: <https://doi.org/10.2514/1.27242>. URL: <https://doi.org/10.2514/1.27242>.
- [60] E. Peral et al. “RainCube, a Ka-band Precipitation Radar in a 6U CubeSat”. In: *Proceedings of the 31st Annual AIAA/USU Conference on Small Satellites*. Logan, UT, USA, 2017.
- [61] K. Price, Rainer Storn, and J. Lampinen. *Differential Evolution—A Practical Approach to Global Optimization*. Vol. 141. Jan. 2005. DOI: 10.1007/3-540-31306-0.
- [62] *Satellite All-Polyimide Thermofoil™ Heaters Datasheet*. Minco. 2023. URL: <https://www.minco.com/catalog/?catalogpage=product&cid=satellite-heaters&id=HAP6747&unit=metric> (visited on 07/20/2023).
- [63] J. C. Smith and J. L. Bell. “2001 Mars Odyssey Aerobraking”. In: *Journal of Spacecraft and Rockets* 42.3 (2005), pp. 406–415. DOI: 10.2514/1.15213. eprint: <https://doi.org/10.2514/1.15213>. URL: <https://doi.org/10.2514/1.15213>.

- [64] DLR Institute of Space Systems. *Integrated Core Avionics (ICA) Facts and Features*. German Aerospace Center (DLR), 2020.
- [65] G. Stephens et al. “The Emerging Technological Revolution in Earth Observations”. In: *Bulletin of the American Meteorological Society* 101.3 (2020), E274–E285. DOI: 10.1175/BAMS-D-19-0146.1. URL: <https://journals.ametsoc.org/view/journals/bams/101/3/bams-d-19-0146.1.xml>.
- [66] *The Red Book*. Sheldahl. 2020. URL: <https://live-sheldahldev.pantheonsite.io/wp-content/uploads/2023/07/RedBook.pdf>.
- [67] F. Topputo and E. Belbruno. “Earth-Mars transfers with ballistic capture”. In: *Celestial Mechanics and Dynamical Astronomy* 121.4 (Feb. 2015), pp. 329–346. DOI: 10.1007/s10569-015-9605-8. URL: <https://doi.org/10.1007/s10569-015-9605-8>.
- [68] C. Treudler et al. “ScOSA - Scalable On-Board Computing for Space Avionics”. In: Proceedings of the 69th International Astronautical Congress 2018. Bremen, Germany, Oct. 2018.
- [69] M. Meng-Tsuan Tsay et al. “LunarCube: A Deep Space 6U CubeSat with Mission Enabling Ion Propulsion Technology”. In: Proceedings of the 29th Annual AIAA/USU Conference on Small Satellites. Logan, UT, USA, 2015.
- [70] T. Villela et al. “Towards the Thousandth CubeSat: A Statistical Overview”. In: *International Journal of Aerospace Engineering* 2019 (Jan. 2019), pp. 1–13. DOI: 10.1155/2019/5063145.
- [71] R. Walker. “Overview of ESA Lunar Interplanetary CubeSat Missions”. Inter-Planetary Small Satellite Conference. Tucson, AZ, USA, 2023. URL: <http://www.intersmallsatconference.com/past/2023/>.
- [72] J.R. Wertz, D.F. Everett, and J.J. Puschell. *Space Mission Engineering: The New SMAD*. Space technology library. Microcosm Press, 2011. ISBN: 9781881883159. URL: <https://books.google.nl/books?id=VmQmtwAACAAJ>.
- [73] R. C. Woolley and Nathan J. Barba. “Delta-Vs and Design Reference Mission Scenarios for Mars Missions”. In: Proceedings of the 36th Annual Small Satellite Conference. Logan, UT, USA, 2022. URL: <https://digitalcommons.usu.edu/smallsat/2022/all2022/257/>.
- [74] *XACT Attitude Control Systems Datasheet*. Blue Canyon Technologies. 2023. URL: <https://storage.googleapis.com/blue-canyon-tech-news/1/2023/04/ACS.pdf> (visited on 04/20/2023).
- [75] Seyoung Yoon et al. “Analysis of the charged particle radiation effect for a CubeSat transiting from Earth to Mars”. In: *Current Applied Physics* 14.4 (2014), pp. 575–581. ISSN: 1567-1739. DOI: <https://doi.org/10.1016/j.cap.2014.01.018>. URL: <https://www.sciencedirect.com/science/article/pii/S1567173914000297>.
- [76] X. Yu et al. “Star of AOXiang: An innovative 12U CubeSat to demonstrate polarized light navigation and microgravity measurement”. In: *Acta Astronautica* 147 (2018), pp. 97–106. ISSN: 0094-5765. DOI: <https://doi.org/10.1016/j.actaastro.2018.03.014>. URL: <https://www.sciencedirect.com/science/article/pii/S0094576517302849>.
- [77] C. Zanoni et al. *The Design of a Drag-Free CubeSat and the Housing for its Gravitational Reference Sensor*. 2016. arXiv: 1605.05496 [astro-ph.IM].



Mission requirements

Table A.1 shows the mission requirements and their respective stakeholder. On top of that, the compliance of the system solution presented in Chapter 4 with each of the requirements is shown.

ID	Stakeholder	Statement	Compliance
MR-01	SH01	The mission shall consist of a space segment or SpaceCraft (SC), a ground segment (GS) and a launch segment (LS).	✓
MR-02	SH01	The mission shall cost less than 10M€.	-
MR-03	SH01	The mission shall be ready to launch in less than 4 years.	✓
MR-04	SH01	The launch of the SC shall nominally occur by 2028.	✓
MR-05	SH01	The system shall be developed, integrated and tested by DLR Institute of Space Systems.	✓
MR-06	SH01	The system shall be operated from the GSOC.	✓
MR-07	SH03	The mission lifetime shall be no more than 2 years including the Earth-Mars transfer.	✓
MR-08	SH03	The SC shall implement the CubeSat form factor as established in the CDS.	✓
MR-09	SH03	The SC shall be implemented following a 12U CubeSat configuration.	✓
MR-10	SH12	The SC shall weigh less than 24 kg.	✓

Table A.1 continued from previous page

ID	Stakeholder	Statement	Compliance
MR-11	SH02	The mission analysis shall be performed using the TU Delft Astrodynamics Toolkit.	✓
MR-12	SH03	The SC shall be sized for the most demanding mechanical, thermal and electromagnetic mission scenario.	✓
MR-13	SH03	The SC shall be launched into an Earth escape trajectory.	✓
MR-14	SH03	The SC shall travel independently from Earth to a Mars orbit.	✓
MR-15	SH03	The SC shall gather data on Mars' atmosphere.	✓
MR-16	SH03	The SC shall collect information about Mars' gravitational field.	✓
MR-17	SH03	The SC shall be able to perform observational analysis of Mars.	✓
MR-18	SH03	The SC shall be able to establish communication with Earth during all mission phases.	✗
MR-19	SH03	The SC shall be able to control its state so as to enable all mission phases.	✓
MR-20	SH03	The SC shall be designed using the available DLR in-house technology.	✓
MR-21	SH03	The SC shall use COTS components for the needed subsystems.	✓
MR-22	SH03	Only technologies at a minimum of TRL 5 shall be implemented in the mission design.	✓
MR-23	SH04	The GS shall be able to provide reliable communication, command, and control of the SC.	✓
MR-24	SH04	The GS shall be able to handle the data generated by the SC.	✓
MR-25	SH04	The GS shall be able to provide orbit and attitude determination and prediction services for the SC.	✗
MR-26	SH05	The system shall undergo testing as defined by the launch provider.	✓
MR-27	SH06	The mission shall implement Telemetry and Telecommand procedures as established by the applicable ECSS standards.	✓
MR-28	SH07	The mission shall follow NASA's General Environment Verification Standard.	✓
MR-29	SH08	The SC shall comply with the COSPAR Planetary Protection policies.	✓
MR-30	SH09	The mission shall obtain and provide documentation of proper licenses for use of radio frequencies.	✓
MR-31	SH10	The scientific data gathered by the system shall be made publicly available to promote research.	✓

Table A.1: Complete list of mission requirements with their respective ID and stakeholder.

B

System requirements

106

Table B.1 shows the system requirements for the mission and their specific ID. On top of that, they have been traced with their corresponding mission requirements. The compliance of the system solution presented in Chapter 4 with each of the requirements is also shown.

ID	Statement	Traced from	Compliance
SR-SYS-01	The system shall consist of a Space Segment or Spacecraft, a Ground Segment and a Launch Segment.	MR-01	✓
SR-SYS-02	The mission cost shall not exceed 10M€.	MR-02	-
SR-SYS-03	The system shall be ready for launch in less than 4 years.	MR-03	✓
SR-SYS-04	The system shall be operational for a maximum of 2 years.	MR-07	✓
SR-SYS-05	The SC shall be implemented using the CubeSat standard as established in the CDS.	MR-08	✓
SR-SYS-06	The SC volume shall not exceed the configuration of a 12U CubeSat as established in the CDS.	MR-09	✓
SR-SYS-07	The total dry mass of the SC shall not be greater than 20 kg.	MR-10	✓
SR-SYS-08	The total wet mass of the SC shall not be greater than 24 kg.	MR-10	✓
SR-SYS-09	The SC shall be launched into a parabolic Earth escape trajectory.	MR-13	✓
SR-SYS-10	The SC shall perform a stand-alone Earth-Mars transfer in less than 15 months.	MR-14	✓

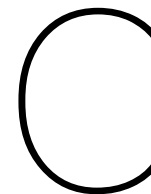
Table B.1 continued from previous page

ID	Statement	Traced from	Compliance
SR-SYS-11	The SC shall achieve autonomous orbital insertion into a Mars 2-sol orbit.	MR-14	✓
SR-SYS-12	The SC shall reach its PSO through a 6-month aerobraking phase.	MR-14	✓
SR-SYS-13	The SC shall nominally operate at a Mars frozen PSO with an altitude of 250 km.	MR-14	✓
SR-SYS-14	The SC shall maintain itself in its PSO for at least 1 month.	MR-14	✓
SR-SYS-15	The SC shall measure water, CO ₂ and dust distribution in Mars' lower atmosphere.	MR-15	✓
SR-SYS-16	The SC shall perform measurements of Mars' gravity field.	MR-16	✓
SR-SYS-17	The SC shall be able to take images in the visible part of the spectrum.	MR-17	✓
SR-SYS-18	The SC shall accommodate the science payloads and enable fulfilling all primary science measurements.	MR-12	✓
SR-SYS-19	The SC shall be able to process all the data gathered by the science payloads and bus.	MR-12	✓
SR-SYS-20	The SC shall be able to provide the required power to enable all operational phases.	MR-12	✓
SR-SYS-21	The SC shall be able to provide enough Delta-V to enable all phases of the mission.	MR-14	✓
SR-SYS-22	The SC shall be able to communicate with the GS without deployable components during LEOP.	MR-18	✓
SR-SYS-23	The system shall be able to establish long-range communication with Earth up to a distance of 1.5 AU.	MR-18	✗
SR-SYS-24	The system shall implement Telemetry and Telecommand procedures as established by the applicable ECSS standards.	MR-27	✓
SR-SYS-25	The system shall obtain and provide documentation of proper licenses for use of radio frequencies.	MR-30	✓
SR-SYS-26	The GS shall provide uninterrupted view of the spacecraft.	MR-18	✓
SR-SYS-27	The SC shall be able to maintain all subsystems within operational temperatures during all mission phases.	MR-12	✓
SR-SYS-28	The SC shall be able to provide attitude estimation and control that enable all operational phases.	MR-19	✓
SR-SYS-29	The SC shall be able to provide state estimation and control that enable all operational phases.	MR-25	✗
SR-SYS-30	The SC shall implement the different operational modes established in the ConOps.	MR-12	✓
SR-SYS-31	The SC shall support autonomous operations according to a mission timeline uploaded from ground.	MR-19	✓

Table B.1 continued from previous page

ID	Statement	Traced from	Compliance
SR-SYS-32	Random vibration testing shall be performed to the levels and duration as defined by the launch provider.	MR-26	✓
SR-SYS-33	Thermal vacuum bakeout shall be performed to ensure proper outgassing of components.	MR-26	✓
SR-SYS-34	The thermal test specification will be defined by the launch provider.	MR-26	✓
SR-SYS-35	Visual inspection of the SC and measurement of critical areas will be performed as defined by the launch provider.	MR-26	✓

Table B.1: Complete list of system requirements with their respective requirement ID, traceability and verification method.



Subsystem requirements

Table C.1 shows the subsystem requirements for the mission and their specific ID. On top of that, they have been traced with their corresponding system requirements. The compliance of the system solution presented in Chapter 4 with each of the requirements is also shown.

ID	Statement	Traced from	Compliance
SR-PL-01	The atmospheric payload (PL-ATM) shall operate in the wavelength range of 1-3 μm .	SR-SYS-15	✓
SR-PL-02	The PL-ATM shall have a spectral resolution of at least 50 nm.	SR-SYS-15	✓
SR-PL-03	The gravity payload (PL-GRA) shall enhance the measurements of Mars' gravity field performed using tracking data.	SR-SYS-16	✓
SR-PL-04	The imager payload (PL-IMG) shall operate in the visible spectrum.	SR-SYS-17	✓
SR-PL-05	The PL-IMG shall take pictures with a resolution of at least 10 Mpx.	SR-SYS-17	✓
SR-PROP-01	The propulsion system shall provide at least 5.1 km/s of Delta-V.	SR-SYS-10	✓
SR-PROP-02	The propulsion system shall have a specific impulse performance of at least 1000 s.	SR-SYS-10	✓
SR-PROP-03	The propulsion system shall be compatible with any operational SC attitude.	SR-SYS-29	✓
SR-PROP-04	The propulsion system shall perform reaction wheel desaturation.	SR-SYS-29	✓

Table C.1 continued from previous page

ID	Statement	Traced from	Compliance
SR-ADCS-01	The ADCS shall provide 3-axis stabilization.	SR-SYS-29	✓
SR-ADCS-02	The ADCS shall provide a torque of at least 10^{-5} Nm.	SR-SYS-29	✓
SR-ADCS-03	The ADCS shall provide momentum storage of at least 16 mNm.s.	SR-SYS-29	✓
SR-ADCS-04	The ADCS shall achieve attitude knowledge better than 0.01 deg (1σ).	SR-SYS-18	✓
SR-ADCS-05	The ADCS shall achieve attitude control better than 0.1 deg (1σ).	SR-SYS-18	✓
SR-ADCS-06	The ADCS shall implement all the modes established above.	SR-SYS-29	✓
SR-GNC-01	The GNC system shall provide a position accuracy in the order of 1 km (1σ) in all three axes.	SR-SYS-30	✗
SR-GNC-02	The GNC system shall provide a velocity accuracy in the order of 1 mm/s (1σ) in all three axes.	SR-SYS-30	✗
SR-AVI-01	The avionics stack shall use a backplane-based configuration.	SR-SYS-18	✓
SR-AVI-02	The avionics stack shall be mechanically compatible with CPCI Serial Space.	SR-SYS-18	✓
SR-OBC-01	The OBC system shall handle data rates of up to 0.5 kBps.	SR-SYS-19	✓
SR-OBC-02	The OBC shall be equipped with at least 400 MB of memory to store the nanosatellite telemetry data.	SR-SYS-19	✓
SR-OBC-03	The OBC shall implement dual modular redundancy.	SR-SYS-19	✓
SR-OBC-04	The OBC shall implement CAN and I2C interfaces for communication with the rest of the SC.	SR-SYS-18	✓
SR-TT&C-01	The TT&C subsystem shall establish communication using X-Band for uplink and downlink during all mission phases.	SR-SYS-23	✗
SR-TT&C-02	The TT&C subsystem shall be able to establish communication using X-Band without the need for deployables.	SR-SYS-22	✗
SR-TT&C-03	The TT&C subsystem shall support a downlink data rate of 2 kbps at a distance of 1.5 AU.	SR-SYS-23	✓
SR-TT&C-04	The TT&C subsystem shall have a downlink BER lower than 10^{-5} .	SR-SYS-23	✓
SR-TT&C-05	The TT&C subsystem shall support two-way Ranging and Doppler measurements of the SC throughout all mission phases.	SR-SYS-30	✗

Table C.1 continued from previous page

ID	Statement	Traced from	Compliance
SR-TT&C-06	The TT&C subsystem shall support Delta-DOR measurements of the SC throughout all mission phases.	SR-SYS-30	✗
SR-TT&C-07	The TT&C subsystem shall be capable of simultaneously handling telemetry, ranging and telecommands.	SR-SYS-23	✓
SR-TT&C-08	The TT&C subsystem shall comply with ESA ECSS telecommunication standards.	SR-SYS-24	✓
SR-TCS-01	The TCS shall preserve all other subsystems within their operational temperature limits during all phases of the mission.	SR-SYS-27	✓
SR-TCS-02	The TCS shall never allow any subsystem to go outside of its survival temperature range.	SR-SYS-27	✓
SR-EPS-01	The EPS shall have Sun-pointing capabilities.	SR-SYS-20	✓
SR-EPS-02	The EPS shall provide at least 90 W to other subsystems at a distance of 1.5 AU from the Sun.	SR-SYS-20	✓
SR-EPS-03	The EPS shall provide at least 49 W of power during eclipse.	SR-SYS-20	✓
SR-STR-01	The structure shall be in compliance with the 12U CubeSat standard established in the CDS [18].	SR-SYS-18	✓
SR-STR-02	The structure shall accommodate openings for the necessary subsystems as established in Subsection 4.1.11.	SR-SYS-18	✓
SR-STR-03	The structure shall shield the necessary subsystems from radiation.	SR-SYS-18	✓

Table C.1: Complete list of subsystem requirements with their respective requirement ID, traceability and verification method.